Journal of Membrane Science 645 (2022) 120041

Contents lists available at ScienceDirect

Journal of Membrane Science

journal homepage: www.elsevier.com/locate/memsci

A critical review and commentary on recent progress of additive manufacturing and its impact on membrane technology

Xin Qian [a], Mayur Ostwal [a], Ayse Asatekin [b], Geoffrey M. Geise [c], Zachary P. Smith [d], William A. Phillip [e], Ryan P. Lively [f], Jeffrey R. McCutcheon [a,*]

[a] Department of Chemical & Biomolecular Engineering, University of Connecticut, United States
[b] Department of Chemical Engineering, Tufts University, United States
[c] Department of Chemical Engineering, University of Virginia, United States
[d] Department of Chemical Engineering, Massachusetts Institute of Technology, United States
[e] Department of Chemical & Biomolecular Engineering, University of Notre Dame, United States
[f] School of Chemical & Biomolecular Engineering, Georgia Institute of Technology, United States

ARTICLE INFO

Keywords:
Membrane
3D printing
Additive manufacturing
Separations

ABSTRACT

Membrane separations has been increasingly recognized as a key technology platform for improving the energy efficiency of many separations processes. Likewise, additive manufacturing (AM), or 3-dimensional (3D) printing as it is often called, is a rapidly emergent technology platform for manufacturing in many industrial sectors. It has become increasingly common to marry these two platforms to take advantage of the additive nature of 3D printing with the increasing need for membrane technology that is adaptable to separations needs. Conventional membrane manufacturing approaches, such as casting, typically result in thick membranes that limit productivity and potentially waste material in a non-performing support layer. Interfacial polymerization (IP) offered a new vision for thin-film composite desalination membranes, yet it was limited to certain chemistries while exhibiting other drawbacks. Additive manufacturing offers certain benefits over these techniques to membranes, including the ability to expand the library of materials that can be processed while also offering a degree of customization that is impossible in conventional manufacturing. This review article evaluates an increasing body of literature on using printing to make membranes and considers the limitations and opportunities for printing to enhance existing membrane technology and expand the reach of membranes into other industries. We also provide a perspective from leading experts in membrane technology to see where there are opportunities to use printing in different membrane science disciplines.

1. Introduction

1.1. The advent of membrane manufacturing technology

Membranes are now ubiquitous to all industries. They are prevalent in water and wastewater treatment, food and beverage processing, pharmaceutical production, industrial gas production, commodity and specialty chemicals, and barrier materials. The continued growth of membrane technology in separations industries has been made possible by innovations in materials and manufacturing technology that have enabled scalable and controlled formation of membranes. Before addressing the recent history and future opportunities of using printing to make membranes, it is important to consider the history of membrane manufacturing and contextualize it with current research trends in membrane science.

Key to the expansion of membranes into these many industries was the development of the asymmetric membrane. The asymmetric membrane comprises a thin, selective layer supported by a porous material made from the same material. Sometimes referred to as the integrated asymmetric membrane, Sidney Loeb and Srinivasan Sourirajan are credited with the development of the first such membranes intended for use in desalination [1]. Their process, now commonly referred to as nonsolvent induced phase separation (NIPS) was used to make cellulose acetate membranes that exhibited a 10–20 fold improvement in water permeance with increased salt rejection over isotropic dense membranes [2].

* Corresponding author.
E-mail address: jeffrey.mccutcheon@uconn.edu (J.R. McCutcheon).

https://doi.org/10.1016/j.memsci.2021.120041
Received 23 April 2021; Received in revised form 26 October 2021; Accepted 1 November 2021
Available online 19 November 2021

Moreover, the process was inherently scalable to a roll-to-roll manufacturing. The relative simplicity of the NIPS process made it easy to fabricate large amounts of membrane area at relatively low cost. With such a step change in reverse osmosis (RO) membrane manufacturing technology that comprised both a performance increase with low-cost manufacturing, RO was born as a viable technology. Moreover, with the knowledge developed to control precipitation of other polymers, asymmetric membranes formed from other materials was enabled. Polysulfone (PSU) [Tweddle et al. [3]), polyethersulfone (PES) (Chaturvedi et al. [4]), polyacrylonitrile (PAN) [5], polyvinylidene fluoride (PVDF) [6], polyimide (PI) [7], self-assembled amphiphilic block copolymer [8,9], and many other commodity polymers were suddenly manufacturable as membranse and thus became household names in the membrane field for water and gas separations.

1.2. Transition to the thin film composite membrane platform

While integrated asymmetric membranes were a major step forward in membrane technology across the field, some of these membranes still lacked performance to meet some industrial needs. Desalination was in increasing demand throughout the latter half of the twentieth century and alternatives to distillation technologies were being sought. While RO offered such savings, the selectivity needed to be improved over the Loeb and Sourirarjan membranes to enable single pass desalination for seawater applications. Different materials, which would then require different processing and manufacturing, would be needed to realize these required improvements in performance.

This performance improvement was accomplished with the development of thin film composite (TFC) membrane by John Cadotte [10,11]. While not the first TFC membrane [12], it became one of the most important membrane platforms that employed a selective layer that was chemically distinct from the support layer.

Such a platform enabled careful selection of materials for optimum performance of either the selective layer or support layer. For instance, the support layer material could be sourced from easily processable and low cost commodity polymers with appropriate mechanical and chemical properties. The selective layer material could be selected from more exotic materials since the layer was thin (less than 1 μm) that could be carefully tuned by changing the chemistry. For early TFCs using aromatic polyamide, such tuning could be accomplished by using different amines and/or acid chlorides of various functionalities. The result was the creation of TFCs for new applications, such as nanofiltration (NF), that expanded the opportunity for RO technology across new industries outside of seawater desalination.

Perhaps even more important was the inherent manufacturability of the TFC platform. In particular, the aromatic polyamide could be made through sequential soaking of the support layer with one monomer followed by the other. The resulting interfacial polymerization could be scaled easily to a roll-to-roll process that produced RO membrane with a step-change improvement over integrated asymmetric membranes. TFC membranes had become the new state-of-the-art (SOTA) for RO. They offered order-of-magnitude performance improvement in both selectivity and permeance over asymmetric membranes. Remarkably, little has changed in this membrane as it has remained the gold standard membrane in reverse osmosis for the last 40 years.

1.3. Fabricating membranes for other separations processes

Interestingly, the TFC membrane platform has not transferred to other membrane separations processes that utilize flat sheet membranes. Membranes for ion exchange [13], gas separations [14], vapor separations [15], ultrafiltration (UF) [16], microfiltration (MF) [17], porous membrane contactors [18], and barrier membranes have largely relied on some type of phase inversion (such as NIPS) or extrusion processes. Though they may come in a variety of geometries (flat sheet, tubular, capillary, or hollow fiber), their manufacturing processes are still reliant largely on decades-old technology. Even more niche membranes, such as nonwovens and ceramics, rely on these conventional manufacturing approaches. Nonwoven membranes are melt or solution spun into mats, reliant on material processing with a solvent or at temperatures above the material's melting point [19]. Monolithic and tubular ceramic membranes are made by an extrusion process before sintering at high temperature [20]. Flat sheet ceramics are fabricated by tape casting a slurry using a knife or slot dye followed by careful evaporation of the solvent from the slurry prior to calcination [21]. Hollow fibers can be formed with dual-layers that enable the formation of TFCs, but materials options are limited to those that can be cast through phase inversion (and not through interfacial polymerization). In all, a vast majority of commercial membranes manufactured today are made through variations of phase inversion casting or extrusion.

1.4. Current gaps in membrane manufacturing

It is difficult to attribute a membrane's performance limitation specifically to a manufacturing limitation. Interestingly, funding drivers push the exploration of new materials for membranes that seek to probe traditional permeability/selectivity tradeoffs rather than specific membrane manufacturing needs. While such research has yielded remarkable new materials with exceptional properties, the challenge has been making these materials into membranes at scales relevant for their application. Thousands of papers have explored the use of new materials for all manner of membrane separation while far fewer have addressed the manufacturability of those materials into quantities and form factors that would make them relevant to the fields they promise to revolutionize.

An excellent example of a technology gap in membrane manufacturing is with mixed matrix membranes (MMMs). MMMs are membranes that contain a second phase that provides a chemical affinity and/or size exclusivity characteristic that target a specific molecule of interest. Good examples include metal organic frameworks (MOFs) [22,23], carbon-based nanomaterials (carbon nanotubes (CNTs), graphene, and graphene oxide (GO)), and zeolites [24]. Nanomaterials have been extensively used to improve the thermal and mechanical properties of many polymeric nanocomposites [25–27]. However, making membranes imbued with these materials is challenging due to their penchant for aggregation and relative disorder within the matrix (i.e. lack of alignment) [25]. The filler can also induce defects in the membrane unless manufacturing is precise and well-controlled. To date, while some commercial MMM have been developed, most membranes lack fillers due to manufacturing difficulties.

A number of questions remain around innovation needs around membrane manufacturing:

1. Are manufacturing limitations the barrier to seeing another step change in membrane performance?
2. What are the potential performance improvements possible with manufacturing innovation?
3. Can we borrow a manufacturing technique from one field (such as interfacial polymerization) and translate it into making membranes for another (such as ion exchange)?
4. Can we rethink how we make membrane structures altogether to leverage manufacturing controls that are currently unavailable with conventional membrane production processes?

1.5. Additive manufacturing

Additive manufacturing (also referred to as "3D printing") is a rapidly emergent manufacturing technique used across many industrial sectors due to its capability of building geometrically intricate structures with various materials in a single step. Printing has historically been seen as a way to precisely and quickly "manufacture" in a reproducible way without the unnecessary loss of material. Traditional printing can

be described as placing material, or ink, where we need it, rather than remove it from where we do not. That same concept has been applied to the manufacturing of more complex 3D structures. Instead of conventional manufacturing techniques for 3D structures, such as the use of molds or for items to be hewn from a block of material, where the unwanted material is removed, we can additively build, in a layer-by-layer approach, a material to precise specifications.

3D printing technology was first developed by Hideo Kodama who used ultraviolet (UV) light to cure polymers. This is the earliest known attempt at stereolithography (SLA) [28]. This precise and controllable approach has rapidly gained attention in printing both conventional materials, such as thermoplastic polymers, ceramic powders, and novel nanomaterials such as carbon nanotubes and graphene. The first SLA machine was invented by Charles Hull in 1983 and his company 3D Systems commercialized the world's first 3D printer SLA-1 in 1988 [29]. Simultaneously, more non-SLA AM techniques were patented. In 1989, selective laser sintering (SLS) was patented by Carl Deckard [30], and the fused deposition modelling (FDM) technology was patented by Scott and Lisa Crump [31]. Later on, laminated object manufacturing (LOM) was commercialized in 1991 by Helisys [32] and continuous liquid interface production (CLIP) appeared in 2012 as an alternative technique to digital light processing (DLP) [33]. In recent decades, 3D printing techniques have been extensively used in numerous industries, such as biomedical [34,35] and tissue engineering [36], pharmaceutical industries [37,38], aerospace [39] and automotive [40] engineering, analytical [41] and electrochemistry [42], sensor technology [43], food engineering [44], metal manufacturing [45] and marine science [46]. In addition to 3D printing and additive manufacturing, readers may find other papers that use synonyms such as rapid prototyping, desktop manufacturing, on-demand manufacturing or direct digital manufacturing.

During its development, 3D printing has achieved progress towards higher resolution, higher printing speed, greater scalability, and lower material consumption. In the last decade, more advanced techniques have been invented, such as DLP that was not only cheaper than SLA but also greatly improved the speed for printing large parts. Two photon polymerization (TPP) came about with substantially higher resolution. Recently a novel vat polymerization technique named continuous liquid interface production (CLIP) avoided the layer by layer procedure of traditional AM and showed ability to independently control the printing speed and resolution. As new techniques have emerged, opportunities for the membrane field became more apparent.

1.6. 3D printing and membranes

As 3D printing techniques have improved their resolution to the micrometer or even nanometer level, researchers have taken an interest in adapting the variants of these techniques to membrane manufacturing. Statistics in Scopus database (Fig. 1) show in the past decade there has been an increase in membrane papers related to 3D printing that has mirrored the increase in papers on 3D printing overall. The earliest work on membrane-related printing technology was focused on customizing spacers for membrane process such as UF [47], RO [47], forward osmosis (FO) [48] and membrane distillation (MD) [49]. From there, other publications emerged on reverse osmosis [50] and gas separation [51] applications. Recent research has realized 3D printing polymeric [52], ceramic [53] and nanoscale [54] materials to form precisely designed membranes in unique shapes.

1.7. Definitions of metrics or this review

Before diving into the methods themselves, it is important to establish baseline metrics that we can use to compare techniques. We show metrics of interest in Table 1. The resolution of the method is often in reference to the controllability of the membrane thickness, though in the case of porous membranes, it may refer to the ability of a technique to control pore size or pore spacing.

Accuracy and precision are critical for manufacturing, especially if one is trying to "dial in" a particular membrane feature size and to control that feature in a reproducible fashion. Other metrics listed would be expected for any manufacturing process, such as cost, mechanical strength and integrity, and material processability. Requirements on each of these factors will be individually discussed in section 4.

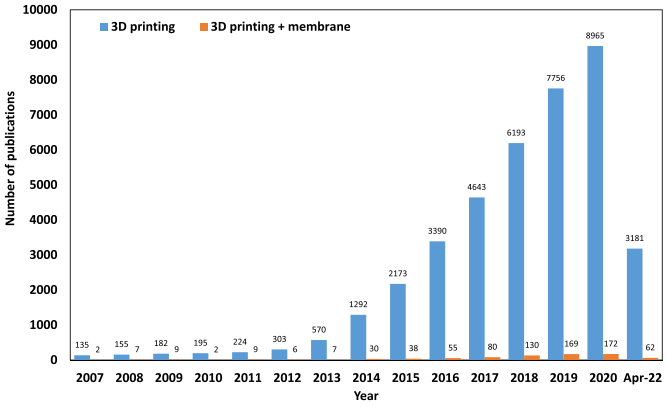

Fig. 1. Number of publications on 3D printing and 3D printing membrane since 2007. (Based on search of keywords "3D printing" and "3D printing + membrane" in Scopus scholar database. Data only includes published research and review articles since 2007.)

Table 1
Key metrics of additive manufacturing, their definition and importance in membrane manufacturing.

Metrics	Definition	Importance in membrane manufacturing
Resolution	Minimum feature size in a given dimension.	Resolution in XY direction determines surface morphology such as pore size and roughness. Z direction resolution determines the minimum thickness.
Accuracy	How closely a final 3D printed part can measure up to its predesigned model.	Dimensional deviation of morphological features between printed membranes and designed model.
Precision	The deviation between printed parts using the same machine and process.	Whether the membranes are consistent in dimension after every print.
Cost	The price of raw materials and printing process.	Whether a lab-scale membrane is appropriate to be
Speed	Rate of material deposition over a certain area.	industrialized by using a specific AM method. Typically
Size	The maximum dimension of the printed part.	assessed on a square meter basis.
Material processability	Whether a printing method allows appropriate processing conditions for different materials.	Determines the variety of materials that an AM technique can process a material into membranes with necessary performance.
Mechanical integrity	The mechanical properties of printed parts.	Whether the printed membranescan maintain its integrity under relevant operating conditions
Safety	Possible danger during operation.	Does the manufacturing process use toxic solvents, materials, or processing approaches that threaten health and life.
Environmental impact	The emission of the AM process and the waste chemicals it produces.	This determines the environmental footprint , chemical wastage, and scrap of the AM technique.

1.8. Structure of this review

This review will provide a commentary and critique on current progress, the future opportunities, and potential pitfalls, of using 3D printing for the manufacturing of membranes. We will first introduce key conventional state-of-art membrane manufacturing methods and their limitations. Based on these limitations, we will review some of the more popular 3D printing techniques that have been reported as potential membrane manufacturing approaches. Certain requirements and challenges imposed on these printing techniques, including level of resolution/accuracy, mechanical properties, cost effectiveness and printing speed/size will be discussed in detail. The focus of the review will be on flat sheet membranes, as few membranes of other geometries can be "printed" at larger scales. We do this for brevity and not to discount the impressive innovations around hollow fiber and tubular membrane manufacturing techniques.

While we will touch on 3D printing opportunities in areas of membrane spacers, modules, and other components, those applications will not be the focus of this review. We will mostly focus on the printing methods used to make membranes themselves. Many of these studies have focused on specific membrane processes, such as wastewater treatment, oil-water separation, and gas separation, rather than on importance of the manufacturing process itself. We will end the review by identifying appropriate applications of this technique in membrane manufacturing and provide commentary on future challenges and improvements in different membrane fields.

2. Conventional membrane manufacturing methods

During the rapid growth of the membrane industry, a number of conventional manufacturing processes have emerged that produce a large majority of the membranes made today. We limit this discussion to polymeric membranes that are manufactured in flat sheet platforms in reasonably large quantities and exclude nonwoven membranes for brevity (these have been reviewed elsewhere [55]). This largely limits discussion of the most common membrane manufacturing techniques: Phase inversion, interfacial polymerization, and extrusion.

2.1. Phase inversion

Phase inversion is a commonly used method for making polymeric integrated asymmetric membranes. The very commonly used phase inversion process is nonsolvent-induced phase separation (NIPS) [56,57]. The polymer dope solution is cast into a film with a knife or dye. That film is then submerged, on one side, in a non-solvent coagulation bath where the solvent and nonsolvent will exchange and the polymer will precipitate and form a thin film [58]. This process was used to make the first asymmetric cellulose acetate RO membrane and has been used since to make many asymmetric polymeric membranes.

Phase inversion has been extensively used in membrane manufacturing due to its wide compatibility with many polymers. This method is also cost effective and fast. A number of key drawbacks, however, are worth mentioning. First, the selective layer of these membrane is often relatively thick. This is because of the integrated nature of the membrane, where the dense selective layer slowly gives way to the supporting structure. This support structure is the second drawback. Most of the material used to make the membrane is relegated to the support structure where it performs no separation function. For expensive materials, this is a wasteful practice.

2.2. Thin film composite via interfacial polymerization

As mentioned above, the TFC membrane largely refers to polyamide thin film membranes made for RO and NF applications. However, this is too narrow of a definition. A TFC membrane refers to any membrane with a thin film selective layer that is chemically distinct from a supporting layer that serves only to provide mechanical support. From a manufacturing standpoint, interfacial polymerization has demonstrated the ability to make large quantities of membrane quickly using a singular chemistry platform (polyamide). The same advantages have not translated well to other materials, though it is worth noting the hollow fiber field has successfully demonstrated TFC hollow fibers through dual layer spinning. Still, interfacial polymerization is the most common approach to making TFC membranes and may offer manufacturing pathways for other condensation polymers [59]. In any case, the TFC has seen the most use for reverse osmosis and nanofiltration membranes.

2.3. Extrusion

There are two types of extrusion for fabricating flat sheet films. Blown film extrusion is often used for making films from poly (lactic acid) (PLA) [60]. The cast film extrusion has been widely used make polypropylene (PP) or polyethylene (PE) films for packaging applications. Extrusion is also commonly used to make PTFE and other flourinated polymer membranes. We note here that ceramic and some hollow fiber membranes are also made by extrusion processes. With hollow fiber spinning, extrusion can sometimes be combined with a phase inversion process where a polyer dope is extruded and then precipitated in a nonsolvent bath.

2.4. Other manufacturing processes

The authors recognize that there are many other fabrication methods for membranes. These may include, but are not limited to, layer by layer assembly, spray coating, electrospinning, dip coating, atomic layer deposition, chemical vapor deposition, and more. However, we are limiting this review to commercial manufacturing methods. While the review will largely cover printing methods at the laboratory scale, we will note the scalability of the methods and whether or not they have potential for large scale manufacturing.

2.5. Gaps and opportunities

2.5.1. Ultra-thin films of non-polyamide polymers

Making ultra-thin membranes for the enhancement of flux performance without sacrificing selectivity has become an important research goal. Currently, interfacial polymerization is the only commercial manufacturing option for making selective barrier layers that are sub-100 nm in thickness. This process is limited to the polyamide family of materials and other condensation polymers. While many have attempted to utilize unique properties of emergent materials, such as self-assembled [61] or chlorine tolerant materials [62], it is challenging to manufacture them into thin films on a larger scale. Identifying manufacturing options for roll-to-roll or otherwise continuous processing of thin films with non-polyamide materials are an opportunity space for commercial membrane development.

2.5.2. Mixed matrix membranes with homogeneous distribution of nanomaterials

As described above, nanomaterial fillers have long been considered for additives to polymeric membrane systems to improve selectivity and permeability. However, homogeneous distribution without aggregation of these nanomaterials is challenging. Many researchers have succeeded in improving the separation performance by forming mixed matrix membranes [63,64], but few have explored new manufacturing approaches that enable evenly distributed nanofillers. Ganesh et al. [65], for example, incorporated graphene oxide and while higher flux and rejection were observed, the GO exhibited a folded and agglomerated morphology. Current manufacturing techniques do not provide such control of nanomaterial distribution.

2.5.3. Aligned/ordered nanomaterials within polymer matrix

Alternative to creating percolation threshold loadings, nanomaterials with high aspect ratios can be used if they can be oriented in such a way as traverse the membrane thickness[66]. Many have tried this with CNTs, which can be opened to provide a cylindrical tube for transport. Orientation of nanotubes has been accomplished through chemical vapor deposition (CVD) growth alignment and subsequent impregnation into a polymer matrix [67,68]. Many of these membranes have demonstrated "enhanced flow" characteristics [69], suggesting that membranes comprised of these materials could yield remarkable fluxes and selectivity. Unfortunately, producing these membranes at scale at competitive pricing has proven elusive.

2.5.4. Hierarchical structures at the nm level

The introduction of additional functional layers plays an important role in tuning membrane structure and performance. These structures might include, for example, a fouling resistant layer on top of a membrane, an inner layer which can carry charge, or multiple layers with varying density. Dip coating approaches have allowed for the nano-scale control of chemistry using polyelectrolytes [70], which in turn can allow for precise placement of nanomaterials within a film material [71]. These methods are largely variations on conventional layer-by-layer assembly and have limited potential for scalable manufacturing.

2.5.5. Interfacial engineering to improve adhesion between composite layers

If we are to consider manufacturing ultra-thin films, then the use of a well adhered support is critical to ensuring mechanical integrity of the membrane. In conventional interfacial polymerization, we note that the *in-situ* formation of a polyamide film occurs with some overlap into the support layer which provides excellent adhesion. Alternative thin film materials may not experience the same level of adhesion, which in turn could lead to delamination, especially in a crossflow environment. Many researchers have sought to improve bonding between thin films and supports through chemical bonding between membrane layers. Li et al. [72] modified PES support with polydopamine (PDA), which later on reacted with piperazine (PIP) monomer and formed covalent bonding between support and polyamide selective layer. Ma et al. [73] cast carbopol as an interlayer between PAN substrate and chitosan active layer to improve adhesion which leverages the –COOH group in carbopol to provide hydrogen bonding with the chitosan. These types of "primer" layers have enhanced adhesion, but they are difficult to manufacture into thin films, leading to the potential of adding significant resistance membrane transport resistance.

2.5.6. Morphological control at the molecular level

Membrane structure-property control at molecular scale has attracted much attention as precision separations becomes more important. To use polyamide as an example again, selective layer "pore size" is adjustable by using alternative amine monomers. Piperazine (PIP), for example, is used to make nanofiltration (NF) membranes as it forms membranes with lower crosslink density. Similar molecular morphological control has major ramifications for solution-diffusion based separations.

3. Additive manufacturing techniques

Before reviewing the literature on additive manufacturing applied to membranes, we need to establish the lexicon that describes the various techniques. According to ASTM 52900 [74] and previous review papers in membrane additive manufacturing techniques [52,53,75,76], there are seven additive manufacturing techniques used for printing different materials and yield various resolution/accuracy. Details of these techniques, including compatible materials, resolution, accuracy, print size/speed, advantages, and disadvantages are provided in Table 2. Among all these techniques, vat polymerization and material jetting are most frequently used for fabricating membranes since other techniques cannot reach the required resolution level to achieve either thin layers or small pore size. The details of these printing processes are illustrated below and basic setup of these 3D printers are presented in Fig. 2.

3.1. Binder jetting (BJT)

Illustrated in Fig. 2(i), this technique was invented and patented at MIT in the early 1990s [77] and has been commercialized. This technique prints a binder into a powder bed to form the product. In this process, an ink jet print head is used to release binder droplets (approximately 80 μm in diameter), which fall onto the powder bed and subsequently form liquid agglomerates bonded to the powder particles. After printing one layer, the powder bed descends and allows new powder to be spread by roller. This process utilizes layer-by-layer conventional ink-jet printing of the binder material until the final product is formed. BJT has wide material compatibility that can print polymeric, metallic, and ceramic powders. This technique is also cost effective and fast. Resolution can be limited, with some commercial systems showing a maximum of 35 μm resolution [76]. Additionally, the printed parts often require post processing such as adding an infiltrant substance or oven sintering. The mechanical strength of the bounded parts is comparatively weaker than other 3D printed sintered or photocured products. BJT has been used to print ceramic membranes from cheap clay powders and binder solution, as discussed in section 5.5.

3.2. Powder bed fusion (PBF) - selective laser sintering (SLS)

This 3D printing technique often utilizes heat, lasers, or electron beams to sinter or melt the powder material layer by layer, as shown in Fig. 2(ii). This approach yields parts with higher mechanical strength than BJT products. Also the laser beam is able to fuse parts with complex geometry. This technique was first patented by Deckard and Beaman at the University of Texas at Austin [78]. Similar to other powder bed based printers, SLS printers use a printing chamber and a powder reservoir. In SLS, a higher point laser is generated from a laser beam to fuse the powder material into solid that forms a 2-dimensional structure. Once the shape of each layer is formed, the powder bed descends and allows new powder to be spread by roller for sintering the next layer. These procedures are repeated until the desired part is finished. Since the product density primarily depends on the peak laser power, the machine usually preheats the bulk material powder below its melting point and subsequently elevates the temperature at certain locations to form the desired product. Unlike other AM techniques such as SLA and FDM, SLS usually does not require support as the powder acts as the support. However, this powder bed technique usually yields rough surfaces compared with VAT techniques and it is usually expensive to operate due the cost of the laser. SLS is used primarily for printing thermoplastic polymers such as nylon, polystyrene, thermoplastic elastomers (TPE) and polyaryletherketone (PAEK) with resolution between 20 and 150 μm. The applications of SLS in printing oil-water separation membranes are discussed in section 5.2.

3.3. Vat photopolymerization (VP)

VP uses a liquid photopolymer in a vat that is cured or hardened by ultraviolet (UV) light layer by layer to form the desired part, as demonstrated in Fig. 2(iii). Unlike BJT and PBF process, VP incorporates curing of photopolymer liquids during printing, so it yields better surface quality and lighter products than powder based printing processes. However, only photosensitive resins can be used and the curing of these resins may result in release of fumes.

3.3.1. Stereolithography (SLA)

SLA is the most common and earliest laser based 3D photopolymerization technique which was first patented by Hull [29] in 1986. In this process, a concentrated beam of UV light is released from a laser

Table 2
Specifications, advantages and disadvantages of 3D printing techniques.

3D printing technique	Company	Resolution	Accuracy	Material	Thickness per layer	Advantages	Disadvantages	Printing speed	Patent/ reference
BJT	ExOne, Digital Metal, Desktop Metal, 3DEO, HP, Stratasys, GE Additive, Voxeljet,	Digital Metal: 35 μm ExOne: 300-400dpi	N/A	Polymer, Metal, Ceramic, Sand	0.05–0.5 mm	1. Wide material Compatibility 2. Fast, simple and inexpensive 3. Can print parts in full color	1. Limited mechanical properties 2. Low density parts 3. Possibility to shrink after printing 4. Additional postprocessing	Exone: 12–20 mm/h Voxeljet: 12–35 mm/h	[76,77,215]
Powder Bed Fusion SLS	3D Systems, Sintratec, EOS GmbH, Sharebot, Red Rock, XYZprinting, Sculpteo, Forecast 3D, Wuhan Binhu, Finnovation, Prodways Group, Formlabs, Renishaw Plc., Dynamic Tools	20–150 μm	Dimensional tolerance of ±0.3% Lower limit of ±0.3 mm	Thermoplastic (Nylon), metal and ceramic powders	EOS GmbH: 0.06–0.15 mm	1. Good mechanical properties 2. Good chemical resistance 3. Able to print complex structure 4. Does not require supporting materials	1. Porous surface 2. Requires post heating or cooling.	EOS GmbH: 20 mm/h Up to 60 mm/h	[76,78]
Vat Polymerization SLA	3D systems, Anycubic, Peopoly, Prusa, XYZprinting, Formlabs, Uniz, DWS, Protolabs, Photocentric, EnvisionTEC, Wuhan Binhu, Phrozen	Formlabs: 25–300 μm Protolabs: X/Y: 200dpi Z: 62.5dpi 3D Systems: 50 μm	Dimensional tolerance of ±0.15% Lower limit of ±0.01 mm	Photopolymers	0.025mm–0.1 mm Protolabs: 0.05 mm	1. Excellent surface quality 3. Able to print complex structure	1. Only works with photo curable materials 2. Questionable mechanical properties 3. Slow and expensive 4. Requires support.	20–36 mm/h	[29,76]
DLP	3D systems, Zortrax, SprintRay, FlashForge, Asiga, B9 Creations, EnvisionTEC, Henkel, Prodways	Formlabs: X/Y: 35–100 μm (depends on projector) Z: 25–300 μm	Forecast 3D: ±0.05 mm	Photopolymers	0.025mm–0.1 mm	1. Can print very intricate designs 2. Accurate 3. Less expensive than SLA	1. Mechanical properties of parts are not durable 2. Parts have worse mechanical properties than FDM 3. Involves toxic resins	20–36 mm/h	[76]
TPP	Nanoscribe, UpNano GmbH, GE	Nanoscribe: X/Y: 100 nm	N/A	Hydrogels, resins, photoresists	Nanoscribe: 10 nm	1. Very high resolution and accuracy 2. High reproducibility	1. Small build size and slow speed 2. Expensive	Nanoscribe: 3 mm^2/h	[76,79,216]
CLIP	Carbon	Carbon: 75 μm	Dimensional tolerance of ±0.3% Lower limit of ±0.3 mm	Photopolymers	0.1 mm	1. High resolution 2. Does not need layer by layer formation 3. Fastest 3D printing technique. 4. Can be used for more viscous and structurally robust materials	1. Lower resolution due to faster speed 2. Small build size	N/A	[76,80,81,82,83]
Material Extrusion FDM/FFF	Prusa3D, Creality3D, Monoprice, Tronxy, Qidi Tech, Ultimaker, Raise3D, Stratasys, JGAurora, XYZprinting	200–300 μm 300-600dpi	Dimensional tolerance of ±0.15% Lower limit of ±0.2 mm	Thermoplastics, polymer-based composites, ceramic slurries and clays, metal powders	Stratasys: 0.17mm–0.33 mm Ultimaker: 0.1mm–0.33 mm 0.5–6 μm	1. Wide material compatibility 2. Durable mechanical properties 3. No post processing 4. Inexpensive	1. Anistoropy in Z (i.e. thickness) direction 2. Lower printing quality. 3. Slow	50–150 mm/h	[31,76] [217,218]

(*continued on next page*)

Table 2 (*continued*)

3D printing technique	Company	Resolution	Accuracy	Material	Thickness per layer	Advantages	Disadvantages	Printing speed	Patent/ reference
Material Jetting IJP	Canon, Epson, HP, Samsung, XYZprinting		Printhead positional error: ±3 μm	Sol-gel materials, polymers, ceramics, nanoparticles, metals, nucleic acid and protein arrays		1. Inexpensive, fast and easy. 2. High printing quality 3. Full color prints 4. Quiet	1. Print head easy to clog 2. Not suitable for high volume printing. 3. May cause blurring	13–15 pages per minute	
ESP	Molecularspray Ltd	Z direction: 4 nm	±0.01%	Any conductive material	4 nm	1. Excellent resolution and accuracy for printing sub-10nm structures. 2. Inexpensive and quiet. 3. Thickness controllable and scalable. 4. Substrate independent. 5. Wide material compatibility.	1. Slow in building Z direction thickness. 2. Tradeoff between resolution and speed 3. Slow 4. Newer process with unknown costs	350 μm/s	[91,92,93, 94,95,96, 126,139, 219]
PJT/MJT	Proto3000, Protolabs, Xometry, Stratasys, Forecast3D	Stratasys: Z: 27 μm Protolabs: XY: 305 μm Z: 30 μm	Stratasys: 14–600 μm	Photopolymers	Stratasys: 14–28 μm	1. Reasonable resolution and accuracy 2. Smooth surface finish 3. Works with multiple materials 4. Full color prints	1. High cost 2. Worse mechanical properties than FDM and SLS printed parts	17 mm/h	[220]

(Abbreviations: BJT: Binder Jetting; SLS: Selective Laser Sintering; SLA: Stereolithography; DLP: Digital Light Processing; TPP: Two Photon Polymerization; CLIP: Continuous Liquid Interface Production; FDM: Fused Deposition Modelling; FFF: Fused Filament Fabrication; IJP: Inkjet Printing; ESP: Electrospray Printing; PJT: Polyjet; MJT: Multijet.).

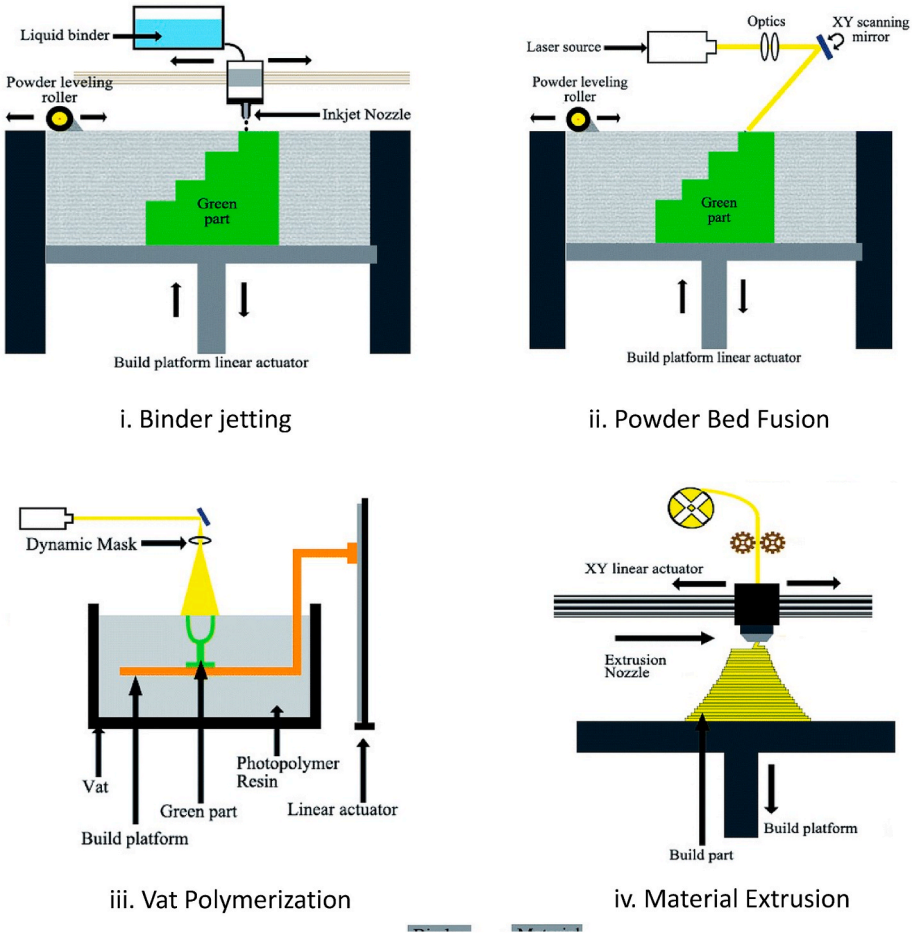

Fig. 2. Schematic diagrams of seven 3D printing techniques. Adapted from [53].

head and focused on a vat of photopolymer resin, which subsequently crosslinks and solidifies to the desired pattern. The building platform then descends, allowing the blade to coat another layer of polymer resin. This process is repeated until the entire 3D product is complete. The product is washed with proper solvent to dissolve all the wet resins or oligomers. SLA is able to print complex structures with good resolution since it applies point to point curing on each layer of resin. Therefore, it is faster when printing small or medium-size parts but not appropriate for larger scale products with multiple parts.

3.3.2. *Digital light processing (DLP)*

DLP technique was originally developed by Texas Instruments in 1987. This technique utilizes a projector that directly displays the light containing the image of the 3D CAD model onto a vat of photopolymer resin. Once the exposed liquid resin hardens the platform moves down, allowing the next layer of resin to be coated on the vat and crosslink into the desired structure. Compared with SLA, this technique is much faster in printing large scale parts and cost effective. However, SLA can yield better resolution and smoother surface than DLP as it prints the entire layer simultaneously and cannot guarantee resolution at each location. Both SLA and DLP were demonstrated successful in making ion exchange membranes, as discussed in section 5.3.1.

3.3.3. *Two-photon polymerization (TPP)*

The first TPP setup was proposed by Maruo et al. [79] in 1997. Unlike SLA which employs a UV laser to produce 2D pattern of photosensitive material layer by layer, TPP utilizes an infrared (IR) laser under which most photosensitive materials become transparent. Therefore, by applying pulses with IR laser the two-photon polymerization can be initiated directly within the small volume of material rather than performing 2D layer and layer polymerization. The IR laser is able to draw 3D patterns inside the material and leave the rest unpolymerized, which will be removed in the post processing step. This method dramatically improves the efficiency of 3D printing with resolution down to 100 nm. Therefore, it is often used to form microstructures such as 3D crystals and artificial fabrication in tissue engineering. The high resolution of this technique induces a tradeoff on its printing speed, maximum part size, and cost. The application in using TPP to make membrane cake filters is demonstrated in section 5.3.2.

3.3.4. *Continuous liquid interface production (CLIP)*

Different to DLP, CLIP (patented by Stratasys, Inc [80]) is an advanced printing technique that combines all the advantages of DLP with continuous printing without sequential layer formation. The core of this technique is the uncured liquid resin dead zone formed by an oxygen permeable window. Previous studies [81,82] reveal that the oxygen inhibits the curing of photopolymer by quenching the initiator or combining with the free radicals. In this process, an oxygen permeable window will be placed underneath the liquid resin container and the UV pattern will be projected through the oxygen window into the resin bath [83]. The liquid resin close to the oxygen permeable window will contain oxygen and forms a dead zone with a thin uncured resin interface. The cured part is located above the dead zone and continuously dragged upward to form the 3D structure. This continuous process achieves independent control on both printing speed and resolution compared with layer by layer bottom-up VP techniques. However, there is always a tradeoff between the printing speed and part resolution as observed by Tumbleston et al. [83]. Although CLIP has not been widely

applied to make membranes, its potential in printing liquid and gas separation membranes has been demonstrated, as summarized in section 5.3.3.

3.3.5. Material extrusion (ME)

This technique is the simplest and most popular method in today's additive manufacturing industry. It employs a nozzle to directly extrude heated material on the substrate, as shown in Fig. 2(iv). The material subsequently solidifies on the substrate at room temperature.

3.3.6. Fused deposition modelling (FDM)/fused filament fabrication (FFF)

FDM was first patented by Scott Crump in 1989 [31] that aimed at extruding polymeric materials on the platform to form 3D structure. Today, this technique is one of the most popular 3D printing methods which is usually used to form composite 3D structures. The material (usually a common thermoplastic filament) is fed into a nozzle, where it is heated up and molten and subsequently extruded on the platform layer by layer. The material then hardens and attaches to the previous layer. FDM is applicable to most thermoplastic polymers as polycarbonate (PC), acrylonitrile butadiene styrene (ABS), PP and polylactic acid (PLA). It is also one of the most cost-effective AM techniques and has a fast printing speed compared with other 3D printing methods. The major limitation on FDM is that it requires high mechanical and thermal stability on the material filament since it will experience melting and strong shear and normal stress during the feeding process. This thermal stress may even yield large distortional strain if the printed material has low modulus, which will ultimately result in problems such as material anisotropy, low resolution, and poor accuracy.

3.3.7. Other techniques

Direct ink writing (DIW) involves computer controlled nozzle to rapidly deposit viscoelastic material on the platform and form more complex structure. It usually employs a computer controlled translation stage to carry a nozzle that deposits ink to write a desired pattern. Many popular 3D printing techniques such as robocasting (patented by Cesarano et al. [84,85]) and inkjet printing can also be considered as DIW techniques. Based on a review of this process, features and application of DIW [86], it could be used to print polymeric, colloidal and polyelectrolytes ink into approximately 1 μm filaments. The filaments are deposited onto the substrate, gelled quickly and are assembled into complex 3D architectures. The viscosity of the ink is particularly important as the rheology will impact the shape and mechanical strength of the final part. Another techniuq, extrusion-based bioprinting (EBB), uses a micro-nozzle to precisely deliver bioink solution and draw 3D human tissue structures [87]. The bioink solution usually involves proteins, hydrogels and bioactive gels. Since most biomaterials are thermosensitive, the printer is usually equipped with an accurate heating system. Both FDM and DIW have been used in printing oil-water separation membranes, as summarized in section 5.1.

3.3.8. Material jetting (MJ)

Material jetting (MJ) is used to deposit material ink/solution or photopolymer droplets to form desired pattern or layer, as illustrated in Fig. 2(v). MJ functions like a 2D printer in the XY plane and additively builds up layers or patterns in the Z direction layer by layer. The manufactured parts can either be directly printed with volatile material or formed by curing the deposited photopolymer with a UV lamp.

3.3.9. Inkjet printing (IJP)

IJP is a very common printing process based on a computer printer that jets out ink droplets on substrates to form desired pattern. The world first inkjet printer was invented by Ichiro Endo, an employee of Canon in Japan. There are two common types of IJP techniques: continuous inkjet and drop-on-demand. IJP has a strict requirement on the substrate in that it governs the spreading of the deposited ink droplets, which can form different shapes and sizes [88]. Here the surface chemistry of the substrate is particularly important. Kang et al. [89] reported the impact of surface wettability on final printed dot size. When the ink droplets hit a wetting surface, the droplets spread and the result is poor resolution. Non-wetting surface usually generate rebounded ink droplets with smaller dot area. The drying of ink droplets will also impact printing resolution as the solute tends to accumulate along the boundary of the dot, which is also known as the coffee-ring effect [88]. Therefore, in order to improve the printing resolution, many efforts have been made to modify the substrate surface. For example, Wang et al. [90] used a charged silicone substrate with surface-energy patterns to repel and dewet the ink, which assisted the formation of 500 nm channels. IJP is among the more common techniques used for printing membranes. These include MF, UF, NF and RO TFC, charge mosaic membranes, oil-water separation membranes and ion exchange membranes. Please refer to section 5.4.1 for more details.

3.3.9.1. Continuous inkjet (CIJ). This technique employs a high pressure pump to transfer liquid ink from a reservoir through a nozzle, from which high speed of ink stream was continuously ejected. An acoustic wave is generated by a piezoelectric crystal that splits the ink stream to a fixed number of droplets. An electrode was used to create an electrostatic field, which charges the droplets during their travel and induces repulsion that separates these ink droplets. The charged droplets are deposited on the substrate and form the designated part. The major advantage of this technique is the fast printing speed without nozzle clogging. Therefore, it is widely used for printing organic solvent based material, allowing the volatile solvent to evaporate before reaching the substrate.

3.3.9.2. Drop on demand (DOD). CJI is a relatively old inkjet printing process and usually requires solvent based inks. As its name implies, DOD differs from CJI in that it aims at depositing ink droplets to create both photorealistic gradients and also vivid blacks. In DOD, piezoelectric material is added in the reservoir. This material is able to control the flow of the ink droplets since it can change shape and control the pressure while being charged at a specific voltage. Therefore, this technique allows printing of a wider variety of ink materials without the requirement of a volatile solvent. It is widely used in the printing industry today as it is able to create gradients and color effects. However, the cost of the print head is much higher than a conventional CJI print head.

3.3.10. Electrospray printing (ESP)

The first experimental research on electrospray was published by Zeleny [91] in 1914. Previously it has been widely used in mass spectrometry for particle ionization [92]. ESP is a novel and increasingly popular membrane AM technique as it can reach almost the highest resolution (up to 4 nm) among all the AM techniques. In one embodiement, ESP process using drum based printer is shown in Fig. 6 (c). In this process, the solution is sprayed at a fixed flow rate onto the rotating drum. The needle tips are charged to provide Columbic repulsion that generates a Taylor cone from the emerging jet. The drum is grounded in order to generate a potential difference between the needle tip and the drum. The voltage can be adjusted so that the Columbic repulsion overcomes the surface tension of the liquid jet. This will result in the formation of exceedingly fine droplets with diameter ranging from nanometer to micrometer scale. The electrospray pattern varies by different voltage, tip to target distance, liquid properties and ambient conditions [93–96]. Before spraying the liquid electrospray pattern must be optimized to reach the cone and jet mode, which provides the most stable pattern and highest printing resolution. By collecting the spray consisting of these fine droplets, the film is formed on a substrate that is attached to the collector surface. ESP has been used for making membranes for membrane distillation, NF, and RO. Examples of using this method are summarized in section 5.4.2.

3.3.11. Polyjet (PJT)/Multijet (MJT)

This technique is often used to form complicated structures as it is a combined IJP/VP technique. It utilizes an inkjet print head to deposit tiny droplets of photopolymer (usually plastic or elastomer) onto the print bed. The inks are usually washable gel-like polymers and solidify when exposed to the UV light attached next to the print head. This technique often prints products with good resolution, but the printed structure requires additional support which need to be removed manually. It can also print mixed materials to achieve better mechanical properties or multiple colors. PJT/MJT have been used membrane support and ion exchange membranes, as discussed in section 5.4.3. and 5.4.4.

4. Requirements and challenges on AM techniques for membrane fabrication

Many have considered some of the above mentioned AM techniques as options to address some of the shortcomings with conventional membrane manufacturing approaches. Due to the significant progress in AM techniques towards greater scalability, better material processability, higher speed, and improved resolution, AM techniques have been explored in the formation of specifically designed membranes components as they are compatible with common membrane materials. To consider which technique is most appropriate to make membranes, let us define the critical metrics that must be considered from the perspective of memrbane applications.

4.1. Resolution

The resolution of the printing technique will dictate various membrane features such as thickness, pore size, pore spacing, or nanomaterial distribution and spacing. Based on specific application demand, certain products may require different levels of surface features or thickness control, which narrows the range of applicable manufacturing methods. In Fig. 3, we illustrate the characteristic features sizes of MF, UF, NF and RO membranes and overlay them with the resolution of every AM technique. AM techniques with resolution lower than 10 μm such as SLS, SLA and FDM have little use in making membranes themselves as they are typically used for forming surface patterns, making films thicker than 10 μm, or fabricating other membrane components such as feed channel spacers and membrane filters [52].

For UF, NF and RO membranes, both pore size and thickness are significant structural parameters that could determine membrane performance. Printing specific pore sizes in any of these membranes as a specific feature of the printing process is unlikely. Pores larger than 0.1 μm in MF could be structured by drawing membrane filaments via DIW or FDM, as indicated in section 5.1. However, when it comes to NF, RO, or other dense membranes (e.g. membranes for gas separations and pervaporation) with smaller pores at sub-10 nm level, most current AM techniques lack resolution. However, we could print materials that could later exhibit the target pore size after solidifying. That means that the technique would need to exhibit the ability to print selective layers of appropriate thickness. For example, RO membranes have selective layer thicknesses that can be below 100 nm. This is below the resolution of many printing techniques. We note that membrane spacers and other structures such as filters, static mixers, and monoliths do not require submicron resolution requirement and are therefore amendable to more AM options.

4.2. Cost

The printed material is one of the major cost in AM and is connected to how expensive the base material is, how much material must be used, and how much must be scrapped. AM techniques by definition have limited scrap due to the fact that, generally, only what is deposited is used. For membranes, the materials costs are substantial, but printing membranes is likely to yield cost benefits over conventional manufacturing due to the lack of chemical wastage. Without the use of chemical baths and by negating the use of separation quality polymer as an underutilized support structure (as is the case with integrated asymmetric membranes), substantial cost savings are possible. This could have ramifications for the making of membranes comprised of expensive materials. If these could be printed into thin films and supported by inexpensive supporting membranes, rare and exotic materials could be made into membranes without wasting material or relegating it to the support layer (as in integrated asymmetric membranes).

Machinery CAPEX and maintenance also contribute to the cost of manufacturing the membrane. Printing equipment may require replacement of light sources, moving parts, heaters, and other components typical with these processes. System clogging, and chemical degradation/corrosion of wetted surfaces will contribute to general maintenance costs. These costs, however, are not, in general, any different than those used for conventional membrane manufacturing.

4.3. Accuracy

Accuracy is defined as the distance of a measurement to the target value. In 3D printing, to quantify accuracy, we introduce dimensional deviation, which is the deviation between the printed part and a model or design. According to Kim et al. [97], a specific part for benchmark tests fabricated by SLS and EOS processes show over 95% consistency with CAD data within the error range of 0.2 mm. FDM and SLA have a little higher dimensional deviation, with =90% and 86% of the of the printed parts being within the error range of 0.2 mm, respectively. In membrane applications, where resolutions must be far less than 0.2 mm, accuracy is a challenging metric to meet.

4.4. Precision

Precision is the repeatability of a measurement and usually describes the deviation between each measurement. To quantify precision, we define a tolerance to variability from membrane to membrane. FDM and SLA can achieve approximately ±0.15% tolerance and SLS reaches ±0.3%. MJ is the most precise AM technique with a dimensional tolerance of ±0.1%. These precisions are of course related to device length scale. With membrane manufacturing, repeatability is essential as every

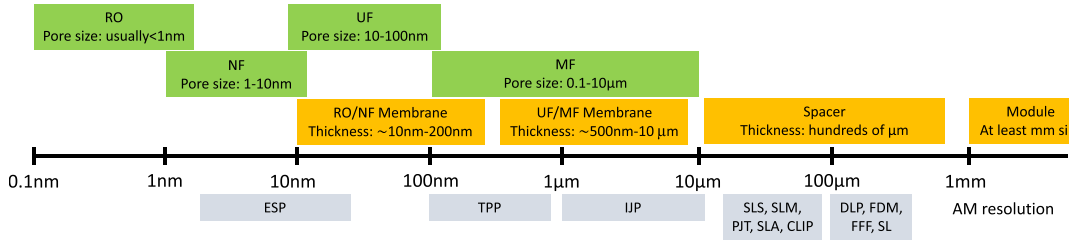

Fig. 3. Range of feature size (green), membrane or component thickness (orange), and AM resolution (grey). (For interpretation of the references to color in this figure legend, the reader is referred to the Web version of this article.)

square meter of membrane must perform similarly to the last one produced. It is worth noting, however, that even commercially available membranes offer "ranges" of performance on their specification sheets. For instance, DuPont's specification sheets for its SW30 seawater RO membranes indicate that manufactured elements may vary by ±20% of the stated permeate flow rate for the standard 4040 individual element. This 40% spread suggests that perhaps even a 40 years old manufacturing technology is not quite as consistent as we might expect.

4.5. Printing speed

Printing speed for membranes dictates the amount of membrane area printable in a set amount of time. It would correspond to a "line speed" of a typical membrane manufacturing process (which might be on the order of meters/min). For a membrane, printing speed depends on how much volume of a material must be deposited over a certain area. For a printing process, additional printing devices can be added in series in order to speed up the line. Alternatively, higher deposition rates could also be used, though this would likely sacrifice resolution. However, if some printing techniques deposit very limited amounts of material yet thick membranes are required, line speed could be hindered. Pre and post-processing time in 3D printing is also a major component that need to be involved when judging the printing speed. Preprocessing time is usually the warming up time of the 3D printers and postprocessing time depends on whether the parts require additional drying, curing or other necessary treatment.

4.6. Printing size

The printing size should be consistent with existing manufacturing practices. For flat-sheet membranes, casting lines between 12 and 40 inches wide tend to be fairly common. Given that printing on paper today is possible on paper that is over 40 inches wide, this metric is likely of limited concern. Some of the printing devices, though, may need significant engineering design to cover large areas with reasonable speed and consistency.

4.7. Material processability

3D printing is compatible with most materials used for membrane fabrication as most AM techniques are capable of printing polymers, ceramic precursors, metal, paper or clay. The materials appropriate for each AM technique are listed in Table 2. The processing conditions determined by material intrinsic properties may further restrict the eligibility of some 3D printing techniques in processing them into membrane components. For example, vat polymerization is only compatible with photosensitive polymer resin. The swelling behavior of some photopolymers, especially cured under heat, imposes problems such as pattern bleeding [98] which causes large deviation from the designed model. Based on previous papers on curing kinetics of bisphenol-A epoxy resin [99], some thermoset polymer resins are not fully crosslinked when the temperature does not reach certain level. The formation of partially crosslinked oligomers will severely reduce the mechanical properties and damage the integrity of the printed parts. Some photocured spacers were also observed to break when soaked in water for long time [76]. This is possibly due to the instability of the photoinitiator or the incomplete curing as discussed above. In FDM, die swell is a detrimental issue due to the viscoeleasticity of the thermoplastic polymers. According to Graessley et al. [100] in capillary flow the swelling ratio of polystyrene is approximately 1.1, which is primarily dependent on the shear stress and polydispersity. It has also been observed in FDM and MJ printing that the nozzle can clog with material, especially when printing viscous polymers or polymers with nanomaterials that can aggregate.

4.8. Structural integrity

The membrane structural integrity is a metric that it determines whether a membrane can remain intact during manufacturing, module installation, and operation. Loss of structural integrity will lead to a loss of selectivity for the membrane. In many 3D printing products, mechanical vulnerability stems from mechanical anisotropy, especially for FDM printed parts, which has an anisotropy level of 50% [101]. Fortunately, many membrane manufacturers are familiar with anisotropic structures. For any membranes printed in a layered format such as through material jetting, one of the critical concerns of printed membranes will be adhesion of the membrane layers to each other and to the substrate. Membranes may undergo high shear in crossflow environments or endure abrasion. A printed membrane must exhibit the same or better mechanical strength as one made from a conventional process for it to be considered an acceptable alternative.

4.9. Environmental, life cycle, and safety metrics

Many 3D printing processes produce hazardous chemicals. These include ultrafine particles (UFPs, particles less than 100 nm) and hazardous volatile organic compounds (VOCs). Some printing processes, even though they are additive, may emit harmful vapors or require post-processing with chemicals that create waste streams. Studies have indicated when printing PLA, ABS or Nylon filaments via FFF, VOCs such as caprolactam and styrene are emitted [102,103]. In VP processes such as SLA and DLP, organic solvents such as IPA and acetone are usually used for removing uncured resin, which produces a large quantity of toxic organic waste. In SLS and PBF it is easy for an operator to breathe in some hazardous polymeric and metal powder particles. Therefore, it is particularly important to identify the potential risk of hazardous emissions on human health and the environmental a for each 3D printing process. Proper handling of these hazards or embedding ideas of green manufacturing in these AM processes could help reduce safety and environmental concern. In general, though, when comparing the generation of waste from AM processes for membranes, we must compare to conventional membrane manufacturing processes. These processes produce their own significant waste streams. In conventional membrane fabrication such as interfacial polymerization, the removal of excessive m-phenylenediamine (MPD) and trimesoyl chloride (TMC) solution could generate large waste stream of monomer. However, in additive manufacturing, the material is selectively bound, sintered, cured or deposited to form the desired membrane structure. This indicates a majority of the material being processed is used to form membrane without resulting in wastage.

5. Recent work on 3D printed membranes

In this section we present the work that has currently been published on using printing approaches to make membranes. We see a number of efforts to use IJP and ESP to make membranes due to their ability to make thin films and MMM membranes. SLS and ME have been considered for making porous membranes. Most PBF, ME and VP methods cannot reach membrane-required resolutions, but they have been used to form surface patterns, base layers, and membrane filaments. Table 3 lists the membranes printed by different materials reported in the literature.

5.1. ME printed membranes

5.1.1. FDM printed membranes

FDM has been used to print membranes intended for use in oil-water separations. Xing et al. [104] printed PLA gravity-driven oil-water separation membranes via FDM that extruded PLA filaments, as shown is Fig. 4 (a). By adjusting the infill setup, the PLA filament width and spacing between adjacent filaments could be tuned so that the pore size

Table 3
3D printed membranes and their fabrication details, application, material and geometry.

Printing technique	Application	3D printed part	Postprocessing	Material	Membrane geometry	Remarks	Reference
Material Extrusion							
FDM	Oil-water separation	Membranes	Chemically etched with strong organic solvents	PLA	Petal thickness: ~100 nm	• Lotus-shaped membranes exhibited 99% separation efficiency with 60,000 LMH flux	[104]
DIW	Oil-water separation	Membranes	Cured at 120 °C for 1hr	PDMS, nanosilica (DNS-2)	Thickness: ~0.8 mm	• Excellent mechanical properties • 99% oil-water selectivity with 23,700 LMH flux	[105]
DIW	Oil-water separation	Membranes	Cured in DI water for 1hr	Cellulose acetate, PVA, silica nanoparticles (SiO2 NPs)	Pore size: 103–631 μm	• Over 99% separation efficiency with 3×10^5 LMH water flux • Strong anti-fouling ability with stable mechanical properties	[107]
DIW	Solar wastewater remediation	3D microlattices	Crosslinked in $CaCl_2$ solution, washing, supercritical drying	g-C_3N_4 nanosheets (CNNS), sodium alginate (SA)	Pore size: 17.81 nm Pore volume: 0.3303 $cm^3\ g^{-1}$	• 2.5 times higher than contrast photodegradation activities, broadband visible-light absorption and virtually no activity loss after three cycles of testing	[108]
DIW	Fouling mitigation for wastewater treatment	Surface patterns	Solidified at room temperature overnight, sintered at 1300 °C for 2hrs	Alumina powders	Thickness: double-coated layers: ~40 μm, top layer: ~8 μm Pore size: double-coated layers: 0.09–0.2 μm, top layer: 0.07–0.09 μm	• Higher flux and much better antifouling performance for patterned ceramic membranes • Flow direction did not impact flux but affected antifouling ability	[109]
Solvent-cast printing (SCP)	Widen material selection for printing isotropic membranes	Membranes	N/A	Poly(benzimidazole) (PBI)	Thickness: 74 ± 2 μm	• SCP could print currently unprintable high-performance high T_g thermoplastics • Better mechanical properties and isotropy than FFF printed films	[112]
Powder Bed Fusion							
SLS	MF	Membranes	N/A	Polyamide-12 (PA2200)	Thickness: >500 μm Mean pore size: 9.8 μm and 14.5 μm Porosity: Maximum 30.7% (depend on laser power)	• High energy density induced denser membrane with lower flux and higher rejection	[113]
SLS	Oil-water separation	Membranes	N/A	Polyamide-12 (PA2200), candle soot	Thickness: 500–800 μm Porosity: 22–28%	• Over 99% Hexane-water separation efficiency with flux between 3300 and 6700 LMH	[114]
SLS	Oil-water separation	Polyamide membranes	ZIF-L coated on PA membranes in solution	Polyamide-12 (PA2200), ZIF-L (Zn $(NO3)_2{\cdot}6H_2O$)	Thickness of ZIF-L layer: 0.15–2.77 μm	• Oil flux of 24,000 LMH and over 99% oil rejection	[106]
SLS	Oil-water separation	PSF membranes	Candle soot coated on membrane under sonication, loose candle soot removed	PSF, candle soot	PSF top layer thickness: 137–355 μm. Candle soot layer depth: 0.8 μm, surface roughness: 0.135 μm	• Oil flux of 19,000 LMH and a 99% separation efficiency • Stable separation efficiency in the 10-cycle hexane-water separation test	[115]
Vat Polymerization							
SLA	Anion exchange membranes (AEMs)	AEMs with surface pattern	Membranes washed with MeOH and water, then quaternized in TMA/MeOH, washed with NaCl	DUDMA-co-PEGDA-co-VBC	Thickness: 200–600 μm	• The membrane resistance is relevant to the interface between layers and the curing time • SLA is not a precise method in printing membranes due to pattern bleeding	[98]

(*continued on next page*)

Table 3 (*continued*)

Printing technique	Application	3D printed part	Postprocessing	Material	Membrane geometry	Remarks	Reference
Solvent based Slurry SLA (3S)	UF	Ceramic membrane	Thermal debinding of binders, sintering	Alumina powder (AES 11C)	Thickness: 200–250 μm Surface roughness: 0.17–0.18 μm Pore size: 7.9–9.8 μm 8.2–13.7 μm	• 32–33° water contact angle, which was in the UF range	[116]
Print-on-demand	Oil–water separation Oil recycling	Graphene coating	Graphene coating deposited onto nickel foam via laser-induced forward transfer strategy	Polyimide, nickel foam	N/A	• Able to collect oil on water surface for at least 10 cycles	[110]
Vat Polymerization							
DLP	Anion exchange membranes (AEMs)	AEMs with surface pattern	Membranes washed with MeOH and water, then quaternized in TMA/MeOH	Poly(DUDA-co-PEGDA-co-VBC)	Base membrane thickness: 250 μm Pattern thickness: 190–589 μm	• Similar permselectivity and water uptake as normal AEMs • Lower ion resistance than flat AEMs with similar thickness	[111]
TPP	Studying filter cake morphology	Colloidal 3D crystals membrane template	Flushed with an aqueous suspension of spherical core-shell microgels	N/A	Sphere size: 6 μm	• The crystal membrane template was able to tune the filter cake orientation • Visualized the filter cake compaction morphology	[119]
CLIP	Liquid and gas separation	Membranes	N/A	A variety of membrane materials	N/A	• CLIP was found to be an appropriate approach to printing separation membranes	[120]
Material Jetting							
IJP	TFC for water treatment and desalination	Fluorinated amine alkaline solution (HFP-mAP-NaOH)	Surface treated with TMC similar with IP, dried and washed	Polysulfone (PSF35), MPD, TMC, 2,2-Bis (3-amino-4-hydroxyphenyl) hexafluoropropane(HFP-mAP)	HFP-mAP coverage: 25%, 50%, 75%, 100% Printed droplet size: ~15 μm	• Similar water permeance as unfluorinated membranes but much higher NaCl rejection (98%)	[124]
IJP	RO and NF TFC	MPD aqueous solution	Surface treated with TMC similar with IP, heat treated at 70 °C for 10min	Polyethersulfone (50 kDa), MPD, TMC	N/A	• More printing layers induced lower water permeance and higher NaCl rejection • IJP did not reach enough resolution to print PA selective layer	[125]
IJP	UF	SPE monomer	UV irradiation, washed with ethanol and DI water	Polyethersulfone (150 kDa), [2-(Methacryloyloxy)ethyl]dimethyl-(3-sulfopropyl)ammonium hydroxide (SPE)	N/A	• Higher protein fouling resistance and slower biofilm growth	[128]
IJP	MF and UF	Dopamine (DA) monomer and sodium periodate (SP)	Further polymerization and washed with DI water	PP, sodium periodate ($NaIO_4$), dopamine hydrochloride	PP membrane proe size: 0.2 μm	• Enhanced flux and antifouling performance, with long-term stability while exposed to various pH	[130]
IJP	Oil–water separation	Polyphenols layer (catechol or tannic acid), sodium periodate	Dried and washed by DI water	PVDF membrane, sodium periodate, catechol (CA), tannic acid (TA)	PVDF membrane pore size: 0.22 μm Smaller pore size when coated with TA or CA	• 99% oil-water separation efficiency and 5.2 times higher water permeance than pristine PVDF membrane	[131]
IJP	Wastewater treatment	silver nanoparticles (AgNPs) coating	Dried overnight	Polyurethane (Bionate 75A), water based silver ink	Thickness: 0.15 mm, unchanged thickness after printing AgNPs	• Strong antimicrobial behavior	[134]
IJP	NF	Graphene oxide (GO) coating	Dried	Single-layer graphene oxide (SLGO) powder, PAN (M-PA400-GPET), NaOH	GO coating thickness: 7.5–60 nm PAN membrane pore size: 20–50 nm	• Over 80 LMH/bar water permeace and 96.7% Methyl Orange (MO) rejection • 10 times higher dye rejection than commercialmembranes	[135]
IJP	Charge mosaic membranes	Polyelectrolytes (PDADMAC and PSS)	Chemically cross-linking	Polycarbonate track-etched membrane (PCTE), poly (diallyldimethylammonium chloride), poly(sodium 4-styrenesulfonate)	PCTE membrane (pore diameter: 30 nm; thickness: 10 μm; porosity: $\sim 3 \times 10^8$ porescm^{-2})	• Dissolved salts could pass more rapidly through membrane than neutral/water molecules	[132,133]

(*continued on next page*)

Table 3 (*continued*)

Printing technique	Application	3D printed part	Postprocessing	Material	Membrane geometry	Remarks	Reference
						• Transport properties could be adjusted by tuning the width of the polyelectrolytes stripes	
IJP	Biocatalytic membranes for micropollutant degradation	PVA-yeast cells layer	PVA crosslinked at 45 °C for 40 min, washed and dried	PVA powder, PSF MF membrane, surface display laccase (SDL) biocatalytic cells	Thickness of PSF membrane: 165–200 μm Pore size of PSF membrane: 800 nm	• Stable enzyme activity • Great bisphenol A (BPA) and acetaminophen (APAP) degradation efficiency	[136]
IJP	Membrane electrode assembly (MEA)	Pt/MWCNTs catalyst layer	Heated dry at 80 °C for 1 h, then hot pressed to form MEA	Nafion 117 membranes, H_2PtCl_6, MWCNTs	N/A	• MEAs printed via catalyst-coated membrane (CCM) method showed better cell performance	[137]
IJP	Proton exchange membranes	Nafion layer	Tempered for 2 h at 85 °C, cell assembly	Nafion® D2020 Dispersion, 2-propanol, gas diffusion electrodes	Overall membrane thickness: 8–25 μm	• The printed MEA had one of the highest power density among all the Nafion membrane fuel cells • Cost saving and long lifetime	[138]
Material Jetting							
ESP	RO TFC	MPD, TMC	Stored in DI water overnight	MPD, TMC, lipophilic ionic liquid, PSF20 UF membrane, PAN50 UF membrane, PAN450 UF membrane,	Thickness per electrospray layer: as low as 4nm/layer Surface roughness: less than 2 nm	• PA thickness was completely independent of substrate material • Highest resolution among 3D printed membranes • Controllable thickness and desalination performance	[126]
ESP	RO TFC	MPD, TMC	Stored in DI water overnight	PES UF membrane, TMC, MPD	ESP thickness growth: 1 nm/min Average surface roughness: 1.2 ± 0.2 nm	• Controllable thickness • Controllable and comparable RO performance to PA membrane made by IP	[139]
ESP	RO TFC	MPD, TMC, MWCNTs	Stored in DI water overnight	PES UF membrane, TMC, MPD, MWCNTs	The introduction of CNTs did not affect the PA selective layer growth rate.	• 6-fold enhancement in water permeance without loss in salt rejection	[54]
ESP	NF TFC	PIP, TMC, Span 80 interlayer	Stored in DI water overnight	PES UF membrane, TMC, PIP, Span 80	ESP thickness growth: 22 nm/h Surface roughness: 15.3 nm	• Improvement in water permeance with only minor loss in Na_2SO_4 rejection	[127]
ESP	Liquid separation	Dopamine	N/A	PES UF membrane (UE006), dopamine hydrochloride	ESP thickness growth: 4.7 nm/h	• 87.9% boric acid rejection and high rejection for neutral red and Congo red dyes	[140]
ESP	Wastewater treatment	PDMS-curing agent/ hexane solution	Cured at 80 °C for 2 days	PVDF (Kynar HSV900), PDMS (SYLGARD® 184), PET non-woven fabrics (grade 3233, 3256 and 3249)	PDMS layer thickness: 3–9.6 μm Surface roughness: as low as 3 nm	• Outstanding phenol mass transfer coefficients (k_0's) of $37.9 \pm 2.8 \times 10{-}7$ m/s with over 99.5% salt rejection • Long-term stability in k_0 and salt rejection while exposed to strong acid and alkaline	[141]
ESP	NF	Zwitterionic copolymer solution, IPA	Stored in DI water or water bath annealing at 50 °C for 2 h.	PTFEMA-*r*-SBMA (zwitterionic copolymer), IPA, trifluoroethanol, DMF, PAN400 UF membrane	Sub-5nm selective layer	• Water permeance up to 180 LMH/bar (30 times higher than peremance of cast membranes) • Full rejection of chlorophyllin • A sharp size cutoff at approximately 1.1 nm	[142]
ESP	Oil-water separation	PVA [151,153] PVA and MWCNTs [152]	Immersed in water/acetone solution, then added glutaraldehyde (GA) and HCl for	PAN (1.36×10^5 g/mol), PVA, GA, HCl, MWCNTs	Thickness of PAN mat: 100 μm Thickness of PVA layer:	• High water permeance of 173.91 LMH/bar with 99.6% oil-water separation	[143-145]

(*continued on next page*)

Table 3 (*continued*)

Printing technique	Application	3D printed part	Postprocessing	Material	Membrane geometry	Remarks	Reference
			PVA crosslinking, hot pressed to control crosslinking degree		~0.5 μm Thickness of PVA layer after hot press: 300 nm	efficiency and a strong anti-fouling performance in crossflow mode • The incorporation of MWCNTs enhanced water permeance to 340 LMH/bar	
ESP	Membrane separation	Cellulose acetate (CA), glutamic acid	Glutamic acid removed by methanol	Cellulose acetate, N-α-benzyloxycarbonyl-$_D$-glutamic acid (Z-$_D$-Glu), N-α-benzyloxycarbonyl-$_L$-glutamic acid (Z-$_L$-Glu)	Thickness: CA with Z-$_D$-Glu: 120 μm CA with Z-$_L$-Glu: 300 μm Diameter of printed CA nanofiber: 200–500 nm	• Higher permselectivity and flux than the membranes electrosprayed without print molecules • This molecularly imprinted membrane was able to break the selectivity-flux trade-off	[148]
ESP	Chiral separation	Polysulfones with aldehyde (PSf-CHO), Z-$_D$-Glu, Z-$_L$-Glu	N/A	PSf-CHO, Z-$_D$-Glu, Z-$_L$-Glu	Membrane thickness: 30–200 μm Fiber diameter: 165–564 nm	• Decent chiral separation ability and great enantiomer transport • Twice higher flux without loss in permselectivity	[149]
ESP	Gas separation	ZIF Precursor solution	Cooled to remove thermal stress, solvent exchange in methanol, dried	Zinc nitrate hexahydrate, sodium formate, benzimidazole, 2-methylimidazole, 2-Hmim	α-alumina substrate thickness: 2 mm, diameter: 20 mm, pore diameter: 0.12 μm, porosity: 40% Thickness of ZIF-7 layer: 2–22 μm Thickness of ZIF-8 layer: 4.5–28.1 μm	• ZIF-7 membranes had 4-10 times higher H2 permeance with decent H2/CO2 separation factor of 9.6 • ZIF-8 membranes exceeded the Robeson's upper bound in the permeability-selectivity tradeoff	[150,151]
Electro-co-spinning/ spraying	MD	Electrosprayed: PVDF-HFP/SiNPs dope solution Electrospun: PVDF-HFP dope solution	DMF vapor-phase welding, functionalized with fluoroalkylsilane (17-FAS)	Poly(vinylidenefluoride)-cohexafluoropropylene (PVDF-HFP), silica nanoparticles (SiNPs)	Before welding: thickness: 132 μm, porosity: 82.2 After welding: thickness: 174 μm, porosity: 80.7	• Excellent NaCl scaling resistance without any decline in flux and distillate conductivity after 420 mL water recovery	[146]
Electro-co-spinning/ spraying	MD	Electrosprayed: PS beads Electrospun: PH fibers	Evaporation of residual solvents in oven at 80 °C for 24hrs	Polystyrene (PS), polyvinylidene fluoride-cohexafluoropropylene (PH)	Pristine PH membrane: thickness: 156 μm, pore size: 0.54 μm PH-PS membrane: thickness: 178 μm, pore size: 0.40 μm	• Over 99% salt rejection, stable flux and anti-wetting performance during the DCMD operation	[152]
Material Jetting							
ESP	MD	PVDF, PDMS and silica fumes blended solution	N/A	PVDF (Kynar HSV900), PDMS, silica fumes, lithium chloride	Membrane thickness: 60 ± 5 μm	• Reasonable anti-scaling/fouling behaviors with a stable flux of 28kg/(m^2h) during 160hrs continuous DCMD operation	[153]
Dual electrospray (DES)-assisted forced polymer blending	Proton exchange membrane fuel cells	Nafion/sBlock blend	Exposed to IPA vapor for densification, hot pressed at 120 °C and annealed at 130 °C	Nafion 521 solution, sBlock	Thickness of Nafion/sBlock membrane: ~30 ± 3 μm	• Higher proton conductivity than the prediction of Maxwell–Eucken structural model	[147]
ESP	UF	Polyelectrolytes: polyethylenimine (PEI), polystyrene sulfonate (PSS)	N/A	PES membrane, PA-PSF TFC membrane,	Thickness of: PEI layer: 130 nm PSS/PEI layer: 470 nm Pore radius of: PES: 2.5 nm PA-PSF TFC: 1.8 nm	The deposition of polyelectrolytes resulted in: • Significant change in ion separation selectivity • Small improvement in flux and an increase in surface hydrophilicity.	[154]
ESP	Anion exchange membrane	Fluoropolymer spots	N/A	Anion-exchange Neosepta AMX membrane, hydrophobic fluoropolymer	N/A	• Expanded electroconvection that enhanced mass transfer and reduce water splitting of the membrane	[155]

(*continued on next page*)

Table 3 (*continued*)

Printing technique	Application	3D printed part	Postprocessing	Material	Membrane geometry	Remarks	Reference
MJT	Oil-water antifouling	ABS support layers	Vacuum filtration to adhere selective layer	Urethane acrylate oligomers, PES (150 kDa)	Thickness of: support: 500 μm Selective layer: 16 ± 1 μm	• Wavy membranes showed 30% higher water permeance (16LMH/bar), 96% oil rejection and 52% higher permeance recovery ratio (89)	[156,157]
PJT	Ion exchange membrane microbial fuel cell	Tangoplus proton exchange membranes	Support removed by water jet	Tangoplus acrylate photopolymer resin, natural rubber latex	Thickness of: Tangoplus membrane: 116 μm Latex membrane: 100 μm CMI-7000 (CEM) membrane: 450 μm	• Enhanced energy output, high ionic conductivity, system stability and resistance to biological deterioration and decent electrical separation	[159]
Binder Jetting	Ceramic membranes	Clay ceramic membranes	Green samples cleaned, dried and sintered.	Kankara clay powder, Maltodextrin	Particle size: 75, 150 and 250 μm	• Membranes printed with smaller clay powders had higher water flux, rejection and mechanical properties	[158]

of the PLA membrane was well controlled. The printed membranes were then chemically etched with strong organic solvents and subsequently treated with polystyrene in order to grow the lotus-shaped nanospheres that enhanced self-cleaning and hydrophobicity. The printed membranes with varying pore size exhibited tunable flux and good oil-water separation efficiency. The membranes were found to have over 99% separation efficiency of various oil-water mixtures and maintained a 60,000 LMH flux. While comparing to other oil-water separation membranes made by different materials and techniques, this FDM printed PLA membrane exhibited extremely high flux, lower cost, strong mechanical durability, and chemical tolerance.

5.1.2. DIW printed membranes

Lv et al. [105] reported the use of DIW technique in printing superhydrophobic nanosilica reinforced polydimethylsiloxane (PDMS) oil-water separation membrane. The PDMS-nanosilica ink was extruded from a computer controlled micronozzle and the filament was printed on a glass substrate layer by layer, as shown in Fig. 4 (b). The pore size of the membrane was precisely controlled by adjusting the filament spacing. Printing this mesh structure helps avoid the weak interfacial adhesion with conventional superhydrophobic membranes coated on the mesh structure. The rheology data showed that printed membrane reinforced with silica exhibited excellent storage modulus and loss modulus at different shear stress. More importantly, the reasonable mechanical strength and chemical robustness guaranteed the membrane's long-term stability in harsh acidic or alkaline conditions. The authors were also able to adjust the flux and oil-water separation efficiency by tuning the pore size of the printed structure. The membrane with 0.37 mm pore size was able to provide a 99% oil-water selectivity while maintaining a 23,700 LMH flux.

Li et al. [107] demonstrated the DIW process of superhydrophilic CA/PVA/Si composite oil-water separation membrane. The PVA and SiO_2 nanoparticles (NPs) were added to the CA ink to enhance the hydrophilicity. The composite ink was extruded from a nozzle onto a glass slide based on the designed structure with precisely controlled pore size. The printed membranes with higher SiO_2 NPs loading exhibited much lower water contact angle than membranes without SiO_2 NPs. By tuning the filament spacing, the authors were able to adjust membrane pore size that induced difference in water flux and separation efficiency of various oil-water mixtures. Membranes with small pores (175 μm) maintained over 99% separation efficiency with 3×10^5 LMH water flux. The authors observed stable separation efficiency under harsh conditions such as low and high pH, strong sonication and multiple bending cycles. These membranes also possessed strong anti-oil fouling ability after several testing cycles.

He et al. [108] used DIW to prepare carbon nitride–based hybrid aerogel membranes and found the membrane structure exhibited high solar wastewater remediation performance. The 3D printing and post-processng process are illustrated in Fig. 5 (a). The building block g-C_3N_4 nanosheets (CNNS) loaded with Au nanobipyramids were mixed with sodium alginate (SA) to form the ink, which was subsequently printed by a nozzle to directly write the pattern via three different routes, directly in air, in $CaCl_2$/glycerol condition or on the Pluronic F127 supporting matrix that induced reversible fluid-to-gel transition. The printed structure was then crosslinked in $CaCl_2$ and dried in CO_2 to form the aerogel. The optical image showed that membranes printed in the Pluronic F127 matrix displayed highest resolution and integrity among the membranes printed via three routes. The authors also characterized solar wastewater remediation performance by evaluating the dye degradation under UV-VIS. The printed hybrid aerogel membranes displayed 93% photodegradation with Methyl Blue (MB) within 60 min with a 2.5 times higher rate constant than pure CNNS. The hybrid aerogel also exhibited no loss in photodegradation activity after 3 cycles. This is attributed to the unique geometry, high surface area and, porous structure.

The DIW technique can also be used for patterning specific structures

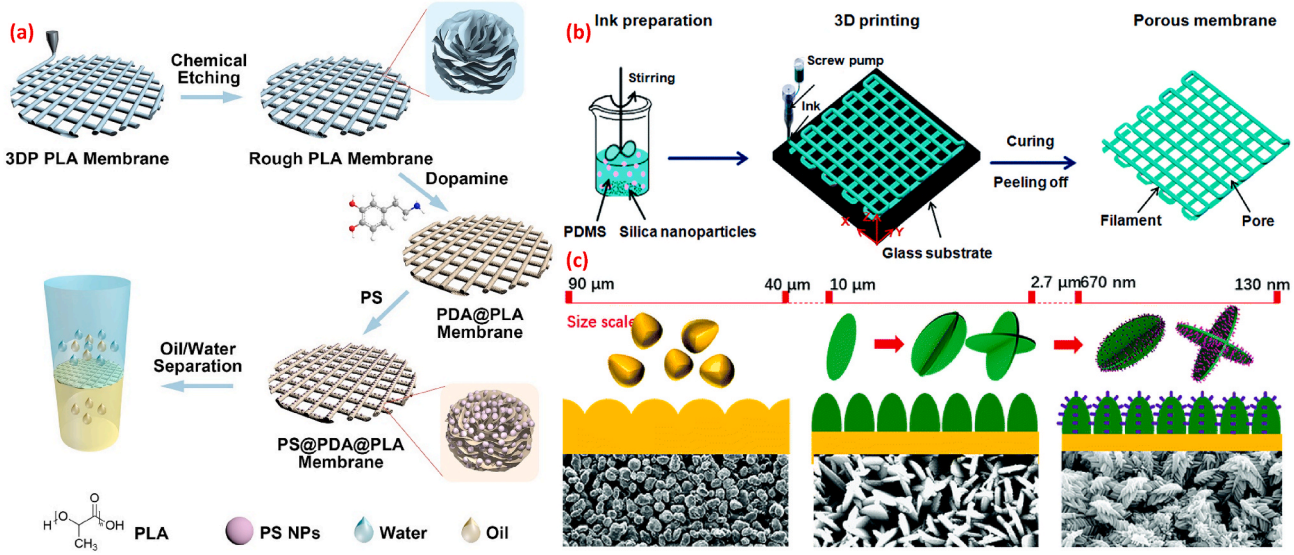

Fig. 4. Some examples of 3D printed oil-water separation membranes: (a) FDM printed PLA superhydrophobic membranes decorated by polystyrene lotus-leaf structure, adapted from [104]; (b) DIW printed PDMS-nanosilica superhydrophobic membrane, adapted from [105]; (c) SLS printed polyamide membrane coated by hierarchical micro/nanostructural ZIF-L layers, adapted from [106].

on membranes to improve membrane flux and antifouling properties. Lyu et al. [109] printed lined patterns on ceramic membranes that showed superior antifouling performance for wastewater treatment. The layer-by-layer coating of the alumina middle layer, 3D printing process, and the morphology of the surface patterns are illustrated in Fig. 5 (b). The Al_2O_3 powder and the binder were first made into suspension ink and then coated onto the support membrane via spin coating and dip coating. After the membranes were formed, the same ink was printed onto the membrane to form the desired lined pattern. The comparison of water flux showed little difference between patterned and unpatterned membranes in dead end mode but higher flux using the patterned membranes in crossflow mode. They demonstrated that the flux was not impacted by the flow direction relative to the patterned lines in the crossflow test. In the fouling test, the printed membranes showed much better antifouling performance than the unpatterned membranes, which had a flux loss of approximately 80% in 30 min. In addition, the flow direction to the patterned lines could also impact the antifouling performance as the perpendicular feed flow direction displayed 47% flux loss while parallel direction has 55% loss. This is due to the stronger vortices formed in the valley areas when the lines were place

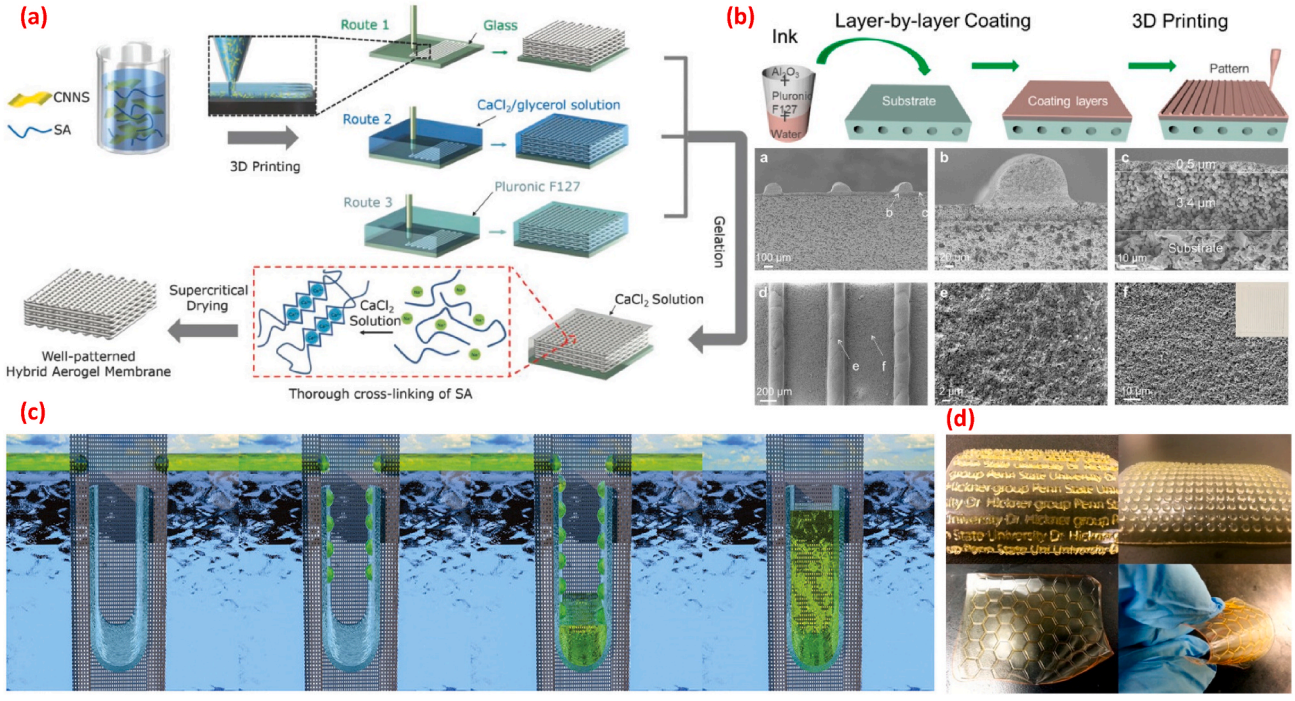

Fig. 5. (a) patterned carbon nitride–based hybrid aerogel membranes via DIW and post crosslinking for broadband solar wastewater remediation, adapted from [108]; (b) DIW printed surface-patterned ceramic membrane with fouling mitigation for wastewater treatment, adapted from [109]; (c) Print-on-demand superhydrophobic/oleophilic membrane and its robotic oil recycling process, adapted from [110]; (d) DLP printed micropatterned anion exchange membrane, adapted from [111].

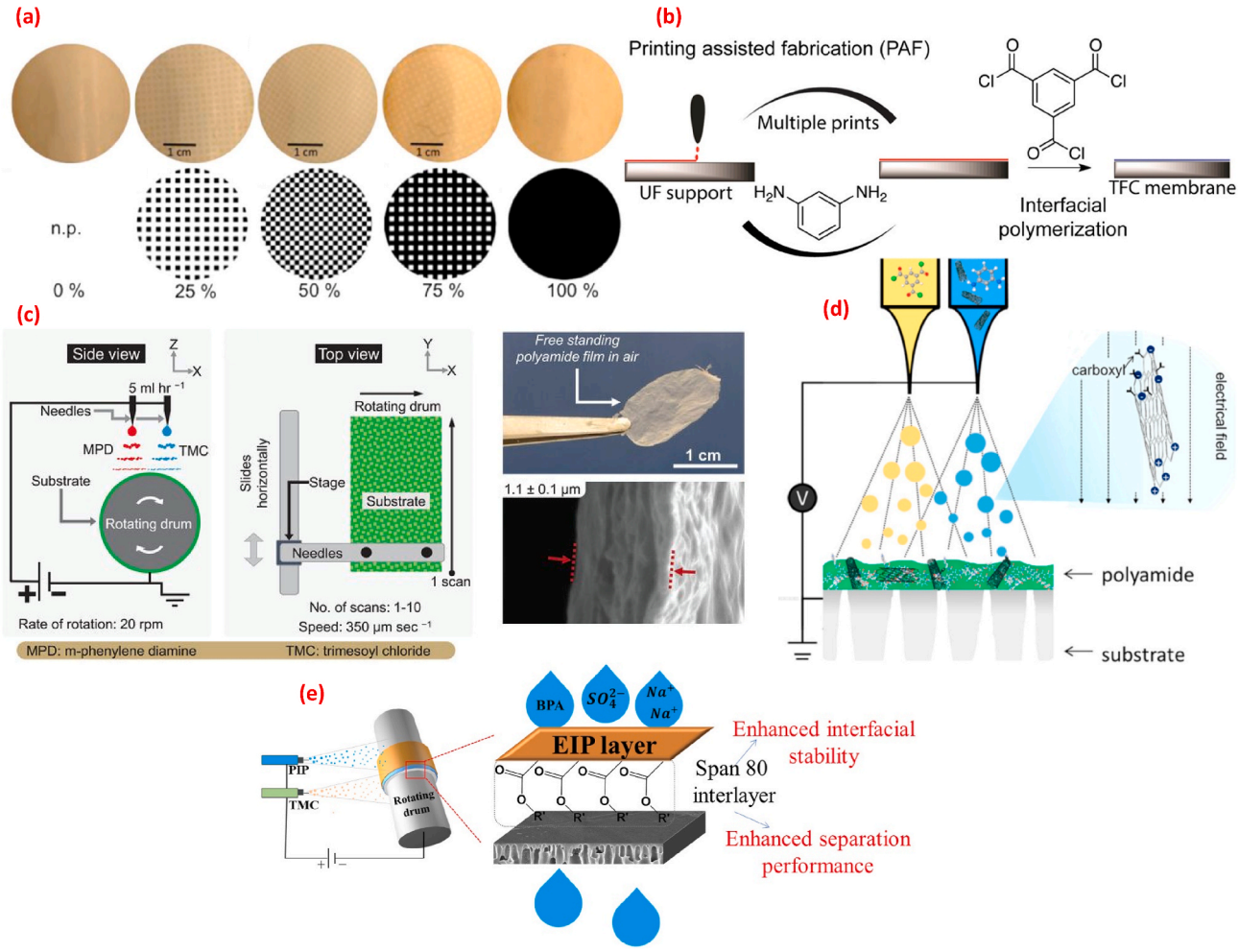

Fig. 6. Examples of 3D printed polyamide TFC membranes: (a) IJP printed various fluorinated amine surface patterns on the MPD impregnated support, which was then immersed in TMC solution to conduct IP. The lower set of pictures show the computer generated patterns used for 3D printing, adapted from [124]; (b) IJP printed MPD aqueous solution on the substrate, which was then immersed in TMC solution to conduct IP, adapted from [125]; (c) ESP printed thickness controllable and free-standing polyamide selective layer, adapted from [126]; (d) ESP printed polyamide-COOH functionalized CNT mixed matrix membranes, adapted from [54]; (e) ESP printed polyamide NF selective layer on top of a Span 80 interlayer, adapted from [127].

perpendicular to the feed flow. This was further verified by computational fluid dynamics. The authors optimized the height of the patterned lines (120 μm) and line spacing (500 μm) for best antifouling performance in perpendicular flow direction.

5.1.3. *Solvent-cast printing (SCP) printed membranes*

Conventional FDM/FFF usually requires to melt the polymer and subsequently extrude the molten polymer through a nozzle. Most high-performance thermoplastic materials have high glass transition temperature (T_g) and melting temperature (Tm), which restrict the 3D printing of such materials via ME. FDM/FFF techniques also needs to reshape the polymer pellets into filament form, which may induce mechanical anisotropy in the printed membrane such as defects, welding, die swelling and melt fracture. Therefore, in order to alleviate such restrictions due to its processing requirements, Singh et al. [112] proposed a novel SCP technique that prints the polymer solution onto the glass substrate and where the solvent subsequently evaporates. This technique was able to print any polymers regardless of the T_m. The authors studied the printing process of poly (benzimidazole) (PBI), which has almost the highest Tg among all the polymers. They proved its printability by SCP due to the high mechanical properties exhibited by the PBI film. The authors also compared the mechanical performance of same film printed via SCP and FFF and found out the SCP printed film showed higher plasticity, lower internal stress, stronger interlayer bonding and higher mechanical isotropy. Therefore, this paper reported a facile approach that could print most polymeric materials with better mechanical properties and higher resolution.

To summarize, ME has been widely used in printing mesh-like membrane structures composed of filaments, which are subjected to postprocessing such as surface modification or crosslinking. These membranes are usually printed with fine features and shapes ideal for porous materials providing oil-water separation with high flux and separation efficiency due to their superior surface properties after surface modification. However, restriction on resolution makes it difficult to form submicron level pores that may further improve separation efficiency. The problem of limited resolution also narrows the use of ME in that it could only be used for forming filaments and membrane surface pattern rather than a thickness controlled coating layer. Another restriction is the requirement on material printability that narrows material selection. In FDM, the high temperature difference between printed filaments may induce interlaminar thermal stress between filaments that will further show deformation, low resolution, weak interfacial bonding and a rough surface. In DIW, if the ink has high surface energy and low shape retention ability, the extruded filaments may undergo collapsing or deformation due to gravity. More viscous ink such as high concentration CNT ink can provide better mechanical performance and surface energy, but a majority of such inks are difficult to extrude and can easily clog the nozzle. What must be clearly articulated,

though, is the value proposition of printing porous membranes when porous membranes are already castable from relatively low cost materials and at production speeds that have driven their costs down. Clear cost or performance benefits relative to existing MF technology have not yet been firmly demonstrated.

5.2. PBF/SLS printed membranes

Other printed oil-water separation membranes have been reported as being made by SLS. The first SLS printed membrane was reported by Yuan et al. [113]. The authors were in particular attempting to make nylon-12 MF membranes in a solvent free manner. In order to investigate the impact of processing conditions on membrane separation behavior, they sintered polyamide-12 powder in an SLS printer using different laser power, hatch spacing, and laser scan count. They discovered that a membrane printed using higher energy density (higher laser power, smaller hatch spacing and more counts) had smaller pores and denser structure. Therefore, these membranes displayed lower water flux and generally higher tensile strength and higher rejection. Based on this optimization in the printing condition, the authors published another paper [114] that modified the polyamide-12 powder with candle soot in order to make an oil-water separation membrane. The membranes were printed by sintering candle soot coated polyamide-12 powder, which was prepared by solvent evaporation of the powder mixture-hexane solution. They also studied the influence of processing conditions (laser power and hatch spacing) on the hydrophobicity, porosity, gravity driven flux and tensile strength of the 3D printed membranes. The membranes exhibited stable hydrophobicity and mechanical performance under harsh conditions such as being treated with various harsh organic solvents for long time, sonicated or abraded by sand paper. This indicated the potential of this membrane in organic mixture separation. The membranes also demonstrated an over 99% hexane-water separation efficiency with reasonable flux between 3300 LMH and 6700 LMH.

The same group also demonstrated high oil-water separation performance of SLS printed polyamide membranes coated with leaf-crossed and flower-like micro/nanoscale zeolitic imidazolate framework (ZIF-L) layer [106], as shown in Fig. 4 (c). The printed polyamide membranes were immersed in the solution where the synthesis of ZIF-L was conducted. The polyamide membranes coated with multiscale ZIF-L exhibited superhydrophilicity and underwater superoleophobicity after being wetted with water. While the polyamide-ZIF membranes were coated with PDMS, the membrane showed extreme superhydrophobicity and superoleophilicity. Different oil (hexane, petroleum ether, heptane and mineral oil) were used to test the oil-water separation performance. These membranes showed excellent oil flux of 24,000 LMH and over 99% oil rejection for all the oil-water mixtures.

In order to broaden the application of SLS in printing different membrane materials, they proposed the use of this technique for a candle soot coated PSF membranes [115]. Pristine PSU powder was sintered by a CO_2 laser in a powder bed. The authors optimized the laser power, hatch spacing and laser scan in SLS process by comparing the porosity, water permeance, mechanical properties and water contact angle of pristine PSU membranes printed under different condition parameters. They subsequently coated the candle soot on the optimum PSU membrane by immersing it in the sonicated candle soot solution. The authors conducted oil-water separation test by testing the separation efficiency in different oil (hexane, petroleum ether, heptane and mineral oil)-water mixture. They found the membrane exhibited high gravity driven oil flux of 19,000 LMH and a 99% separation efficiency for all these oil-water mixtures. This membrane also demonstrated its stable separation efficiency in the 10-cycle hexane-water separation test.

SLS is able to print the base layer or the matrix of oil-water separation membranes. The superhydrophobicity-oleophilicity needs to be achieved by either mixing the polymer powder with hydrophobic candle soot or depositing a layer of hydrophobic ZIF or candle soot on the base layer surface. Compared with the mesh-shaped oil-water separation membranes printed by ME, SLS printed membranes exhibit lower gravity-driven oil flux and similar separation efficiency. This is mainly attributed to the much higher pore size of the mesh-structured membrane (above 100 μm) compared with the pore size of a printed polyamide base layer (10–15 μm).

5.3. VP printed membranes

5.3.1. SLA/DLP printed membranes

Ray et al. [116] implemented the novel solvent based slurry stereolithography (3S) technique in fabricating hydrophilic UF ceramic membranes. Unlike traditional SLA, 3S combines photopolymerzation, thermal debinding and sintering to process the slurry material. In this work, the authors mixed photopolymer resin, Al powder, solvent, dye and dispersant to form the slurry material. The slurry was first printed layer by layer, and cured by a DLP projector to form the green part. The green part was subsequently debound when the temperature was raised to 600 °C in a heating chamber in order to burn off the binder. Then the temperature was elevated extremely slowly to 1100 °C in order to sinter the material. During the sintering step the ceramic powder would fill in the gaps left by the binder material and form the ceramic membrane. The content of Al in the membrane was found to be approximately 50% after 3S printing. The authors observed the membrane pore size ranging from 7.9 to 9.8 nm while a small sized Al powder was used. The membrane had 225–230 μm thickness and a surface roughness of 0.17–0.18 μm. The water contact angle was observed to be 32–33°.

Li et al. [110] proposed the use of print-on-demand technique to fabricate tubular graphene-nickel foam composite membrane for oil-water separation. The authors placed polyimide films on top of the nickel foam as the precursor material. This 3D printing technique was based on SLA that employed a laser beam to photochemically convert the aromatic rings of polyimide molecule into graphene. The membrane was then assembled into a self-floating superhydrophobic/oleophilic oil recycling device that was able to collect the oil on water surfaces. The oil-recycling process of the self-floating device is shown in Fig. 5 (c). This device was tested to be reusable and could still take up oil after 10 cycles.

In 2019, Capparelli et al. [98] published a paper that reported the use of SLA in printing patterned anion exchange membranes (AEMs). Micropatterns has been demonstrated to improve the surface properties such as mixing and lower resistance of AEMs. The authors printed the cross-linked diurethane dimethacrylate (DUDMA) -co- poly(ethylene glycol) diacrylate (PEGDA) -co- vinylbenzyl chloride (VBC) membranes by photocuring a resin mixture consisting two oligomers, a crosslinker and a quaternization precursor. The surface patterns were created by applying additional resins in designated areas, which were subsequently cured by a digital light source. They were able to control the pattern-base area ratio and the pattern design on the membrane surface, allowing the study of their influence on membrane properties. The ion resistance was found to be relevant to pattern-base ratio and curing time but independent of pattern design. The permselectivity and water uptake were found to be independent of both pattern-base ratio and surface design. However, pattern bleeding resulted from low accuracy was observed in the scanning electron microscope (SEM) images of the printed membranes. This could induce deviation in the pattern shape and pattern-base ratio, which was subsequently corrected in order to improve accuracy of the measurement. Therefore, SLA was proved to be able to print membrane surface patterns and provide functional membranes. However, the accuracy of this technique is still low to precisely form the desired pattern shape. The same research group used a custom photolithographic setup to print photocurable materials into patterned AEMs [111]. This setup was composed of a digital projector, converging lens, a front-surface mirror, a glass substrate. This setup was similar to the printing apparatus used in previous work [117,118]. The photopolymer resin mixture was cast on the glass substrate with a controllable

thickness and was subsequently exposed to the digital pattern for curing. The morphology of the DLP printed surface patterns is presented in Fig. 5 (d). A base layer of 250 μm was created and the pattern was formed on the based layer by curing additional photopolymer materials. The authors found consistent permselectivity on the printed membranes with general AEMs, suggesting the success in making AEMs via DLP. The authors also observed lower ionic resistance on the patterned membrane compared with other flat AEMs with equivalent effective thickness. This was explained by the parallel resistance model that explored the resistance-thickness relationship to compare the flat and patterned membranes. This model also provided an insight of the amount of material needed for patterning to reach the maximum ionic resistance.

5.3.2. TPP printed membranes

Linkhorst et al. [119] printed hard colloidal 3D crystals membrane template via a TPP printer and studied the morphology and the particle distribution in the filter cake. The membrane was composed of size-adjustable crystal spheres that aligned with each other. The filter cake was formed by flushing an aqueous suspension of spherical core-shell microgels on the membrane. The authors demonstrated the microgels formed crystallites following the angle of the template, which indicates tuning membrane template via 3D printing was able to manipulate the filter cake orientation. The authors also precisely visualized the filter cake compaction towards the template surface and measured the distance between particles in the filter cake both at natural and compressed state.

5.3.3. CLIP printed membranes

In 2015, Mecham reported the potential of using CLIP in printing liquid and gas separation membranes in North American Membrane Society conference [120]. In this presentation the group demonstrated the ability of this technique to continuously print a variety of membrane materials rather than conventional layer by layer printing techniques. They also addressed the permeance and selectivity performance of membrane printed by CLIP. Although till now there has not been any work that successfully produced CLIP printed membranes, porous membranes have played a significant role in the CLIP process, especially when functioning as the oxygen permeation window. Lin et al. [121] proposed the use of a porous track-etched membranes. The pore size of this track-etched polyethylene terephthalate (PET) film could be precisely controlled so that the oxygen permeation was maximized. The membrane was placed at the bottom of the liquid resin pool, allowing oxygen to permeate through the membrane and form the inhibition layer between the membrane and liquid resin. Due to the high permeability of the track-etched membrane, CLIP printer could achieve the maximum printing speed, which was always the most challenging limitation on CLIP. The track-etched membrane also realized this continuous printing process by only using air rather than pure oxygen.

Conventional CLIP process has suffered from the drawback of slow resin refilling speed, which induced problems such as low printing speed and defects in the cured parts. Wang et al. [122] proposed a composite layer comprising a nano-textured PDMS contact layer and a polymer oxygen-permeable membrane to function as the oxygen permeation window. The nano-textured PDMS layer was located between the resin pool and the porous membrane. The introduction of the PDMS layer was able to double the resin refilling speed and reduce the printing time by 25%. This composite layer could also reduce the vacuum caused by slow resin refilling and realize 3D printing large cross section areas.

VP has not been extensively used in printing membranes due to its limited resolution, accuracy and narrow material compatibility. Based on the SEM images showing pattern bleeding indicated in [98], the dimensional deviation of the printed pattern is above micron level. Therefore, it is extremely difficult to print submicron level NF and RO membranes via VP. Additionally, most photopolymers are thermoset with strong hydrophobicity, which may be ideal for oil-water separation but will induce low water flux in liquid filtration. The strong chemical robustness of most thermoset polymers could also guarantee their long-term performance in highly aggressive organic solvent. According to the preliminary work on ion exchange membranes [98,111], VP is able to print membranes with low ion resistance and decent ion exchange capacity. Most VP methods such as DLP and SLA can provide controllable curing of the membrane that can prevent swelling in most ion exchange applications. Many potential ion exchange resins, such as various crosslinked polystyrenes, have shown great potential in electrodialysis and membrane fuel cell applications. However, none of these polystyrene resins has been photopolymerized as ion exchange membranes.

5.4. MJ printed membranes

5.4.1. IJP printed membranes

Inkjet printing has been a key technology in membrane fabrication and functionalization as it significantly reduces the quantity of materials used compared to other conventional techniques such as IP, casting and dip coating. This printing process has been regarded as yielding less footprint and reducing membrane production cost. Since most inkjet-printed membranes are polymer based, the most crucial factor of material printability lies in the surface tension and the viscosity of the polymer ink. Gans et al. [123] published a review article that illustrated the application of inkjet-printed polymer and their printability requirements. The most challenging issue during polymer IJP is the strain hardening that displayed a 'bead-on-string' structure rather than continuous ink droplets. This strain hardening phenomena was primarily attributed to the high Mw (high viscosity) of the polymer ink and high elongation rate. Therefore, IJP imposes a restriction on selection of printable polymers and their molecular weight should not exceed the maximum Mw (approximately 100,000 g/mol) to prevent strain hardening.

The first 3D printed polyamide TFC membrane was proposed by Badalov et al. [124] via IJP technique. The authors printed fluorinated amine on PSF20 support in order to increase the hydrophobicity of the selective layer. The PSF support was first cleaned and immersed in pristine MPD solution. The excess solution was then removed from the impregnated support, which was subsequently loaded onto the inkjet printer. The fluorinated amine solution was printed on the membrane surface to form specific patterns based on the computer design. The membrane was then treated with TMC solution to finish the IP process. The printed surface pattern with a variety of coverages are shown in Fig. 6 (a). Since the printed droplet size was measure be ~15 μm, the authors were able to print specific patterns as designed on the membrane surface and precisely control the fluorinated area coverage. The highly fluorinated membrane exhibited similar water permeance as unfluorinated interfacial polymerized control membrane but showed 98% NaCl rejection compared to the 93% rejection of the control membrane.

The same research group later demonstrated controllable printing of polyamide selective layer via inkjet printing MPD aqueous solution in another paper [125]. The printing and subsequent IP processes are illustrated in Fig. 6 (b). The PES UF support was first wetted with DI water and then printed with 2.5% w/v MPD aqueous solution for different printing layers in order to vary the selective layer thickness and crosslinking density. The membrane was subsequently treated by TMC solution following the same procedure used in IP. XPS results indicated that membranes with more printing layers displayed higher crosslinking degree, together with higher surface hydrophobicity as revealed by contact angle results. It was also illustrated that increasing printing layers could induce a membrane with lower water permeance and higher NaCl rejection. From the permeance and rejection data it showed that a membrane made by IP shows higher permeance and rejection than most inkjet printed membranes, which is likely attributed to the low resolution of this inkjet printing technique in depositing the aqueous MPD droplets.

Numerous studies have been focused on membrane modification through inkjet printing. Bernstain et al. [128] for the first time demonstrated efficient printing assisted modification on UF support by inkjet grafting SPE polymeric layer. The SPE monomer was first printed on the support and then irradiated by UV light to finish the surface grafting. Surface modification by conventional methods such as dip coating usually had significant impact on membrane permeance and selectivity. Membrane modified by inkjet printing showed a very small decline in permeance and a slight change in molecular weight cutoff (MWCO). The introduction of the grafted layer induced higher protein fouling resistance and slower biofilm growth while being exposed to bacteria.

Commercial TFC RO membranes has been previously demonstrated to exhibit substantially higher FO osmotic flux while being modified with PDA [129]. Membrane surface modification by mussel-inspired PDA is also an attractive research topic due to its superior antifouling ability. However, due to the high cost of dopamine, its relatively long polymerization time, and its wasteful nature attributed to dip coating, conventional PDA coating may not be ideal. Li et al. [130] deposited PDA onto PP support by inkjet printing the dopamine (DA) monomer solution and sodium periodate (SP) solution simultaneously from two individual cartridges, as shown in Fig. 7 (a). Inkjet printing could precisely control the amount, ratio and the deposition location of materials, which was found to greatly enhance the rate of PDA polymerization. Authors found the membrane wettability was sharply improved after the formation of printed PDA-SP. The printed membrane also showed enhanced flux and antifouling performance, together with a long-term stability while exposed to a variety of pH conditions. The same group also demonstrated the use of IJP in 3D printing oil-water separation membranes. Polyphenol-based coating has been suffering from inefficient processing procedure although it was regarded as an ideal candidate for membrane surface functionalization. Li et al. [131] published a paper that first employed IJP to coat the polyphenols layer (catechol or tannic acid (TA)) on PVDF membrane surface, as illustrated in Fig. 7 (b). A pattern of catechol acid or TA was first printed for one layer on the PVDF membrane and another layer of SP was printed on top of the polyphenols for oxidization. The oxidized polyphenol was found to show improved surface hydrophilicity than the pristine PVDF membrane. The printed membrane also exhibited a 99% oil-water separation efficiency and a 5.2 times higher water permeance than the pristine PVDF membrane. The printed membrane also demonstrated decent stability under long-term acidic conditions.

There are many other studies that introduced nanofillers onto membrane surface via inkjet printing. Lee et al. [134] reported the deposition of silver nanoparticles (AgNPs) onto electrospun polyurethane (PU) fibrous membrane by a commercial inkjet printer. The printing of the AgNPs did not significantly change the thickness of the membrane although the weight content of the nanofiller was observed to be approximately 23.8 wt%. This AgNPs modified membrane was found to have strong antimicrobial behavior. Fathizadeh et al. [135] successfully printed ultra-thin graphene oxide (GO) layer on NaOH modified PAN support using inkjet printing. The printing time and GO ink concentration was control so that the thickness of the selective layer could be precisely adjusted. This study demonstrated that inkjet printing could reach selective layer thickness as low as 7.5 nm with reasonable water permeance and dye rejection. The thinnest membrane (7.5 nm) yielded

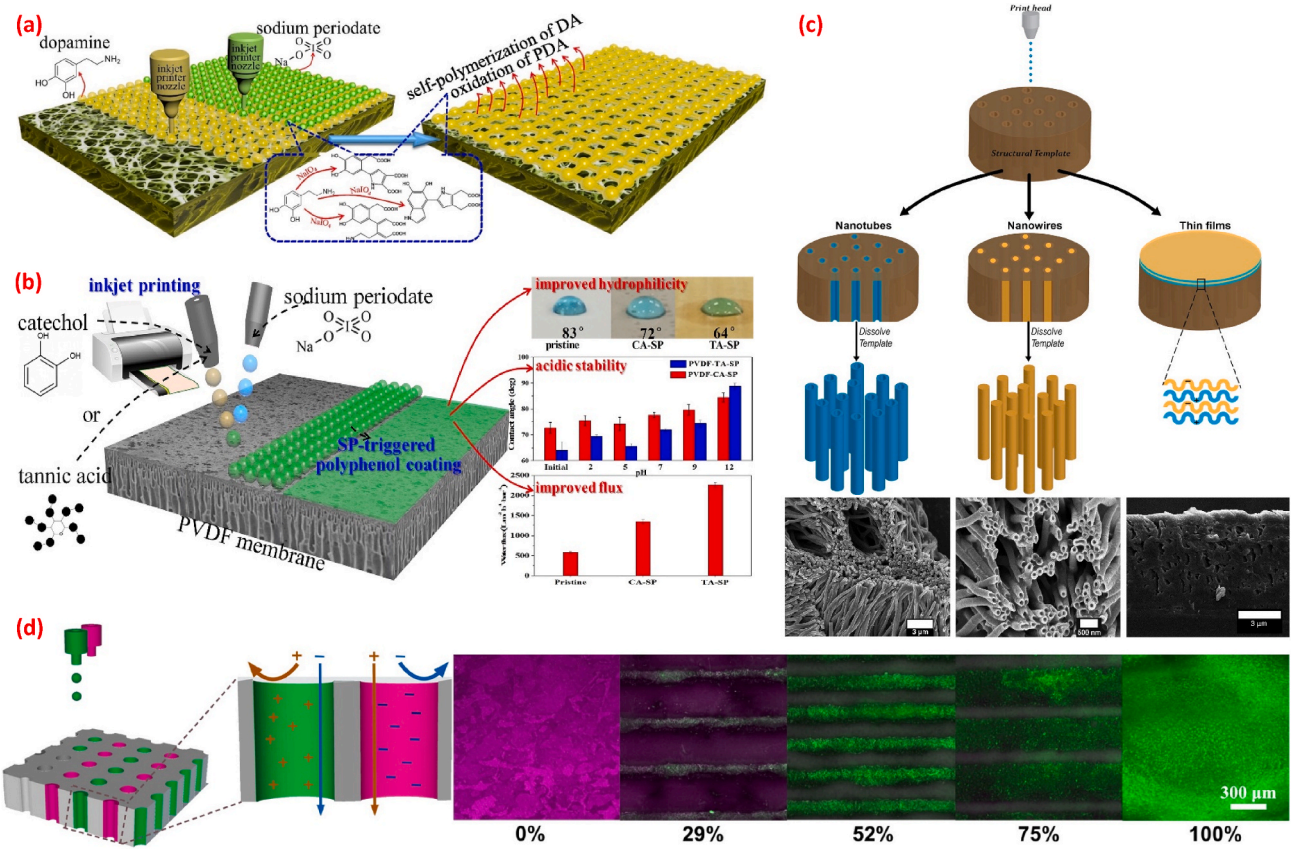

Fig. 7. (a) IJP of dopamine and oxidant sodium periodate to form PDA antifouling layer, adapted from [130]; (b) IJP of polyphenol hydrophilic oil-water separating layer, adapted from [131]; (c) IJP with template synthesis. From left to right: polyelectrolyte nanotubes by printing PAH and PSS alternately on a PCTE membrane template, PVA nanowires printed on a PCTE membrane template, formation of LbL thin films on top of a PCTE membrane by printing alternating layers of PAH and PSS, adapted from [132]; (d) left: charged mosaic membrane by printing poly(diallyldimethylammonium chloride) (PDADMAC) and poly(sodium 4-styrenesulfonate) (PSS) polyelectrolytes respectively on the PCTE template; right: fluorescent micrographs of membranes with areal fractions of the positively charged domain from 0 to 100% by printing stripes of various width, adapted from [133].

over 80 LMH/bar water permeace and the 60 nm membrane reached 96.7% Methyl Orange (MO) rejection. The authors conducted dye rejection test on dyes with varying size and charge and found that this membrane showed sized based rejection, 10 times higher dye rejection than commercial NF membranes, stable permeance and rejection while removing pharmaceutical contaminants.

Gao et al. [132] demonstrated the application of inkjet printing in fabricating patterned nanostructured polymeric membranes. They explored the possibility of printing a variety of functional polymers layer by layer on a tracked etched polycarbonate (PCTE) membrane to form the nanostructures. For example, bilayers of poly(allylamine hydrochloride) (PAH) and poly(styrenesulfonate) (PSS) with fixed MWCO could be printed either as nanotubes on the pore wall or as a TFC selective layer on the surface of the PCTE membranes. Poly(vinyl alcohol) (PVA) aqueous solution could also be printed to fill the pores of the PCTE membranes and form nanotubes or nanowires. They also succeeded in forming patterned LBL structures by printing a fluorescent polymer (FITC-PAH) on the PCTE membranes. The formation of these structures are shown in Fig. 7 (c). These nanostructured membranes exhibited reasonable water permeability, streaming current of the nanotubes, and high water permeance with comparable salt rejection of the TFC selective layer. Furthermore, in their recent work [133] they demonstrated the application of this technique in forming charge mosaic membranes, as presented in Fig. 7 (d). Here they printed two charged polyelectrolytes individually on the PCTE membranes and successfully formed distinct cationic and anionic domains (stripes) within the membrane pores as nanowires. Therefore, dissolved salts could be transported more rapidly through this membrane structure than neutral/water molecules. They also demonstrated that the transport properties of the membrane could be adjusted by tuning the width of the printed polyelectrolytes stripes. This work is an indication to the future of selective transport of ionic solutes.

IJP can be used to print functionalized yeast cells as the selective layer of biocatalytic membranes (BCMs) due to its ability to catalyze the degradation of persistent micropollutants. Chen et al. [136] proposed the fabrication of BCMs by printing yeast cells containing surface displayed laccase (SDL) biocatalyst onto PSF MF membrane substrate. PVA powder and 4 mL yeast cell solution with varying cell concentration was made into 1 wt% PVA-yeast cell aqueous ink and was subsequently printed on the MF substrate via IJP. After 3D printing the PVA was crosslinked to form the selective layer. The enzymatic activities of BCMs was found to increase with higher cell concentration and printing layers. The membranes were observed with decent stability in enzyme activity when tested in repeated ABTS oxidation reaction cycles for as long as 20 days. As a comparison, the SDL cells showed declined enzyme activity while tested in the same condition. In wastewater micropollutant removal tests, compared to SDL cells the printed membranes displayed improved bisphenol A (BPA) degradation efficiency and similar acetaminophen (APAP) degradation efficiency. Therefore, this work successfully demonstrated the effectiveness of incorporation of SDL cells to BCMs in treating emerging contaminants in membrane-based separation.

IJP has also been demonstrated as a promising technique in printing ion exchange membranes for membrane electrode assemblies (MEAs). Yazdanpour et al. [137] used IJP to print Pt/MWCNTs ink as catalyst on Nafion substrate for the electrodes. They found out MEAs printed via catalyst-coated membrane (CCM) method showed better cell performance than conventionally made cells. In another work Klingele et al. [138] applied drop-on-demand IJP method to print Nafion membrane onto MEAs. The thickness of the Nafion layer could be significantly reduced, which resulted in very low membrane resistance. This printed MEA also exhibited one of the highest power density among all the Nafion membrane fuel cells. This MEA was also cost saving not only due to savings on material but also because it had high power density and could operate well under dry condition to avoid the use of humidifier. The authors also found out this membrane exhibited a promising lifetime under aggressive mechanical and chemical conditions.

5.4.2. ESP printed membranes

ESP has been a particularly attractive AM approach for making membranes. A key point of this technique is that it offers very fine control of thickness but can also deposit either polymers or monomers to form polymers into a film upon deposition. This makes ESP especially valuable in making TFC membranes. ESP has been used to make polyamide TFC membranes, PVA TFC membranes, molecularly imprinted membranes, ceramic membranes, metal organic frameworks (MOF) membranes and ion exchange membranes.

One of the more exciting opportunities to use ESP is in the printing of TFC membranes that are used for RO and NF. As shown in Fig. 6 (c), both Chowdhury et al. [126] and Ma et al. [139] used a drum based 3D printer to synthesis polyamide selective layer by spraying MPD aqueous and TMC-Hexane solution separately. The electrospray setup and the printed free-standing polyamide selective layer are presented in Fig. 6 (c). The support layer is fixed on the rotating drum to collect the spray of monomer solutions. The polymerization was triggered when the spray of one monomer overlaps with the other monomer deposited on the support. Table compares the spray and solution conditions used in these two papers. In Chowdhury's work, a lipophilic ionic liquid was added into TMC/hexane solution at 1 μL/mL to achieve cone-jet spray pattern between 4 and 7 kV. Both work indicated that 3D printed Polyamide membranes display high resolution and precise thickness control of 4 nm/printing layer in Chowdhury's work and a 1 nm/min film growth in Ma's work. Chowdhury also electrosprayed the polyamide selective layer on different substrates and found the polyamide thickness was independent of substrate material. In terms of roughness control, Chowdhury was able to limit the surface roughness to around 4 nm and Ma's Polyamide membranes exhibited an average surface roughness (Ra) of 1.2 $\pm$ 0.2 nm. Both membranes were much smoother than the interfacial polymerized polyamide membranes with ridge and valley morphology and a Ra value of 58 $\pm$ 2 nm [139]. The desalination performance of these printed membranes were also observed to be controllable and comparable with commercial polyamide membranes.

The same group also introduced CNT nanofiller in the electrosprayed polyamide TFC membranes [54] and found out remarkable improvement in membrane permeance without impacting salt rejection. Here the authors used lower monomer solution concentration to print polyamide-CNTs NF membrane with the same electrospray setup used in the previous study, as shown in Fig. 6 (d). The TEM thickness measurement indicated that the introduction of CNTs did not affect the polyamide selective layer growth rate. The polyamide-CNTs membranes showed 6-fold enhancement in water permeance without loss in salt rejection. This nanofiller incorporated NF membrane showed much higher water flux but lower salt rejection than commercial NF270 and NF90 membranes.

Tang's group also explored the use of electrospray in printing polyamide NF membranes with PIP aqueous solution and TMC/hexane-acetone solution [127]. The printing process and parameters were similar to those in the electrospray process of polyamide RO membranes, as shown in Fig. 6 (e). Compared to other commercial NF membrane and lab-made polyamide membrane by IP, the electrosprayed membranes exhibited tremendous improvement in water permeance with only minor loss in Na_2SO_4 rejection. Similar to the polyamide RO membranes, they also succeeded in tuning the NF membrane's water permeance and salt rejection by controlling the PIP concentration and electrospray time. In order to further enhance the interfacial stability between the polyamide selective layer and support layer, a Span 80 interlayer was introduced to form a composite membrane. Compared to polyamide NF membranes this membrane displayed smoother polyamide surface, higher surface hydrophilicity, enhanced anti-backwash ability and BPA removal efficiency.

Other studies report using ESP in forming other polymeric TFC membranes. Wang et al. [140] demonstrate a "living" electrospray

technique in making PDA membranes, as illustrated in Fig. 8 (a). Here the authors sprayed the dopamine aqueous solution onto PES substrate via ESP. Since the polymerization rate of dopamine largely depends on the oxygen in the air, the rate of polymerization was significantly enhanced due to the high surface area of the electrospray droplets and the much higher dopamine concentration in these droplets. Therefore, the authors observed uniform and smooth PDA surface after the fast polymerization provided by ESP. The authors also achieved precise and facile control on the PDA layer thickness by adjusting the ESP time. The PDA membranes showed 87.9% boric acid rejection and high rejection for neutral red and Congo red dyes, suggesting the potential of this membrane's application in textile wastewater purification. In another work, Huang et al. [141] reported the use of ESP in printing PDMS TFC membrane for phenol removal in aqueous-aqueous condition, as shown in Fig. 8 (b). The PDMS-curing agent/hexane solution was electrosprayed on the PVDF substrate and selective thickness was controlled by tuning the electrospray time. The optimal membrane showed an outstanding phenol mass transfer coefficients (k_0) of $37.9 \pm 2.8 \times 10^{-7}$ m/s with over 99.5% salt rejection. These membranes also exhibited long-term stability in k_0 and salt rejection while exposed to strong acid and alkaline conditions. Compared with other PVDF/PDMS nanofibrous membranes, these electrosprayed membranes had similar salt flux but outstanding k_0, which indicated its significance in phenol removal. Qian et al. [142] printed thickness-controllable zwitterionic copolymer selective layer with a thickness well below 50 nm via ESP, as shown in Fig. 8 (c). The ultra-thin selective layer, when supported by a PAN 400 support as NF TFC membrane, exhibited a water permeance up to 180 LMH/bar with full rejection of chlorophyllin. This NF membrane also had a sharp size cutoff at approximately 1.1 nm similar to that of the membrane made by phase inversion using the same material [61].

In additional to the success of ESP in fabricating TFC membranes, Hsiao's group demonstrated the application of this printing technique in forming PVA/PAN thin film nanofibrous composite (TFNC) membranes for low pressure oil-water separation, as shown in Fig. 8 (d) [144]. The PVA layer was formed by electrospraying PVA aqueous solution on the electrospun PAN nanofibrous substrate and the thickness was controlled by adjusting the electrospray time. The PVA was further swollen and chemically crosslinked to form the water-insoluble barrier layer. The authors also optimized water content in the solution used for PVA swelling and the swelling time and found out the crosslinked barrier layer displayed a thickness of roughly 0.5 μm. This TFNC membrane exhibited mechanical robustness and superior separation performance. Under crossflow conditions, the TFNC membrane showed a high water permeance of 173.91 LMH/bar with 99.6% oil-water separation efficiency and anti-fouling performance. In another work [145], this group incorporated oxidized MWCNTs in the PVA barrier layer to form UF TFNC membranes for oil-water separation. The MWCNTs were mixed with PVA powder in the aqueous solution and subsequently electrospun onto the PAN substrate. The incorporation of the oxidized MWCNTs enhanced the membrane water permeance to 340.01 LMH/bar, which reached the UF level. This membrane also maintained 99.5% oil-water separation efficiency and stable mechanical performance. In another paper [143], the same group successfully controlled the crosslinking degree of electrosprayed PVA TFNC membranes, which could function as both NF and UF membranes. The PVA was electrosprayed onto the electrospun PAN substrate following the same procedures illustrated in their previous paper [144]. The PVA was then moisturized and hot pressured into sandwich structure, followed by the chemical crosslinking of PVA barrier layer. The PVA barrier layer after hot press exhibited much lower thickness (300 nm) compared with the swollen PVA layer illustrated in the previous work [144]. Two TFNC with different PVA crosslinking degree was prepared by controlling the crosslinker concentration. The highly crosslinked membranes exhibited decent NF performance with 3.55 LMH/bar water permeance and 91.1% Vitamin B12 rejection. The TFNC membrane with lower PVA crosslinking degree displayed a UF behavior with 57.67 LMH/bar water permeance and 98.4% BSA rejection.

Sueyoshi et al. [148] employed ESP technique to form molecularly imprinted nanofibrous CA membranes. They incorporated glutamic acid in the ESP dope solution so that they were able to achieve both molecular imprinting and ESP deposition simultaneously. The resulting membranes showed great affinity between CA functional groups and the print molecules when a small quantity of print molecules were used. The molecularly imprinted membranes also demonstrated higher permselectivity and flux than the membranes electrosprayed without print molecules. This result indicated that this molecularly imprinted membrane was able to break the trade-off relationship that was observed for most membranes. In another work [149], the same group also

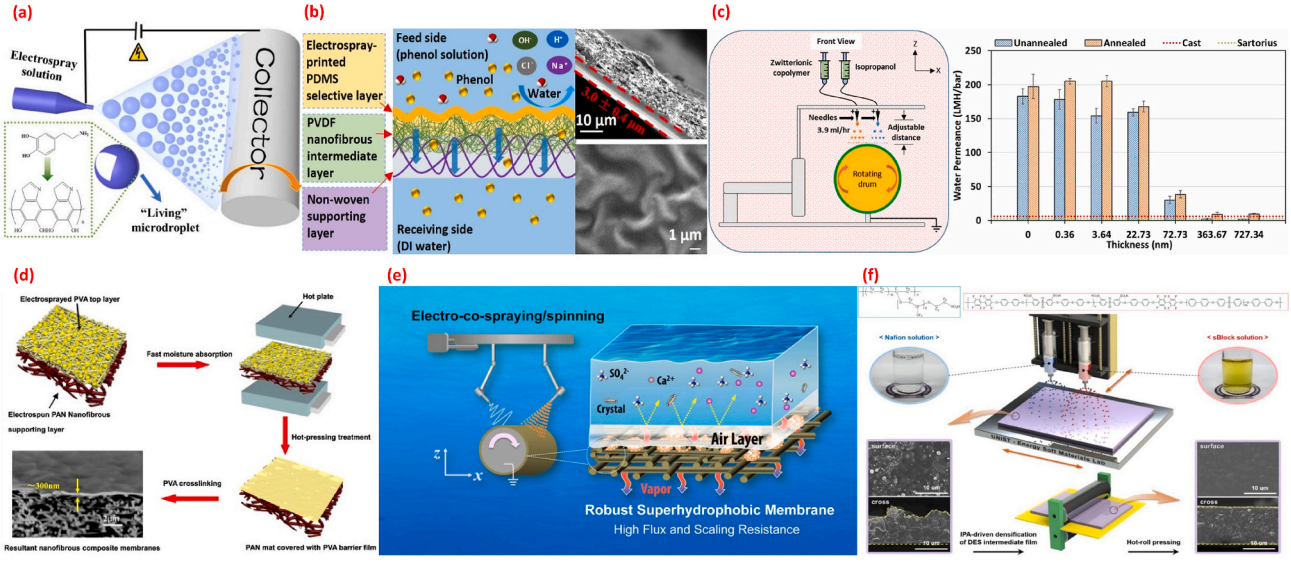

Fig. 8. (a) "living" electrospray for depositing PDA layer, adapted from [140]; (b) three-tiered composite membrane with electrosprayed PDMS selective layer for phenol removal, adapted from [141]; (c) electrospray printing of ultra-thin zwitterionic copolymer NF selective layer with water permeance up to 200 LMH/bar, adapted from [142]; (d) electrospray PVA selective layer on top of electrospun PAN nanofibrous substrate, followed by hot press and PVA crosslinking, adapted from [143–145]; (e) construction of a superhydrophobic MD composite membrane with electrosprayed SiNPs/PVDF-HFP microbeads embedded in electrospun PVDF-HFP fibrous web, adapted from [146]; (f) dual electrospray of Nafion/sBlock blend membranes, adapted from [147].

demonstrated the application of ESP in forming molecularly imprinted PSF-aldehyde nanofiber membranes. This membrane displayed decent chiral separation ability and great enantiomer transport. This electrosprayed membrane also exhibited two orders of magnitude higher flux than conventionally made molecularly imprinted membranes without loss in permselectivity.

ESP is also an effective method in making MOFs membranes. Melgar et al. [150] developed the electrospray printing of ZIF-7 gas separation membranes. Conventional in-situ synthesis of ZIFs membranes are usually time consuming and material-wasting without any scalability control. In this work the authors electrosprayed the ZIFs precursor solution (dissolved in DMF) on a disk-shaped α-alumina substrate. The temperature of the substrate was precisely controlled around the boiling point of DMF in order to avoid both the deposition of dry individual crystals and the penetration of the precursor solution into the substrate. They also achieved precise control of the ZIF-7 membrane thickness by adjusting the amount of precursor solution that was sprayed. The ESP synthesis of ZIF-7 membranes tremendously reduced the processing time under 20min compared with 2–6hrs synthesis time for in-situ or secondary growth methods. Additionally, the electrosprayed ZIF-7 membranes exhibited 4–10 times higher H_2 permeance than conventionally made ZIF-7 membranes. The electrosprayed membranes also exhibited a decent H_2/CO_2 separation factor of 9.6 at 25 °C. In another work [151] the same group used the same technique to print ZIF-8 membranes on the same heated substrate. The resulting ZIF-8 membranes showed decent H_2/CO_2 selectivity and H_2 permeability that exceeded the Robeson's upper bound in the permeability-selectivity tradeoff.

ESP is also a promising method in making superhydrophobic membranes for membrane distillation (MD). Su et al. [146] made silica nanoparticles (SiNPs) intercalated polymeric nanofibrous membranes via electro-co-spinning/spraying, as shown in Fig. 8 (e). The PVDF-HFP dope solution was electrospun simultaneously with the electrospraying of PVDF-HFP/SiNPs dope solution onto pre-electrospun PVDF-HFP substrate. This method is a completely scalable technique for making high-flux and robust superhydrophobic membranes compared with other recently reported superhydrophobic MD membranes. On the other hand, this membrane exhibited excellent scaling resistance without any decline in flux and distillate conductivity after 420 mL water recovery. In terms of mineral scaling mitigation, this printed membrane was more scaling-resistant than the commercial or electrospun membranes due to moderate increase in flux and distillate conductivity at high water recovery level. In another paper, Jia et al. [152] demonstrated the same technique in electrospinning PH fibers and electrospraying PS beads to form a composite membrane for MD. This technique successfully showed a good structural integrity in the composite membrane with uniform mixing of the PH fibers/PS beads and a clear hierarchical and porous structure. The superhydophobic membranes also displayed over 99% salt rejection, stable flux and anti-wetting performance during the direct contact membrane distillation (DCMD) operation. Liao et al. [153] explored the use of ESP in printing different polymeric membranes for MD application. In this work they electrosprayed various blended solutions composed of PVDF, PDMS and silica fumes onto the electrospun PVDF nanofibrous support. This technique successfully made the first anti-abrasive membrane for MD with strong superhydrophobicity. Additionally, the printed membranes showed decent anti-scaling/fouling behaviors in various high concentration salt solutions with a stable flux of 28kg/(m^2h) during 160hrs continuous DCMD operation, which proved its potential anti-scaling/fouling application in seawater and wastewater treatment.

ESP could also be used to modify membrane surface charge by incorporating polyelectrolytes. Lim et al. [147] has successfully blended polyelectrolytes mixtures which were thermodynamically immiscible while being incorporated in conventional membrane fabrication process. They proposed an alternative method that used the dual-electrospray technique to individually spray the Nafion and sBlock blend, as demonstrated in Fig. 8(f). As a result, the deposition of the blend induced higher proton conductivity than the prediction of Maxwell–Eucken structural model. In 2020, Korzhova et al. [154] electrosprayed the polyelectrolytes onto commercial UF membranes and could adjust the membrane surface zeta potential in the range of −40 to +40 mV by depositing the negative PSS or the positive PEI. The adjustment in surface charge induced a significant change in ion separation selectivity of the membrane due to the change in the interaction between ions and membrane surface. Based on this, the authors were able to alter the rejection of monovalent and divalent cations and anions. Additionally, the deposition of polyelectrolytes resulted in a small improvement in flux and an increase in surface hydrophilicity, which could help mitigate membrane fouling.

ESP was also used to hydrophobize the surface of anion exchange membranes. Korzhova et al. [155] printed hydrophobic non-conducting spots of a fluoropolymer on the anion exchange membranes to tailor its chronopotentiometric behavior. Due to the tangential electric force generated by the hydrophobic spots, the electroconvection was expanded and this caused earlier and higher amplitude of oscillations on the chronopotentiograms. The electroconvection was also able to enhance mass transfer and reduce water splitting of the membrane.

5.4.3. MJT printed membranes

Al-Shimmery et al. [156] used a Multijet 3D printer to precisely fabricate both flat and wavy double-sinusoidal shaped ABS support layers. The fabrication of the fouling resistant TFC membrane is illustrated in Fig. 9 (a). The PES selective layer was formed via phase inversion on a glass plate and then transferred onto the ABS support by vacuum filtration. The wavy membranes exhibited 30% higher water permeance (16LMH/bar), 96% oil rejection and 52% higher permeance recovery ratio (89) compared with the flat membranes. The permeance after cleaning with NaOCl solution recovered to 70% of the initial permeance of the wavy membranes. In another work [157] the authors studied the BSA fouling performance of these membranes printed by the Multijet printer. They found out that the wavy membranes could retain 88% of their initial water permeance when washed by water after 10 BSA filtration cycles. Under various Re numbers, the wavy membranes all exhibited superior anti-fouling performance than the flat membranes after any BSA filtration cycle. This decent anti-fouling and cleanability behavior indicates that this 3D printed membrane is ideal for future membrane processes due to the low operational and replacement cost.

5.4.4. PJT printed membranes

Philamore et al. [159] compared three ion exchange membranes in a microbial fuel cell (MFC) configuration. Tangoplus acrylate photopolymer resin was printed by a Polyjet printer to form 116 μm membranes and natural rubber latex was cast into 100 μm membranes. These membranes were individually loaded onto a MFC as proton exchange membrane in comparison with the commercial CMI-7000 membrane. The printed and cast membranes exhibited enhanced energy output, high ionic conductivity, system stability, resistance to biological deterioration, and reasonable ion separation. This research provided a rapid and easy path to make membranes from novel materials at lower manufacturing cost.

5.5. BJT printed membranes

Hwa et al. [158] reported the application of BJT aiming at printing ceramic membranes from cheap clay powders, as presented in Fig. 9 (b). This printing process mainly involved the mixing of Maltodextrin binder solution with Kankara clay powder. The sample design was fed into the printer, which then extruded the binder solution form an inkjet print head onto the powder bed to form the cylindrical porous samples. The samples were then dried and sintered to form the ceramic material. The authors studied the impact of clay powder size in membrane structure and filtration performance. The membranes printed with powders at any size displayed a book-like microstructure under SEM, which was an

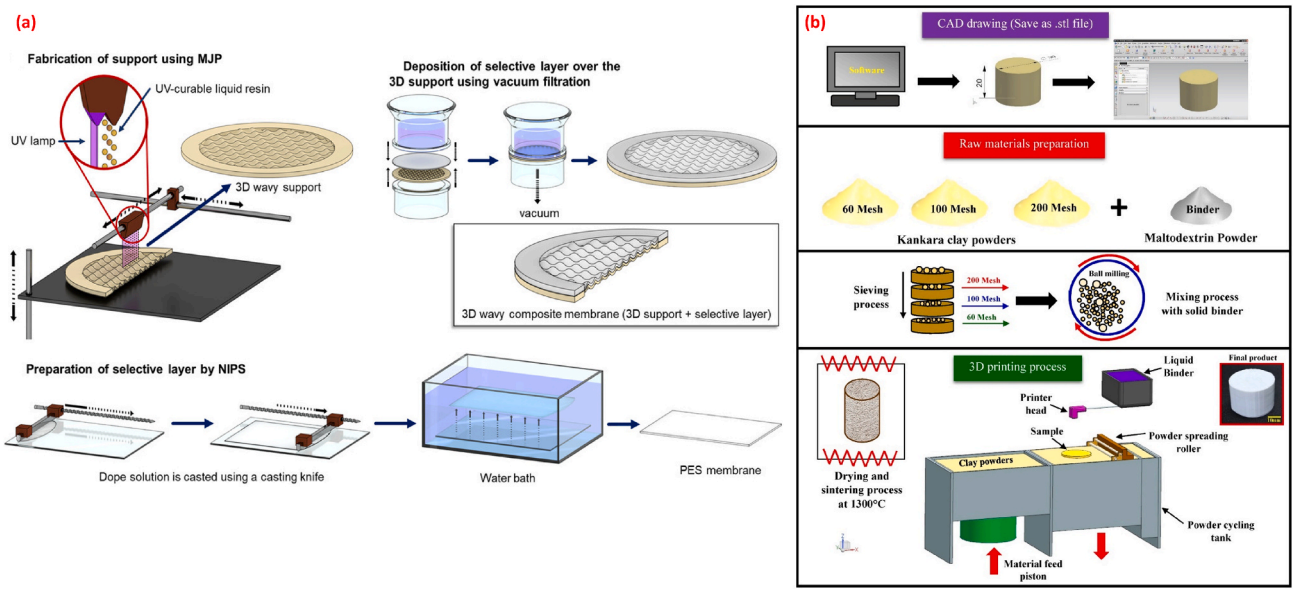

Fig. 9. (a) Fouling resistant TFC membrane consisting MJT printed ABS support layer and the PES selective layer formed by NIPS, adapted from [156,157]; (b) BJT printed cheap ceramic membranes, adapted from [158].

indication of this printing technique using binder solution to stick the powders. Both water filtration and the mechanical test all showed that membranes printed by smaller clay powders had higher water flux, rejection and mechanical properties than membranes printed by bigger clay powders. This was due to the packing behavior of their aggregation as smaller powder could be easier to be packed and form smaller and more uniform pores. This work for the first time proposed this alternative way of the challenging BJT technique in membrane fabrication as this technique usually lacks resolution and accuracy.

6. 3D printed membrane objects and components

While the focus of this review is the presentation of work on printed membrane technologies, we do note the other opportunities in the membrane space for use of additive manufacturing. We do not provide comprehensive reviews of these areas for brevity, but nevertheless believe that they should be mentioned in the context of this paper.

6.1. Membrane gas-liquid contactors

The first 3D printed membrane contactor was based on the DLP technique to form triply periodic minimal surface (TPMS) - PDMS membranes. Femmer et al. [160,161] demonstrated a versatile method to form these pre-developed TPMS structures [162] by first printing the acrylate based sacrificial photoresist mold by DLP. The TPMS structures were designed with optimized mechanical properties and had wrinkle-free local smoothness in order to prevent fouling. The mold was then immersed in PDMS prepolymer solution and then degassed and cured at 65 °C. Once the PDMS polymer filled the space within the mold, the entire structure was soaked in NaOH solution to remove the mold. The membrane was then bonded to glass slide for testing the gas transport behavior in water. The printed membranes had a thickness of 1 mm with 0.15–0.28% porosity that differed from varying membrane structures. The membranes, especially the Schwarz-P geometry showed much better gas transport properties than common hollow fiber membranes. This excellent contacting and transport properties were due to the superior internal structure that improved the gas diffusion. In their subsequent study [163] the authors compared the heat transfer performance of 4 TPMS geometries with conventional flat sheet and hollow fiber membranes. All 4 TPMS structures showed superior heat transfer coefficient to the flat sheet and hollow fiber membranes, with Schwarz-D structure exhibiting the best heat transfer characteristics. Al-Shimmery et al. [164] printed TPMS oil-water separation porous contactors by using a Multijet printer based on the Schwarz-P and Gyroid structures. Membrane contactors with cylindrical pores were also printed as comparison. The internal structures and contactor thickness could be precisely controlled. The TMPS contactors showed superior oil-water separation performance as the 3D printed Gyroid contactor had the highest separation efficiency of 93% compared to the 71% separation efficiency of the cylindrical contactor. The high surface area and tortuosity of the TPMS contactors resulted in longer residence time of the oil droplets.

6.2. Spacers and turbulence promotors

Turbulence promoter/static mixers are usually used in tubular membranes to improve the flux and reduce fouling while also to keep channels open for flow. Conventional extruded spacers provide adequate performance for most modules today, but their manufacturing process prevents optimization of spacer geometries to maximize turbulence while minimizing pressure drop. Armbruster et al. [165] compared the flux performance and energy consumptions of 9 different printed turbulence pormotors. These promoters were printed by the Polyjet printer from photosensitive acrylate based polymer and inserted into a ceramic tubular membrane for flux test. Eight promoters had the twisted-tape structure with different helix geometry, and another one was based on the Kenics geometry. The membranes containing a promoter showed at least 53% higher permeate flux than the pristine ceramic membrane, while the membrane with the Kenics promoter exhibited 140% higher flux. Although the energy consumption and the pressure drop went up when a promoter was installed, the flux was improved at equal levels of energy consumption was applied. In order to mitigate the pressure drop issue induced by the twisted-tape promoters, the authors modified the structure of the promoters in their subsequent study [166]. The modified promoters include a shortened twisted tape aiming at reducing pressure drop at the end of the promoter and a spaced twisted tape promoter that could help alleviate the pressure decline at the rod area. In the fouling test with low foulant concentration, the modified promoters exhibited considerably lower pressure drop and energy consumption but the same fouling mitigation performance as the full-length twisted tape promoters. While the fouling resistance of the modified promoters turned weaker at high foulant concentration,

they exhibited much lower pressure drop and energy consumption than the regular promoters. Tsai et al. [167] printed circular, diamond and elliptic type turbulence promoters by a FDM printer in order to study the optimum promoter geometry for enhancing flux and fouling mitigation in a crossflow microfiltration device. The addition of the promoters was able to reduce the cake generation due to the enhancement of the local shear stress. The authors also found out that the elliptic type promoter was able to improve the flux by 30–64% for different crossflow velocities.

6.3. Hollow fiber, tubular, and monolithic membrane geometries

Most of this review has focused on printing flat sheet membranes. We relegate this article mostly to this membrane geometry for the reason that printing technology has for centuries been designed largely for paper. Printing on cylindrical membranes is challenging and may not be necessary, given the unique multi-layered extrusion and NIPS processes offered by the membrane science community. Where printing has been valuable, though, is in the production of customized spinnerettes with exotic geometries that would be difficitult to machine while being prohibitively expensive. Luelf et al. [168] fabricated spinnerets with different opening shapes by a Polyjet printer in order to produce hollow fibers with different geometry. The authors were able to combine the co-extrusion with rotational assembly to form both Titanium and PES based tri-bore and helical tri-bore hollow fibers by using these spinnerets. They also studied the velocity profile in the helical tri-bore hollow fiber and found out higher radical flow in the shell and counter movements. The helical shape of the fiber served the same function as feed spacers in membrane module in enhancing mass transfer.

Further leveraging the opportunities for 3D printing with hollow fiber membranes, Li et al. [169] used a 3D printed baffle in the hollow fiber vacuum membrane distillation (HF-VMD) system. They found out the baffle could help reduce the temperature drop and enhance the heat transfer of the HF-VMD system without consuming additional power. The velocity profile comparison on the baffled and non-baffled module indicated that the baffle could improve the feed flux near the membrane and achieve a uniform velocity distribution. The authors observed an over 6% improvement in permeate flux and 65% increase in membrane shear stress when the baffle was incorporated.

7. Future perspectives for 3D printing in membrane technologies

We present here the future opportunities for additive manufacturing across membrane disciplines.

7.1. Water treatment and desalination membranes

Since much of the above work is relegated to examples of printed membranes for water treatment applications, we will refrain from being repetitive. Of the most important needs in water treatment membranes is customizability. With so many source waters and so many target contaminants, membranes must be customizable for a wide variety of separations needs. Water treatment system designers have limited options when it comes to RO, NF, or UF membranes with respect to their performance. With such a range of contaminant compositions, salinities, temperatures, and chemistries, a one-membrane-fits-all approach is simply not feasible. We need customizable, on-demand membranes that can provide a user with a membrane targeted to perform for a specific set of contaminants in a specific environment. While the development of structure-property-performance relationships is critical to identifying membrane chemistries that will perform for a desired separation [170], we cannot enable those chemistries to be formed into membranes using only conventional manufacturing approaches. As of now, additive manufacturing is the only option available that allows for careful tuning of chemistry and structure independently while being inherently scalable on a roll-to-roll process. Printing offers a type of scalability that allows membrane science to grow beyond the thumbnail sized membrane made in the lab and move into scales that can make impact. For areas like water treatment, where the product is of low value, the ability to scale cheaply is critical to any techno-economic analysis.

7.2. Gas separations

There are two major technical challenges that need to be overcome to enable AM for gas separations: (1) membrane materials must be compatible with known AM techniques, and (2) selective layers must be formed with thin dimensions in the z-direction. Most of the recent advancements in the literature have only addressed one of these two requirements.

In terms of the first challenge, almost all high-performance gas separation polymers are synthesized via step polymerization to allow for the incorporation of rigid backbone chemistries, which benefit diffusion and diffusion selectivity. However, these desired materials specifications result in polymers that are not easily processed in their melt state, thereby precluding the use of traditional AM approaches such as FDM. By replacing filament extruders with capillary nozzles, Pattison and Hart [171] demonstrated that concentrated solutions of cellulose acetate – one of the most common commercial gas separation membrane materials – could be 3D printed into various polymer parts using an SCP technique. Zhang et al. [172] demonstrated a related approach for concentrated solutions of Polymer of Intrinsic Microporosity (PIM-1), which is a state-of-the-art gas separation material, indicating that even ladder polymers are amenable to this approach. Other researchers have been developing methods to form composite materials through AM, including the development of zeolite/polymer and MOF/polymers composites, although these approaches and those with pure PIMs have only investigated gas adsorption applications and not membrane applications, likely due to dimensional restrictions in thickness. Various so-called MOF inks are being developed [173,174], so the toolkit of compatible materials for AM is expanding in the gas separation space.

In terms of the second challenge, ESP is the only AM approach used today that can form films significantly thinner than traditional solution-based casting methods currently employed for gas separation membranes. For ESP, there have recently been major advancements in forming ultra-thin RO membranes using traditional MPD and TMC monomers [126]. However, interfacial polymerization of polyamides is known to produce gas separation membranes with very low permeability, even after modifying monomer structures [175]. Therefore, significant advancements are needed in polyamide chemistry to enable this method to become competitive for gas separation applications. Another possibility to decrease thickness of 3D printed membranes is to develop high-performance gas separation polymers from resins that can be photopolymerized, and hence, are amenable to techniques such as SLS and CLIPs. Unfortunately, monomers commonly used for these approaches today are based on (meth)acrylates, thiolenes, and thiolynes [176], and these formulations often lack the backbone stiffness required to achieve high diffusion rates and diffusivity selectivities found in polymers formed through step polymerization.

While still in its infancy, there are early indications that AM could become a viable manufacturing option for gas separations if compatible chemistries and improved resolution in thickness can be achieved.

7.3. Ion exchange

Ion exchange membranes are critical components of electromembrane processes, which include a range of technologies spanning batteries to fuel cells to electrodialysis [177–180]. These membranes are often polymeric in nature, but the scope and variety of the chemistry used to prepare these materials has historically been relatively limited. For example, early ion exchange materials were largely styrenic

networks functionalized with either sulfonate, carboxylate, amine, or quaternary ammonium functional groups to prepare strong or weak cation or anion exchangers [181]. The invention of Nafion launched considerable interest in perfluorinated strong cation exchange materials [182]. More recently, a desire to move away from fluorination has contributed to interest in broadening ion exchange membrane chemistry, and growing interest in electromembrane processes has also driven research activity in ion exchange membranes [183,184].

Additive manufacturing could further efforts to explore new ion exchange membrane chemistry and structure by providing pathways to make membranes that, perhaps for thermodynamic or kinetic reasons, are not accessible via conventional processing. For example, additive manufacturing may be useful for preparing ion exchange membranes where co-monomers need to be brought together precisely at the right place and time. It could be particularly useful if the co-monomers are not miscible or are disparate in size or diffusivity in a manner that would preclude conventional solution casting or extrusion. The approach could unlock interesting phase-segregated or composite materials with highly tuned conductive transport pathways that could be key to achieving highly conductive and selective membranes [177,185–187].

Another example where additive manufacturing could be useful is in the preparation of complex membrane electrode assemblies and/or shaped or flexible batteries for structural or wearable energy storage devices. If membrane additive manufacturing were to be coupled to electrode deposition, the technique might offer unique opportunities to control ionomer, binder, and electrode morphology, which are critical for device performance [188], and prepare electrodes with optimized form factors. Similarly, as interest in shaped or flexible energy storage grows, a need exists for custom-shaped membrane separators with varying mechanical properties [189,190]. Additive manufacturing could provide an interesting pathway to realizing the benefits of shaped batteries that would require shaped membrane separators.

7.4. Non-aqueous liquid separations

Membrane-based separations of organic solvents and non-aqueous liquids is one of the most rapidly growing areas of membrane science [191]. A variety of membrane materials have been explored, including solvent-resistant polymers, crosslinked polymers, microporous polymers, mixed matrix membranes, molecularly mixed composite membranes, ceramic membranes, and carbon membranes, among others. However, this rapidly growing field has almost exclusively utilized the traditional membrane manufacturing methods discussed at the outset of this article. A recent article from Van der Bruggen et al. is perhaps the first to describe the creation of solvent-stable membranes using SLS techniques [114]. The SLS technique was capable of producing organic solvent microfiltration membranes that were stable in a variety of aggressive solvents (e.g., tetrahydrofuran, dimethylsulfoxide). The membranes were found to be useful for proof-of-concept oil/water separations. However, the SLS technique was not utilized to impart any specific microscopic patterning or other engineered structure on the surface of the membrane.

With this first report as motivation, there are several clear challenges that exist at the intersection of AM and organic solvent separations. For small molecule separations (e.g., toluene from triisopropylbenzene), a high quality skin layer free from defects is essential for successful operation. These separations are burdened with high osmotic pressures, thus sub-100 nm membranes are almost certainly required to take advantage of the low driving forces [192]. This suggests AM techniques such as ESP will be impactful for these types of separations. It is likely that polymer-based methods capable of making defect-free skin layers (e.g., ESP [126]) will be useful for organic solvent reverse osmosis (OSRO) separations. However, certain applications require solute-solute separations, and these are often addressed via the use of organic solvent nanofiltration (OSN) membranes with precisely engineered micropores in the membrane skin layer. Creation of features of this size is currently beyond the capabilities of existing printers (which to date have only achieved MF-style or RO-style membranes), and is an open area for exploration.

7.5. Intellectual property considerations

AM/3DP for membrane manufacturing points towards endless possibilities to design, develop and rapidly prototype complex membrane architectures and membrane modules with precise control and fidelity that are not possible with current manufacturing methods and as such is a rapidly developing field as described above (cf. Section 1.6 and Fig. 1) with enormous growth potential. Realizing this potential, however, relies on the commercialization efforts that are dependent on intellectual propertly

In addition to numerous peer-reviewed publications reviewed above, there have also been numerous worldwide patents granted on printed membranes. These include graphene oxide printed directly on NF/UF supports through inkjet printing [193], ion exchange membranes with inkjet printer [194,195], RO membranes with flow modifier structures disposed on the membrane surface using direct-write technique [196], fabrication (or modification) of polymer membranes for water treatment utilizing ink-jet printing [197], RO membrane and zwitterionic copolymer membranes using electrospray [198,199], ceramic membranes fabricated using direct ink writing [200], among others. A few examples of these (patents) are described below along with commercial activity in this area.

Yu and Fathizadeh developed a technology to directly print graphene oxide (GO) on NF /UF membranes using inkjet printing [193]. Specifically, GO ink (mixed GO nanoplatelets with a solvent (water or organic solvent)) was directly printed on commercial NF or UF membrane either in single- or multi-print mode to achieve a desired thickness of the GO layer (2–100 nm) with the resulting membrane exhibiting higher water flux and salt rejection. This technology is currently being scaled up by G2O Water Technologies [201], UK for variety of separation applications.

Thin film composite membranes with tunable thickness from zwitterionic amphiphilic copolymers were developed using electrospray technique [199]. The printed membranes exhibited >100-fold increase in water permeance compared to those made by conventional methods, without loss of selectivity (dye rejection). In addition to virtually no waste production, this technology also demonstrated significant reduction in the constituent polymer consumption compared to conventional method to make the membranes, thus creating a potential incentive for technology adoption in cases where expensive materials are used for membrane fabrication.

Inkjet printing was used to rapidly fabricate chemically patterned charged mosaic membranes possessing distinct with anionic and cationic domains that traverse the membrane thickness [195]. It is impossible to fabricate such membranes by any conventional membrane fabrication method and thus provides one example where additive manufacturing can be utilized to produce membranes with complex architectures.

We note one commercialization effort in Singapore. 3D printed high flux UF membranes are being produced by Nano Sun Pte Ltd [202]. The membranes are produced by printing PVDF nanofibers on a backing material using proprietary 3D printer which are subsequently compressed to produce membranes. MF or UF membranes can be made using this technology by adjusting the thickness of the fibers.

AquaMembranes [203] in US have developed and commercialized printed spacer technology where spacer elements are directly printed on commercial RO membranes eliminating the need for traditional feed spacers. Printing spacers in such a fashion resulted in ~30–40% more membrane area (and thus proportional increase in the produced permeate) in the membrane module compared with conventional membrane module while maintaining similar rejection.

With continuing efforts to address existing challenges and related

intellectual property development, the case for adoption of these AM techniques for membrane manufacturing looks promising.

7.6. Perspective of 4D printing

4D printing was originally introduced in a TED talk about printing shape transformation material in 2012 and has attracted attention. 4D printing is an advanced 3D printing technology in which the printed material exhibits shape-change behavior such as deformation, twisting and folding [204]. Most shape changes of polymeric material come from swelling, stress relaxation or creep behavior. 4D printing is progressing toward controlled and predictable shape changes. As of now, many 3D printers are compatible with various shape-changeable hydrogels and shape-memory polymers. DIW 3D printers are able to simultaneously print multiple materials with different shape-changing ability to create controlled local stress and perform programmable shape-changing behavior. Naficy et al. [205] printed two hydrogel inks via DIW to form a composite hinge structure which was sensitive to both hydration and heat, as shown in Fig. 10 (a). The hybrid hinge could be bended when fully swollen with controlled bending angle at different temperature. The hybrid hinge also has shape memory function that showed almost completely reversible shape shifting. Yang et al. [206] used FDM to print carbon black/PU composite material into photosensitive shape memory devices. As shown in Fig. 10 (b), they demonstrated the shape memory polymer could adsorb light or sunshine to generate heat, which was able to trigger the shape recovery.

Many AM techniques can be used to 4D print single material. For example, Raviv et al. [207] proposed the shape deformation of a MJT printed UV curable polymeric hydrogel. As shown in Fig. 11 (a), the polymer can either be formed as an assembly of repeated rigid disks that undergo liner stretching overtime or as a ring shape that performs ring stretching primitive. Folding primitive can be achieved by printing a joint structure with disks between the bars to control the final folding angle. Furthermore, the ring stretching structures can be assembled together to form a porous grid that can deform into a double curvature surface with both convex and concave, as shown in Fig. 11 (b). As shown in Fig. 11 (c), the folding joint structure also demonstrated a 2D folding deformation such as sinusoidal wave, hyperbolic surface and shape-changeable letters. Zarek et al. [208] demonstrated the use of SLA in printing shape memory polymers into shape-adjustable structures. The polymer could be deformed above the melting point and could recover to its original shape by reheating above the melting temperature.

Smart and responsive membranes subjected to different stimuli (such as heat, light, or chemical environment) can temporarily alter the membrane structure or chemistry before reverting back to their original state [209]. However, there are only a few studies succeeding in printing responsive membranes. Zhang et al. [210] printed thermal sensitive lightweight PLA/paper composite membrane sheets via FDM. PLA strips were printed on paper sheets at different orientation. Under the heating and cooling cycle, these sheets exhibited different degree of distortion and form helical shapes due to the difference in the coefficient of thermal expansion (CTE) between PLA and paper. The PLA was also printed on paper sheets in staggered segments with a corrugating shape formation during the heating and cooling cycle. The authors proposed this reversible thermal responsive self-folded material can be applied in wave switch. In another study, Gillono et al. [211] printed a light responsive membrane that could generate internal free volume. The membranes were synthesized with a mixture of PEGDA, the azobenzene dye methyl red (MR) or disperse red 1 methacrylate (DR1M) and photo-initiator (2 phr) via DLP. The membrane was exposed to laser light when testing CO_2 permeability. Since the photoisomerization of the azobenzene dye expanded free volume in the membrane, the CO_2 permeability proportionally increased with the laser intensity. The authors demonstrated this smart membrane could be used for CO_2 separation as the generation of free volume did not significantly change the permeability of other gases such as O_2. This light responsive membrane could also be used to build a connector prototype that functioned as CO_2 flow controller by adjusting the laser exposure based on the pH of the acid solution.

Although 4D printing has not been extensively used in making smart membranes, other responsive mechanisms have substantial potential to be exploited in combination with 4D printing in membrane fabrication. Hester et al. [212] cast self-organizing polymer blends to prepare membranes with pH-responsive flux performance when varying the pH of the feed solution from 2 to 8. Grooth et al. [213] demonstrated the ionic strength responsive polyzwitterionic membrane which was formed by dip-assisted LbL assembly of PDADMAC/PSBMA. They found the growth of additional layers was inhibited at 0.5 M NaCl concentration, resulting in thinner layers. At 1.5 M NaCl concentration, they also observed an increased swelling behavior that induced over 100% improvement in membrane permeability. The thermal-responsive Poly (N-isopropylacrylamide) (PNIPAm) polymer has been blended with other polymers to form temperature responsive membrane. The PNIPAm polymer swells and shrinks the membrane pore structures below its lower critical solution temperature (LCST) at 32 °C. While heated above 32 °C, the polymer dehydrates and loses 90% of its volume, which significantly impacts the membrane pore structure. Frost et al. [214] grafted PNIPAm onto track-etched PET membranes via surface initiated atomic transfer radical polymerization (ATRP) and formed a temperature responsive UF membrane. They found out the membrane pore size was switched from 21 nm to 69 nm when the feed solution temperature was elevated from 23 °C to 45 °C. This temperature elevation also induced a decrease in the rejection of silica nanoparticles from 99% to 35%. As of now, none of these responsive membranes has been 3D printed. It will be interesting and important to explore their controllable and responsive performance at lower thickness level.

8. Closing remarks

This review provides a perspective on past work and future opportunities for 3D printing in the membrane field. Integrating 3D printing with membrane science is compelling as it offers a new manufacturing approach to making membranes at scale using a wide variety of

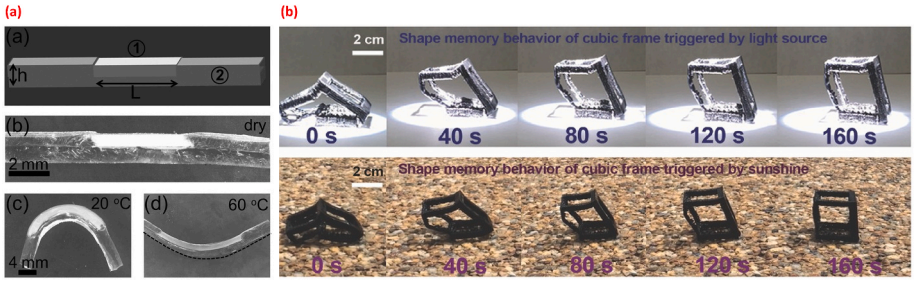

Fig. 10. (a) The composite hybrid hinge at dry state (upper two images) and fully swollen at 20 °C and 60 °C (lower two images), adapted from [205]; (b) shape memory behavior of carbon black/PU composite devices triggered by light source and natural sunshine, adapted from [206].

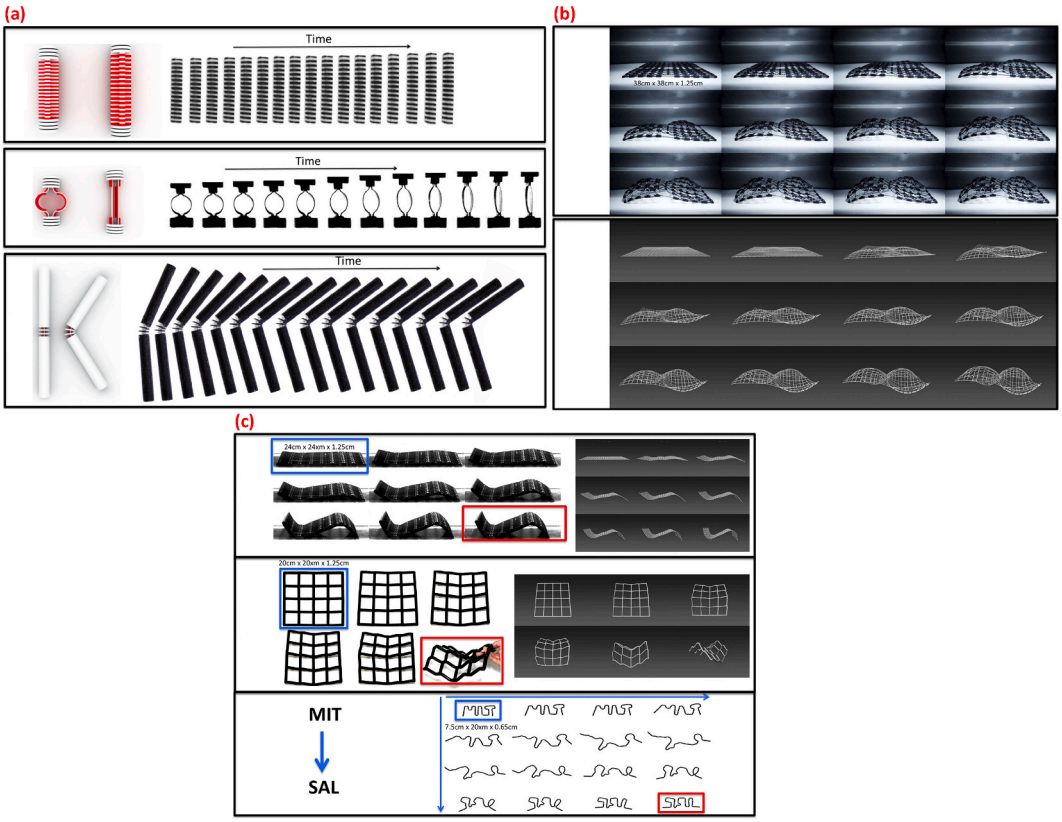

Fig. 11. (a) linear stretching primitive (upper image) composed of rigid disks, ring stretching primitive (middle image) and folding primitive (lower image) joint structure, adapted from [207]; (b) 2D folding and stretching structure consisting ring stretching primitive, adapted from [207]; (c) 2D folding structures composed of folding joint primitive, displaying sinusoidal wave (upper image) and hyperbolic surface (middle image). The lower image is the time-varying curve that changes its shape overtime, adapted from [207].

materials. It often seems that much of the published work in membrane science today focuses on materials development alone and not the manufacturing innovations required to put these materials into practice at scales relevant to their intended use. On the other hand, widespread application of AM for membrane manufacturing may be premature as the cost of the membranes may ultimately limit its use in fields where membranes are already quite inexpensive.

Where AM may create the most value, however, is in enabling the use of emergent materials into high performance membranes. With the incredible wealth of new materials developed over the last half century of membrane science, we have largely relied on traditional manufacturing approaches to put those materials into practice. Such an approach has limited the adoption of new materials in commercial membranes. AM's inherent flexibility offers a new pathway for implementing novel materials into membranes and may ultimately lead to expansion of commercial membrane offerings across many separations disciplines.

Declaration of competing interest

Jeffrey McCutcheon is the Founder of a faculty affiliated company at the University of Connecticut that is commercializing additive manufacturing technology for membranes.

Acknowledgements

This material is based upon work supported by the National Alliance for Water Innovation (NAWI), funded by the U.S. Department of Energy, Office of Energy Efficiency and Renewable Energy (EERE), Advanced Manufacturing Office, under Funding Opportunity Announcement Number DE-FOA-0001905. The Author also acknowledges funding from the National Science Foundation (CMMI #2001544 and #2001624).

References

[1] S. Loeb, S. Sourirajan, High Flow Porous Membranes For Separating Water From Saline Solutions, 1964.
[2] S. Loeb, The Loeb-Sourirajan Membrane: How It Came About, ACS Symp. Ser. Am. Chem. Soc., Washington, DC, 1981.
[3] T.A. Tweddle, O. Kutowy, W.L. Thayer, S. Sourlrajan, Polysulfone ultrafiltration membranes, Ind. Eng. Chem. Prod. Res. Dev. 22 (1983) 320–326, https://doi.org/10.1021/i300010a030.
[4] B.K. Chaturvedi, A.K. Ghosh, V. Ramachandhran, M.K. Trivedi, M.S. Hanra, B. M. Misra, Preparation, Characterization and performance of polyethersulfone ultrafiltration membranes, Desalination 133 (2001) 31–40, https://doi.org/10.1016/S0011-9164(01)00080-7.
[5] I.C. Kim, H.G. Yun, K.H. Lee, Preparation of asymmetric polyacrylonitrile membrane with small pore size by phase inversion and post-treatment process, J. Membr. Sci. 199 (2002) 75–84, https://doi.org/10.1016/S0376-7388(01)00680-9.
[6] D. Wang, K. Li, W.K. Teo, Preparation and characterization of polyvinylidene fluoride (PVDF) hollow fiber membranes, J. Membr. Sci. 163 (1999) 211–220, https://doi.org/10.1016/S0376-7388(99)00181-7.
[7] H. Kawakami, M. Mikawa, S. Nagaoka, Formation of surface skin layer of asymmetric polyimide membranes and their gas transport properties, J. Membr. Sci. 137 (1997) 241–250, https://doi.org/10.1016/S0376-7388(97)00198-1.
[8] A. Jung, S. Rangou, C. Abetz, V. Filiz, V. Abetz, Structure formation of integral asymmetric composite membranes of polystyrene-block-poly(2-vinylpyridine) on a nonwoven, Macromol. Mater. Eng. 297 (2012) 790–798, https://doi.org/10.1002/mame.201100359.
[9] K.V. Peinemann, V. Abetz, P.F.W. Simon, Asymmetric superstructure formed in a block copolymer via phase separation, Nat. Mater. 6 (2007) 992–996, https://doi.org/10.1038/nmat2038
[10] J.E. Cadotte, Evolution of composite reverse osmosis membranes, ACS Symp. Ser. (1985) 273–294, https://doi.org/10.1021/bk-1985-0269.ch012.
[11] J.E. Cadotte, Interfacially synthesized reverse osmosis Membrane, 1981. https://patents.google.com/patent/US4277344A/en.
[12] P.S. Francis, J.E. Cadotte, J.A. Hunter, W.S. Gillam, H.E. Podall, Fabrication and evaluation of new ultrathin reverse osmosis membranes, U. S. Dep. Inter. Off. Saline Water Res. Dev. Progr. Rep. (1967) 51.

[13] S.M. Hosseini, S.S. Madaeni, A.R. Khodabakhshi, Preparation and characterization of ABS/HIPS heterogeneous anion exchange membrane filled with activated carbon, J. Appl. Polym. Sci. 118 (2010) 3371–3383, https://doi.org/10.1002/app.32369.

[14] K. Xie, Q. Fu, G.G. Qiao, P.A. Webley, Recent progress on fabrication methods of polymeric thin film gas separation membranes for CO2 capture, J. Membr. Sci. 572 (2019) 38–60, https://doi.org/10.1016/j.memsci.2018.10.049.

[15] B.D. Freeman, I. Pinnau, Polymer membranes for gas and vapor separation, copyright, advisory board, foreword, ACS Symp. Ser. (1999), https://doi.org/10.1021/bk-1999-0733.fw001.

[16] Q.Z. Zheng, P. Wang, Y.N. Yang, D.J. Cui, The relationship between porosity and kinetics parameter of membrane formation in PSF ultrafiltration membrane, J. Membr. Sci. 286 (2006) 7–11, https://doi.org/10.1016/j.memsci.2006.09.033.

[17] S.J. Shin, J.P. Kim, H.J. Kim, J.H. Jeon, B.R. Min, Preparation and characterization of polyethersulfone microfiltration membranes by a 2-methoxyethanol additive, Desalination 186 (2005) 1–10, https://doi.org/10.1016/j.desal.2005.03.092.

[18] N. Ghasem, M. Al-Marzouqi, N. Abdul Rahim, Effect of polymer extrusion temperature on poly(vinylidene fluoride) hollow fiber membranes: properties and performance used as gas-liquid membrane contactor for CO 2 absorption, Separ. Purif. Technol. 99 (2012) 91–103, https://doi.org/10.1016/j.seppur.2012.07.021.

[19] K.H. Lee, H.Y. Kim, Y.M. La, D.R. Lee, N.H. Sung, Influence of a mixing solvent with tetrahydrofuran and N,N-dimethylformamide on electrospun poly(vinyl chloride) nonwoven mats, J. Polym. Sci., Part B: Polym. Phys. 40 (2002) 2259–2268, https://doi.org/10.1002/polb.10293.

[20] M.C. Almandoz, C.L. Pagliero, N.A. Ochoa, J. Marchese, Composite ceramic membranes from natural aluminosilicates for microfiltration applications, Ceram. Int. 41 (2015) 5621–5633, https://doi.org/10.1016/j.ceramint.2014.12.144.

[21] M. Jabbari, R. Bulatova, A.I.Y. Tok, C.R.H. Bahl, E. Mitsoulis, J.H. Hattel, Ceramic tape casting: a review of current methods and trends with emphasis on rheological behaviour and flow analysis, Mater. Sci. Eng. B Solid-State Mater. Adv. Technol. 212 (2016) 39–61, https://doi.org/10.1016/j.mseb.2016.07.011.

[22] H. Wang, S. Zhao, Y. Liu, R. Yao, X. Wang, Y. Cao, D. Ma, M. Zou, A. Cao, X. Feng, B. Wang, Membrane adsorbers with ultrahigh metal-organic framework loading for high flux separations, Nat. Commun. 10 (2019) 1–9, https://doi.org/10.1038/s41467-019-12114-8.

[23] H.B. Tanh Jeazet, C. Staudt, C. Janiak, Metal-organic frameworks in mixed-matrix membranes for gas separation, Dalt. Trans. 41 (2012) 14003–14027, https://doi.org/10.1039/c2dt31550e.

[24] J. Caro, M. Noack, P. Kölsch, R. Schäfer, Zeolite membranes - state of their development and perspective, Microporous Mesoporous Mater. 38 (2000) 3–24, https://doi.org/10.1016/S1387-1811(99)00295-4.

[25] O.G. Kravchenko, X. Qian, S.G. Kravchenko, R. Misiego, R.B. Pipes, I. Manas-Zloczower, Role of hierarchical morphology of helical carbon nanotube bundles on thermal expansion of polymer nanocomposites, J. Mater. Res. 32 (2017) 2738–2746, https://doi.org/10.1557/jmr.2017.214.

[26] Y. Chen, H. Bin Zhang, M. Wang, X. Qian, A. Dasari, Z.Z. Yu, Phenolic resin-enhanced three-dimensional graphene aerogels and their epoxy nanocomposites with high mechanical and electromagnetic interference shielding performances, Compos. Sci. Technol. 152 (2017) 254–262, https://doi.org/10.1016/j.compscitech.2017.09.022.

[27] O.G. Kravchenko, D. Pedrazzoli, D. Kovtun, X. Qian, I. Manas-Zloczower, Incorporation of plasma-functionalized carbon nanostructures in composite laminates for interlaminar reinforcement and delamination crack monitoring, J. Phys. Chem. Solids. 112 (2018) 163–170, https://doi.org/10.1016/j.jpcs.2017.09.018.

[28] Hideo Kodama, Automatic method for fabricating a three- dimensional plastic model with photo- hardening polymer, Rev. Sci. Instrum. 52 (1998) 2–6.

[29] C.W. Hull, Apparatus for Production of Three-Dmensonal Objects by Stereo Thography, 1984. https://patents.google.com/patent/US4575330.

[30] C.R. Deckard, Method and Apparatus for Producing Parts by selective sintering, 1989. https://patents.google.com/patent/US4863538.

[31] S.S. Crump, Apparatus and Method for Creating Three-Dimensional objects, 1992, https://doi.org/10.2116/bunsekikagaku.28.3_195.

[32] M. Feygin, A. Shkolnik, M.N. Diamond, E. Dvorskiy, Laminated object Manufacturing system, 1996.

[33] H.D. Dean, J.E. Wallace, A.G. Mikos, M. Wang, A. Siblani, K. Kim, J.P. Fisher, Continuous Digital Light Processing Additive Manufacturing of Implants, 2012.

[34] J.K. Placone, A.J. Engler, Recent Advances in Extrusion-Based 3D Printing for Biomedical Applications, 2018, https://doi.org/10.1002/adhm.201701161.

[35] T. Han, S. Kundu, A. Nag, Y. Xu, 3D printed sensors for biomedical applications: a review, Sensors 19 (2019), https://doi.org/10.3390/s19071706.

[36] U. Jammalamadaka, K. Tappa, Recent advances in biomaterials for 3D printing and tissue engineering, J. Funct. Biomater. 9 (2018), https://doi.org/10.3390/jfb9010022.

[37] W. Jamróz, J. Szafraniec, M. Kurek, R. Jachowicz, 3D printing in pharmaceutical and medical applications, Pharm. Res. (N. Y.) 35 (2018). Article 176.

[38] S.J. Trenfield, A. Awad, A. Goyanes, S. Gaisford, A.W. Basit, 3D printing pharmaceuticals: drug development to frontline care, Trends Pharmacol. Sci. 39 (2018) 440–451, https://doi.org/10.1016/j.tips.2018.02.006.

[39] S.C. Joshi, A.A. Sheikh, 3D printing in aerospace and its long-term sustainability, Virtual Phys. Prototyp. 10 (2015) 175–185, https://doi.org/10.1080/17452759.2015.1111519.

[40] C.W.J. Lim, K.Q. Le, Q. Lu, C.H. Wong, An overview of 3-D printing in the manufacturing, aerospace, and automotive industries, IEEE Poten. 35 (2016) 18–22.

[41] B. Gross, S.Y. Lockwood, D.M. Spence, Recent advances in analytical chemistry by 3D printing, Anal. Chem. 89 (2017) 57–70, https://doi.org/10.1021/acs.analchem.6b04344.

[42] A. Ambrosi, M. Pumera, 3D-printing technologies for electrochemical applications, Chem. Soc. Rev. 45 (2016) 2740–2755, https://doi.org/10.1039/c5cs00714c.

[43] Y. Xu, X. Wu, X. Guo, B. Kong, M. Zhang, X. Qian, S. Mi, W. Sun, The Boom in 3D-Printed Sensor Technology, 2017, https://doi.org/10.3390/s17051166.

[44] Z. Liu, M. Zhang, B. Bhandari, Y. Wang, 3D printing: printing precision and application in food sector, Trends Food Sci. Technol. 69 (2017) 83–94, https://doi.org/10.1016/j.tifs.2017.08.018.

[45] T. Duda, L.V. Raghavan, 3D metal printing technology, IFAC-PapersOnLine. 49 (2016) 103–110, https://doi.org/10.1016/j.ifacol.2016.11.111.

[46] J.S. Mohammed, Applications of 3D printing technologies in oceanography, Meth. Ocean. ogr. 17 (2016) 97–117, https://doi.org/10.1016/j.mio.2016.08.001.

[47] N. Sreedhar, N. Thomas, O. Al-Ketan, R. Rowshan, H. Hernandez, R.K. Abu Al-Rub, H.A. Arafat, 3D printed feed spacers based on triply periodic minimal surfaces for flux enhancement and biofouling mitigation in RO and UF, Desalination 425 (2018) 12–21, https://doi.org/10.1016/j.desal.2017.10.010.

[48] N. Yanar, M. Son, E. Yang, Y. Kim, H. Park, S.E. Nam, H. Choi, Investigation of the performance behavior of a forward osmosis membrane system using various feed spacer materials fabricated by 3D printing technique, Chemosphere 202 (2018) 708–715, https://doi.org/10.1016/j.chemosphere.2018.03.147.

[49] N. Thomas, N. Sreedhar, O. Al-Ketan, R. Rowshan, R.K. Abu Al-Rub, H. Arafat, 3D printed spacers based on TPMS architectures for scaling control in membrane distillation, J. Membr. Sci. 581 (2019) 38–49, https://doi.org/10.1016/j.memsci.2019.03.039.

[50] K.P. Lee, T.C. Arnot, D. Mattia, A review of reverse osmosis membrane materials for desalination-Development to date and future potential, J. Membr. Sci. 370 (2011) 1–22, https://doi.org/10.1016/j.memsci.2010.12.036.

[51] R.W. Baker, B.T. Low, Gas separation membrane materials: a perspective, Macromolecules 47 (2014) 6999–7013, https://doi.org/10.1021/ma501488s.

[52] J.Y. Lee, W.S. Tan, J. An, C.K. Chua, C.Y. Tang, A.G. Fane, T.H. Chong, The potential to enhance membrane module design with 3D printing technology, J. Membr. Sci. 499 (2016) 480–490, https://doi.org/10.1016/j.memsci.2015.11.008.

[53] H. Dommati, S.S. Ray, J.C. Wang, S.S. Chen, A comprehensive review of recent developments in 3D printing technique for ceramic membrane fabrication for water purification, RSC Adv. 9 (2019) 16869–16883, https://doi.org/10.1039/c9ra00872a.

[54] X.H. Ma, H. Guo, Z. Yang, Z.K. Yao, W.H. Qing, Y.L. Chen, Z.L. Xu, C.Y. Tang, Carbon nanotubes enhance permeability of ultrathin polyamide rejection layers, J. Membr. Sci. (2019) 139–145, https://doi.org/10.1016/j.memsci.2018.10.055, 570–571.

[55] I.M. Hutten, Handbook of Nonwoven Filter Media, 2007.

[56] H.H. Wang, J.T. Jung, J.F. Kim, S. Kim, E. Drioli, Y.M. Lee, A novel green solvent alternative for polymeric membrane preparation via nonsolvent-induced phase separation (NIPS), J. Membr. Sci. 574 (2019) 44–54, https://doi.org/10.1016/j.memsci.2018.12.051.

[57] D.M. Wang, J.Y. Lai, Recent advances in preparation and morphology control of polymeric membranes formed by nonsolvent induced phase separation, Curr. Opin. Chem. Eng. 2 (2013) 229–237, https://doi.org/10.1016/j.coche.2013.04.003.

[58] X. Dong, A. Al-Jumaily, I.C. Escobar, Investigation of the use of a bio-derived solvent for non-solvent-induced phase separation (NIPS) fabrication of polysulfone membranes, Membranes 8 (2018), https://doi.org/10.3390/membranes8020023.

[59] Y. Yao, P. Zhang, C. Jiang, R.M. DuChanois, X. Zhang, M. Elimelech, High performance polyester reverse osmosis desalination membrane with chlorine resistance, Nat. Sustain. 4 (2021) 138–146, https://doi.org/10.1038/s41893-020-00619-w.

[60] N. Mallegni, T.V. Phuong, M.B. Coltelli, P. Cinelli, A. Lazzeri, Poly(lactic acid) (PLA) based tear resistant and biodegradable flexible films by blown film extrusion, Materials 11 (2018), https://doi.org/10.3390/ma11010148.

[61] P. Bengani, Y. Kou, A. Asatekin, Zwitterionic copolymer self-assembly for fouling resistant, high flux membranes with size-based small molecule selectivity, J. Membr. Sci. 493 (2015) 755–765, https://doi.org/10.1016/j.memsci.2015.07.025.

[62] R. Verbeke, W. Arts, E. Dom, M. Dickmann, W. Egger, G. Koeckelberghs, A. Szymczyk, I.F.J. Vankelecom, Transferring bulk chemistry to interfacial synthesis of TFC-membranes to create chemically robust poly(epoxyether)films, J. Membr. Sci. 582 (2019) 442–453, https://doi.org/10.1016/j.memsci.2019.02.016.

[63] A.F. Ismail, P.S. Goh, S.M. Sanip, M. Aziz, Transport and separation properties of carbon nanotube-mixed matrix membrane, Separ. Purif. Technol. 70 (2009) 12–26, https://doi.org/10.1016/j.seppur.2009.09.002.

[64] B. Zornoza, C. Tellez, J. Coronas, J. Gascon, F. Kapteijn, Metal organic framework based mixed matrix membranes: an increasingly important field of research with a large application potential, Microporous Mesoporous Mater. 166 (2013) 67–78, https://doi.org/10.1016/j.micromeso.2012.03.012.

[65] B.M. Ganesh, A.M. Isloor, A.F. Ismail, Enhanced hydrophilicity and salt rejection study of graphene oxide-polysulfone mixed matrix membrane, Desalination 313 (2013) 199–207, https://doi.org/10.1016/j.desal.2012.11.037.

[66] A.K. An, E.J. Lee, J. Guo, S. Jeong, J.G. Lee, N. Ghaffour, Enhanced vapor transport in membrane distillation via functionalized carbon nanotubes anchored into electrospun nanofibres, Sci. Rep. 7 (2017) 1–11, https://doi.org/10.1038/srep41562.

[67] B.J. Hinds, N. Chopra, T. Rantell, R. Andrews, V. Gavalas, L.G. Bachas, Aligned multiwalled carbon nanotube membranes, Science 303 (2010) 62–65, 80.

[68] L. Zhang, B. Zhao, X. Wang, Y. Liang, H. Qiu, G. Zheng, J. Yang, Gas transport in vertically-aligned carbon nanotube/parylene composite membranes, Carbon N. Y. 66 (2014) 11–17, https://doi.org/10.1016/j.carbon.2013.08.007.

[69] M. Majumder, N. Chopra, R. Andrews, B.J. Hinds, Enhanced flow in carbon nanotubes, Nature 438 (2005) 44.

[70] J.E. Gu, S. Lee, C.M. Stafford, J.S. Lee, W. Choi, B.Y. Kim, K.Y. Baek, E.P. Chan, J. Y. Chung, J. Bang, J.H. Lee, Molecular layer-by-layer assembled thin-film composite membranes for water desalination, Adv. Mater. 25 (2013) 4778–4782, https://doi.org/10.1002/adma.201302030.

[71] W. Choi, J. Choi, J. Bang, J.H. Lee, Layer-by-layer assembly of graphene oxide nanosheets on polyamide membranes for durable reverse-osmosis applications, ACS Appl. Mater. Interfaces 5 (2013) 12510–12519, https://doi.org/10.1021/am403790s.

[72] Y. Li, Y. Su, J. Li, X. Zhao, R. Zhang, X. Fan, J. Zhu, Y. Ma, Y. Liu, Z. Jiang, Preparation of thin film composite nanofiltration membrane with improved structural stability through the mediation of polydopamine, J. Membr. Sci. 476 (2015) 10–19, https://doi.org/10.1016/j.memsci.2014.11.011.

[73] J. Ma, M. Zhang, H. Wu, X. Yin, J. Chen, Z. Jiang, Mussel-inspired fabrication of structurally stable chitosan/polyacrylonitrile composite membrane for pervaporation dehydration, J. Membr. Sci. 348 (2010) 150–159, https://doi.org/10.1016/j.memsci.2009.10.051.

[74] Standard terminology for additive manufacturing – general principles – terminology, in: ISO/ASTM 52900:2015(E), 2015.

[75] L.D. Tijing, J.R.C. Dizon, I. Ibrahim, A.R.N. Nisay, H.K. Shon, R.C. Advincula, 3D printing for membrane separation, desalination and water treatment, Appl. Mater. Today. 18 (2020) 100486, https://doi.org/10.1016/j.apmt.2019.100486.

[76] Z.X. Low, Y.T. Chua, B.M. Ray, D. Mattia, I.S. Metcalfe, D.A. Patterson, Perspective on 3D printing of separation membranes and comparison to related unconventional fabrication techniques, J. Membr. Sci. 523 (2017) 596–613, https://doi.org/10.1016/j.memsci.2016.10.006.

[77] E.M. Sachs, J.S. Haggerty, M.J. Cima, P.A. Williams, Three-dimensional Printing Techniques, 1993.

[78] C.R. Deckard, Apparatus for Producing Parts by Selective Sintering, 1997.

[79] S. Maruo, O. Nakamura, S. Kawata, Three-dimensional microfabrication with two-photon-absorbed photopolymerization 22 (1997) 132–134.

[80] J.S. Batchelder, J.B. Hedlund, P.E. Hopkins, S.A. Chillscyzn, Continuous Liquid Interface Production system with Viscosity Pump, 2017.

[81] S.C. Ligon, B. Husár, H. Wutzel, R. Holman, R. Liska, Strategies to reduce oxygen inhibition in photoinduced polymerization, Chem. Rev. 114 (2014) 577–589, https://doi.org/10.1021/cr3005197.

[82] Y. Yagci, S. Jockusch, N.J. Turro, Photoinitiated polymerization: advances, challenges, and opportunities, Macromolecules 43 (2010) 6245–6260, https://doi.org/10.1021/ma1007545.

[83] J.R. Tumbleston, D. Shirvanyants, N. Ermoshkin, R. Januszewicz, A.R. Johnson, D. Kelly, K. Chen, R. Pinschmidt, J.P. Rolland, A. Ermoshkin, E.T. Samulski, J. M. DeSimone, Continuous liquid interface production of 3D objects, Science 347 (2015) 1349–1352, https://doi.org/10.1126/science.aaa2397, 80.

[84] J. Cesarano III, P.D. Calvert, Freeforming objects with Low-Binder slurry, 2000.

[85] J. Cesarano III, R. Segalman, P. Calvert, Robocasting provides moldless fabrication from slurry deposition, Ceram. Ind. VO - 148 (1998) 94. https://ezp.lib.unimelb.edu.au/login?url=https://search.ebscohost.com/login.aspx?direct=true&db=edsggo&AN=edsgcl.20872588&site=eds-live&scope=site.

[86] J.A. Lewis, Direct ink writing of 3D functional materials, Adv. Funct. Mater. 16 (2006) 2193–2204, https://doi.org/10.1002/adfm.200600434.

[87] I.T. Ozbolat, K.K. Moncal, H. Gudapati, Evaluation of bioprinter technologies, Addit. Manuf. 13 (2017) 179–200, https://doi.org/10.1016/j.addma.2016.10.003.

[88] M. Kuang, L. Wang, Y. Song, Controllable printing droplets for high-resolution patterns, Adv. Mater. 26 (2014) 6950–6958, https://doi.org/10.1002/adma.201305416.

[89] B.J. Kang, J.H. Oh, Influence of C4F8 plasma treatment on size control of inkjet-printed dots on a flexible substrate, Surf. Coating. Technol. 205 (2010) 158–163, https://doi.org/10.1016/j.surfcoat.2010.07.010.

[90] J.Z. Wang, Z.H. Zheng, H.W. Li, W.T.S. Huck, H. Sirringhaus, Dewetting of conducting polymer inkjet droplets on patterned surfaces, Nat. Mater. 3 (2004) 171–176, https://doi.org/10.1038/nmat1073.

[91] J. Zeleny, The electrical discharge from liquid points, Phys. Rev. III (1914) 69–91. http://link.aps.org/doi/10.1103/PhysRev.3.69.

[92] J.B. Fenn, M. Mann, C.K. Meng, S.F. Wong, C.M. Whitehouse, Electrospray ionization for mass spectrometry of large biomolecules, Science 246 (1989) 64–71, https://doi.org/10.1126/science.2675315, 80.

[93] A.M. Gañán-Calvo, J. Dávila, A. Barrero, Current and droplet size in the electrospraying of liquids. Scaling laws, J. Aerosol Sci. 28 (1997) 249–275, https://doi.org/10.1016/S0021-8502(96)00433-8.

[94] R.P.A. Hartman, D.J. Brunner, D.M.A. Camelot, J.C.M. Marijnissen, B. Scarlett, Electrohydrodynamic atomization in the cone-jet mode physical modeling of the liquid cone and jet, J. Aerosol Sci. 30 (1999) 823–849, https://doi.org/10.1016/S0021-8502(99)00033-6.

[95] S. Martin, A. Perea, P.L. Garcia-Ybarra, J.L. Castillo, Effect of the collector voltage on the stability of the cone-jet mode in electrohydrodynamic spraying, J. Aerosol Sci. 46 (2012) 53–63, https://doi.org/10.1016/j.jaerosci.2011.11.003.

[96] J. Li, On the stability of electrohydrodynamic spraying in the cone-jet mode, J. Electrost. 65 (2007) 251–255, https://doi.org/10.1016/j.elstat.2006.08.006.

[97] G.D. Kim, Y.T. Oh, A benchmark study on rapid prototyping processes and machines: quantitative comparisons of mechanical properties, accuracy, roughness, speed, and material cost, Proc. Inst. Mech. Eng. Part B J. Eng. Manuf. 222 (2008) 201–215, https://doi.org/10.1243/09544054JEM724.

[98] C. Capparelli, C.R. Fernandez Pulido, R.A. Wiencek, M.A. Hickner, Resistance and permselectivity of 3D-printed micropatterned anion-exchange membranes, ACS Appl. Mater. Interfaces 11 (2019) 26298–26306, https://doi.org/10.1021/acsami.8b04177.

[99] A. Patel, A. Maiorana, L. Yue, R.A. Gross, I. Manas-Zloczower, Curing kinetics of biobased epoxies for tailored applications, Macromolecules 49 (2016) 5315–5324, https://doi.org/10.1021/acs.macromol.6b01261.

[100] W.W. Graessley, S.D. Glasscock, R.L. Crawley, Die Swell in Molten Polymers, 1970, p. 544, https://doi.org/10.1122/1.549177.

[101] J.R.C. Dizon, A.H. Espera, Q. Chen, R.C. Advincula, Mechanical characterization of 3D-printed polymers, Addit. Manuf. 20 (2018) 44–67, https://doi.org/10.1016/j.addma.2017.12.002.

[102] P. Steinle, Characterization of emissions from a desktop 3D printer and indoor air measurements in office settings, J. Occup. Environ. Hyg. 13 (2016) 121–132, https://doi.org/10.1080/15459624.2015.1091957.

[103] P. Azimi, D. Zhao, C. Pouzet, N.E. Crain, B. Stephens, Emissions of ultrafine particles and volatile organic compounds from commercially available desktop three-dimensional printers with multiple filaments, Environ. Sci. Technol. 50 (2016) 1260–1268, https://doi.org/10.1021/acs.est.5b04983.

[104] R. Xing, R. Huang, W. Qi, R. Su, Z. He, Three-dimensionally printed bioinspired superhydrophobic PLA membrane for oil-water separation, AIChE J. 64 (2018) 3700–3708, https://doi.org/10.1002/aic.16347.

[105] J. Lv, Z. Gong, Z. He, J. Yang, Y. Chen, C. Tang, Y. Liu, M. Fan, W.M. Lau, 3D printing of a mechanically durable superhydrophobic porous membrane for oil-water separation, J. Mater. Chem. A. 5 (2017) 12435–12444, https://doi.org/10.1039/c7ta02202f.

[106] S. Yuan, J. Zhu, Y. Li, Y. Zhao, J. Li, P. Van Puyvelde, B. Van Der Bruggen, Structure architecture of micro/nanoscale ZIF-L on a 3D printed membrane for a superhydrophobic and underwater superoleophobic surface, J. Mater. Chem. A. 7 (2019) 2723–2729, https://doi.org/10.1039/c8ta10249j.

[107] X. Li, H. Shan, W. Zhang, B. Li, 3D printed robust superhydrophilic and underwater superoleophobic composite membrane for high efficient oil/water separation, Separ. Purif. Technol. 237 (2020) 116324, https://doi.org/10.1016/j.seppur.2019.116324.

[108] P. He, X. Tang, L. Chen, P. Xie, L. He, H. Zhou, D. Zhang, T. Fan, Patterned carbon nitride–based hybrid aerogel membranes via 3D printing for broadband solar wastewater remediation, Adv. Funct. Mater. 28 (2018) 1–8, https://doi.org/10.1002/adfm.201801121.

[109] Z. Lyu, T.C.A. Ng, T. Tran-Duc, G.J.H. Lim, Q. Gu, L. Zhang, Z. Zhang, J. Ding, N. Phan-Thien, J. Wang, H.Y. Ng, 3D-printed surface-patterned ceramic membrane with enhanced performance in crossflow filtration, J. Membr. Sci. 606 (2020) 118138, https://doi.org/10.1016/j.memsci.2020.118138.

[110] G. Li, X. Mo, Y. Wang, C.Y. Chan, K.C. Chan, All 3D-printed superhydrophobic/oleophilic membrane for robotic oil recycling, Adv. Mater. Interfaces. 6 (2019) 1–5, https://doi.org/10.1002/admi.201900874.

[111] J. Seo, D.I. Kushner, M.A. Hickner, 3D printing of micropatterned anion exchange membranes, ACS Appl. Mater. Interfaces 8 (2016) 16656–16663, https://doi.org/10.1021/acsami.6b03455.

[112] M. Singh, A.P. Haring, Y. Tong, E. Cesewski, E. Ball, R. Jasper, E.M. Davis, B. N. Johnson, Additive manufacturing of mechanically isotropic thin films and membranes via microextrusion 3D printing of polymer solutions, ACS Appl. Mater. Interfaces 11 (2019) 6652–6661, https://doi.org/10.1021/acsami.8b22164.

[113] S. Yuan, D. Strobbe, J.P. Kruth, P. Van Puyvelde, B. Van der Bruggen, Production of polyamide-12 membranes for microfiltration through selective laser sintering, J. Membr. Sci. 525 (2017) 157–162, https://doi.org/10.1016/j.memsci.2016.10.041.

[114] S. Yuan, D. Strobbe, X. Li, J.P. Kruth, P. Van Puyvelde, B. Van der Bruggen, 3D printed chemically and mechanically robust membrane by selective laser sintering for separation of oil/water and immiscible organic mixtures, Chem. Eng. J. 385 (2020) 123816, https://doi.org/10.1016/j.cej.2019.123816.

[115] S. Yuan, D. Strobbe, J.P. Kruth, P. Van Puyvelde, B. Van Der Bruggen, Superhydrophobic 3D printed polysulfone membranes with a switchable wettability by self-assembled candle soot for efficient gravity-driven oil/water separation, J. Mater. Chem. A. 5 (2017) 25401–25409, https://doi.org/10.1039/c7ta08836a.

[116] S.S. Ray, H. Dommati, J.C. Wang, S.S. Chen, Solvent based Slurry Stereolithography 3D printed hydrophilic ceramic membrane for ultrafiltration application, Ceram. Int. 46 (2020) 12480–12488, https://doi.org/10.1016/j.ceramint.2020.02.010.

[117] J. Muskin, M. Ragusa, T. Gelsthorpe, Three-dimensional printing using a photoinitiated polymer, J. Chem. Educ. 87 (2010) 512–514, https://doi.org/10.1021/ed800170t.

[118] A.R. Schultz, P.M. Lambert, N.A. Chartrain, D.M. Ruohoniemi, Z. Zhang, C. Jangu, M. Zhang, C.B. Williams, T.E. Long, 3D printing phosphonium ionic liquid

networks with mask projection microstereolithography, ACS Macro Lett. 3 (2014) 1205–1209, https://doi.org/10.1021/mz5006316.
[119] J. Linkhorst, J. Lölsberg, S. Thill, J. Lohaus, A. Lüken, G. Naegele, M. Wessling, Templating the morphology of soft microgel assemblies using a nanolithographic 3D-printed membrane, Sci. Rep. 11 (2021) 1–7, https://doi.org/10.1038/s41598-020-80324-y.
[120] S. Mecham, A. Nebipasagil, R. Janusziewicz, B.D. Freeman, J.M. DeSimone, Continuous liquid interface production (CLIP) of precise membrane structures, in: North Am. Membr. Soc., 2015.
[121] W. Lin, H. Liu, H. Huang, J. Huang, K. Ruan, Z. Lin, H. Wu, Z. Zhang, J. Chen, J. Li, Y. Ge, J. Zhong, L. Wu, J. Liu, Enhanced continuous liquid interface production with track-etched membrane, Rapid Prototyp. J. 25 (2019) 117–125, https://doi.org/10.1108/RPJ-12-2017-0251.
[122] L. Wang, Y. Luo, Z. Yang, W. Dai, X. Liu, J. Yang, B. Lu, L. Chen, Accelerated refilling speed in rapid stereolithography based on nano-textured functional release film, Addit. Manuf. 29 (2019) 100791, https://doi.org/10.1016/j.addma.2019.100791.
[123] B.J. De Gans, P.C. Duineveld, U.S. Schubert, Inkjet printing of polymers: state of the art and future developments, Adv. Mater. 16 (2004) 203–213, https://doi.org/10.1002/adma.200300385.
[124] S. Badalov, Y. Oren, C.J. Arnusch, Ink-jet printing assisted fabrication of patterned thin film composite membranes, J. Membr. Sci. 493 (2015) 508–514, https://doi.org/10.1016/j.memsci.2015.06.051.
[125] S. Badalov, C.J. Arnusch, Ink-jet printing assisted fabrication of thin film composite membranes, J. Membr. Sci. 515 (2016) 79–85, https://doi.org/10.1016/j.memsci.2016.05.046.
[126] M.R. Chowdhury, J. Steffes, B.D. Huey, J.R. McCutcheon, 3D printed polyamide membranes for desalination, Science 361 (2018) 682–686, https://doi.org/10.1126/science.aar2122, 80.
[127] S. Yang, J. Wang, L. Fang, H. Lin, F. Liu, C.Y. Tang, Electrosprayed polyamide nanofiltration membrane with intercalated structure for controllable structure manipulation and enhanced separation performance, J. Membr. Sci. 602 (2020) 117971, https://doi.org/10.1016/j.memsci.2020.117971.
[128] R. Bernstein, C.E. Singer, S.P. Singh, C. Mao, C.J. Arnusch, UV initiated surface grafting on polyethersulfone ultrafiltration membranes via ink-jet printing-assisted modification, J. Membr. Sci. 548 (2018) 73–80, https://doi.org/10.1016/j.memsci.2017.10.069.
[129] J.T. Arena, S.S. Manickam, K.K. Reimund, B.D. Freeman, J.R. McCutcheon, Solute and water transport in forward osmosis using polydopamine modified thin film composite membranes, Desalination 343 (2014) 8–16, https://doi.org/10.1016/j.desal.2014.01.009.
[130] R. Li, J. Liu, A. Shi, X. Luo, J. Lin, R. Zheng, H. Fan, S.V. Selasie, H. Lin, A facile method to modify polypropylene membrane by polydopamine coating via inkjet printing technique for superior performance, J. Colloid Interface Sci. 552 (2019) 719–727, https://doi.org/10.1016/j.jcis.2019.05.108.
[131] R. Li, H. Fan, L. Shen, L. Rao, J. Tang, S. Hu, H. Lin, Inkjet printing assisted fabrication of polyphenol-based coating membranes for oil/water separation, Chemosphere 250 (2020) 126236, https://doi.org/10.1016/j.chemosphere.2020.126236.
[132] P. Gao, A. Hunter, S. Benavides, M.J. Summe, F. Gao, W.A. Phillip, Template synthesis of nanostructured polymeric membranes by inkjet printing, ACS Appl. Mater. Interfaces 8 (2016) 3386–3395, https://doi.org/10.1021/acsami.5b11360.
[133] P. Gao, A. Hunter, M.J. Summe, W.A. Phillip, A method for the efficient fabrication of multifunctional mosaic membranes by inkjet printing, ACS Appl. Mater. Interfaces 8 (2016) 19772–19779, https://doi.org/10.1021/acsami.6b06048.
[134] S.J. Lee, D.N. Heo, M. Heo, M.H. Noh, D. Lee, S.A. Park, J.H. Moon, I.K. Kwon, Most simple preparation of an inkjet printing of silver nanoparticles on fibrous membrane for water purification: technological and commercial application, J. Ind. Eng. Chem. 46 (2017) 273–278, https://doi.org/10.1016/j.jiec.2016.10.039.
[135] M. Fathizadeh, H.N. Tien, K. Khivantsev, J.T. Chen, M. Yu, Printing ultrathin graphene oxide nanofiltration membranes for water purification, J. Mater. Chem. A. 5 (2017) 20860–20866, https://doi.org/10.1039/c7ta06307e.
[136] Y. Chen, P. Gao, M.J. Summe, W.A. Phillip, N. Wei, Biocatalytic membranes prepared by inkjet printing functionalized yeast cells onto microfiltration substrates, J. Membr. Sci. 550 (2018) 91–100, https://doi.org/10.1016/j.memsci.2017.12.045.
[137] M. Yazdanpour, A. Esmaeilifar, S. Rowshanzamir, Effects of hot pressing conditions on the performance of Nafion membranes coated by ink-jet printing of Pt/MWCNTs electrocatalyst for PEMFCs, Int. J. Hydrogen Energy 37 (2012) 11290–11298, https://doi.org/10.1016/j.ijhydene.2012.04.139.
[138] M. Klingele, M. Breitwieser, R. Zengerle, S. Thiele, Direct deposition of proton exchange membranes enabling high performance hydrogen fuel cells, J. Mater. Chem. A. 3 (2015) 11239–11245, https://doi.org/10.1039/c5ta01341k.
[139] X.H. Ma, Z. Yang, Z.K. Yao, H. Guo, Z.L. Xu, C.Y. Tang, Interfacial polymerization with electrosprayed microdroplets: toward controllable and ultrathin polyamide membranes, Environ. Sci. Technol. Lett. 5 (2018) 117–122, https://doi.org/10.1021/acs.estlett.7b00566.
[140] J. Wang, X. Pei, G. Liu, Q. Han, S. Yang, F. Liu, "Living" electrospray – a controllable polydopamine nano-coating strategy with zero liquid discharge for separation, J. Membr. Sci. 586 (2019) 170–176, https://doi.org/10.1016/j.memsci.2019.05.071.
[141] J.J. Huang, Y. Tian, L. Chen, Y. Liao, M. Tian, X. You, X. You, R. Wang, R. Wang, Electrospray-printed three-tiered composite membranes with enhanced mass transfer coefficients for phenol removal in an aqueous-aqueous membrane extractive process, Environ. Sci. Technol. 54 (2020) 7611–7618, https://doi.org/10.1021/acs.est.0c00475.
[142] X. Qian, T. Ravindran, S.J. Lounder, A. Asatekin, J.R. McCutcheon, Printing zwitterionic self-assembled thin film composite membranes: tuning thickness leads to remarkable permeability for nanofiltration (submitted, in revision), J. Memb. Sci (n.d.).
[143] L. Shen, X. Yu, C. Cheng, C. Song, X. Wang, M. Zhu, B.S. Hsiao, High filtration performance thin film nanofibrous composite membrane prepared by electrospraying technique and hot-pressing treatment, J. Membr. Sci. 499 (2016) 470–479, https://doi.org/10.1016/j.memsci.2015.11.004.
[144] H. You, Y. Yang, X. Li, K. Zhang, X. Wang, M. Zhu, B.S. Hsiao, Low pressure high flux thin film nanofibrous composite membranes prepared by electrospraying technique combined with solution treatment, J. Membr. Sci. 394–395 (2012) 241–247, https://doi.org/10.1016/j.memsci.2011.12.047.
[145] H. You, X. Li, Y. Yang, B. Wang, Z. Li, X. Wang, M. Zhu, B.S. Hsiao, High flux low pressure thin film nanocomposite ultrafiltration membranes based on nanofibrous substrates, Separ. Purif. Technol. 108 (2013) 143–151, https://doi.org/10.1016/j.seppur.2013.02.014.
[146] C. Su, T. Horseman, H. Cao, K.S.S. Christie, Y. Li, S. Lin, Robust superhydrophobic membrane for membrane distillation with excellent scaling resistance, Environ. Sci. Technol. (2019), https://doi.org/10.1021/acs.est.9b04362.
[147] J.M. Lim, H.J. Lee, H.W. Kim, J. Yong Lee, J.T. Yoo, K.W. Park, C.K. Lee, Y. T. Hong, S.Y. Lee, Dual electrospray-assisted forced blending of thermodynamically immiscible polyelectrolyte mixtures, J. Membr. Sci. 481 (2015) 28–35, https://doi.org/10.1016/j.memsci.2015.01.057.
[148] Y. Sueyoshi, C. Fukushima, M. Yoshikawa, Molecularly imprinted nanofiber membranes from cellulose acetate aimed for chiral separation, J. Membr. Sci. 357 (2010) 90–97, https://doi.org/10.1016/j.memsci.2010.04.005.
[149] Y. Sueyoshi, A. Utsunomiya, M. Yoshikawa, G.P. Robertson, M.D. Guiver, Chiral separation with molecularly imprinted polysulfone-aldehyde derivatized nanofiber membranes, J. Membr. Sci. (2012) 89–96, https://doi.org/10.1016/j.memsci.2012.01.033, 401–402.
[150] V.M. Aceituno Melgar, H.T. Kwon, J. Kim, Direct spraying approach for synthesis of ZIF-7 membranes by electrospray deposition, J. Membr. Sci. 459 (2014) 190–196, https://doi.org/10.1016/j.memsci.2014.02.020.
[151] V.M. Aceituno Melgar, H. Ahn, J. Kim, M.R. Othman, Highly selective microporous ZIF-8 membranes prepared by rapid electrospray deposition, J. Ind. Eng. Chem. 21 (2015) 575–579, https://doi.org/10.1016/j.jiec.2014.03.021.
[152] W. Jia, J.A. Kharraz, J. Guo, A.K. An, Superhydrophobic (polyvinylidene fluoride-co-hexafluoropropylene)/(polystyrene) composite membrane via a novel hybrid electrospin-electrospray process, J. Membr. Sci. 611 (2020) 118360, https://doi.org/10.1016/j.memsci.2020.118360.
[153] Y. Liao, G. Zheng, J.J. Huang, M. Tian, R. Wang, Development of robust and superhydrophobic membranes to mitigate membrane scaling and fouling in membrane distillation, J. Membr. Sci. 601 (2020) 117962, https://doi.org/10.1016/j.memsci.2020.117962.
[154] E. Korzhova, S. Déon, Z. Koubaa, P. Fievet, D. Lopatin, O. Baranov, Modification of commercial UF membranes by electrospray deposition of polymers for tailoring physicochemical properties and enhancing filtration performances, J. Membr. Sci. 598 (2020), https://doi.org/10.1016/j.memsci.2019.117805.
[155] E. Korzhova, N. Pismenskaya, D. Lopatin, O. Baranov, L. Dammak, V. Nikonenko, Effect of surface hydrophobization on chronopotentiometric behavior of an AMX anion-exchange membrane at overlimiting currents, J. Membr. Sci. 500 (2016) 161–170, https://doi.org/10.1016/j.memsci.2015.11.018.
[156] A. Al-Shimmery, S. Mazinani, J. Ji, Y.M.J. Chew, D. Mattia, 3D printed composite membranes with enhanced anti-fouling behaviour, J. Membr. Sci. 574 (2019) 76–85, https://doi.org/10.1016/j.memsci.2018.12.058.
[157] S. Mazinani, A. Al-Shimmery, Y.M. John Chew, D. Mattia, 3D printed fouling-resistant composite membranes, ACS Appl. Mater. Interfaces 11 (2019) 26373–26383, https://doi.org/10.1021/acsami.9b07764.
[158] L.C. Hwa, M.B. Uday, N. Ahmad, A.M. Noor, S. Rajoo, K. Bin Zakaria, Integration and fabrication of the cheap ceramic membrane through 3D printing technology, Mater. Today Commun. 15 (2018) 134–142, https://doi.org/10.1016/j.mtcomm.2018.02.029.
[159] H. Philamore, J. Rossiter, P. Walters, J. Winfield, I. Ieropoulos, Cast and 3D printed ion exchange membranes for monolithic microbial fuel cell fabrication, J. Power Sources 289 (2015) 91–99, https://doi.org/10.1016/j.jpowsour.2015.04.113.
[160] T. Femmer, A.J.C. Kuehne, M. Wessling, Print your own membrane: direct rapid prototyping of polydimethylsiloxane, Lab Chip 14 (2014) 2610–2613, https://doi.org/10.1039/c4lc00320a.
[161] T. Femmer, A.J.C. Kuehne, J. Torres-Rendon, A. Walther, M. Wessling, Print your membrane: rapid prototyping of complex 3D-PDMS membranes via a sacrificial resist, J. Membr. Sci. 478 (2015) 12–18, https://doi.org/10.1016/j.memsci.2014.12.040.
[162] P.J.F. Gandy, S. Bardhan, A.L. Mackay, J. Klinowski, Nodal surface approximations to the P, G, D and I-WP triply periodic minimal surfaces, Chem. Phys. Lett. 336 (2001) 187–195, https://doi.org/10.1016/S0009-2614(00)01418-4.
[163] T. Femmer, A.J.C. Kuehne, M. Wessling, Estimation of the structure dependent performance of 3-D rapid prototyped membranes, Chem. Eng. J. 273 (2015) 438–445, https://doi.org/10.1016/j.cej.2015.03.029.
[164] A. Al-Shimmery, S. Mazinani, J. Flynn, J. Chew, D. Mattia, 3D printed porous contactors for enhanced oil droplet coalescence, J. Membr. Sci. 590 (2019) 117274, https://doi.org/10.1016/j.memsci.2019.117274.

[165] S. Armbruster, O. Cheong, J. Lölsberg, S. Popovic, S. Yüce, M. Wessling, Fouling mitigation in tubular membranes by 3D-printed turbulence promoters, J. Membr. Sci. 554 (2018) 156–163, https://doi.org/10.1016/j.memsci.2018.02.015.
[166] S. Armbruster, F. Stockmeier, M. Junker, M. Schiller-Becerra, S. Yüce, M. Wessling, Short and spaced twisted tapes to mitigate fouling in tubular membranes, J. Membr. Sci. 595 (2020) 117426, https://doi.org/10.1016/j.memsci.2019.117426.
[167] H.Y. Tsai, A. Huang, J.F. soesanto, Y.L. Luo, T.Y. Hsu, C.H. Chen, K.J. Hwang, C. D. Ho, K.L. Tung, 3D printing design of turbulence promoters in a cross-flow microfiltration system for fine particles removal, J. Membr. Sci. 573 (2019) 647–656, https://doi.org/10.1016/j.memsci.2018.11.081.
[168] T. Luelf, D. Rall, D. Wypysek, M. Wiese, T. Femmer, C. Bremer, J.U. Michaelis, M. Wessling, 3D-printed rotating spinnerets create membranes with a twist, J. Membr. Sci. 555 (2018) 7–19, https://doi.org/10.1016/j.memsci.2018.03.026.
[169] Q. Li, B. Lian, W. Zhong, A. Omar, A. Razmjou, P. Dai, J. Guan, G. Leslie, R. A. Taylor, Improving the performance of vacuum membrane distillation using a 3D-printed helical baffle and a superhydrophobic nanocomposite membrane, Separ. Purif. Technol. 248 (2020) 117072, https://doi.org/10.1016/j.seppur.2020.117072.
[170] J.R. McCutcheon, Unraveling the mysteries of the thin film composite reverse osmosis membrane, Joule. 5 (n.d.) 528–530. doi: 10.1016/j.joule.2021.03.004.
[171] S.W. Pattinson, A.J. Hart, Additive manufacturing of cellulosic materials with robust mechanics and antimicrobial functionality, Adv. Mater. Technol. 2 (2017), https://doi.org/10.1002/admt.201600084.
[172] F. Zhang, Y. Ma, J. Liao, V. Breedveld, R.P. Lively, Solution-based 3D printing of polymers of intrinsic microporosity, Macromol. Rapid Commun. 39 (2018), https://doi.org/10.1002/marc.201800274.
[173] M.S. Denny, M. Kalaj, K.C. Bentz, S.M. Cohen, Multicomponent metal-organic framework membranes for advanced functional composites, Chem. Sci. 9 (2018) 8842–8849, https://doi.org/10.1039/c8sc02356e.
[174] J.C. Moreton, J.M. Palomba, S.M. Cohen, Liquid-phase Applications of metal–organic framework mixed-matrix membranes prepared from poly (ethylene- co -vinyl acetate), ACS Appl. Polym. Mater. 2 (2020) 2063–2069, https://doi.org/10.1021/acsapm.0c00230.
[175] J. Petersen, K.V. Peinemann, Novel polyamide composite membranes for gas separation prepared by interfacial polycondensation, J. Appl. Polym. Sci. 63 (1997) 1557–1563, https://doi.org/10.1002/(SICI)1097-4628(19970321)63:12<1557::AID-APP6>3.0.CO;2-N.
[176] A. Bagheri, J. Jin, Photopolymerization in 3D printing, ACS Appl. Polym. Mater. 1 (2019) 593–611, https://doi.org/10.1021/acsapm.8b00165.
[177] A. Alabi, A. AlHajaj, L. Cseri, G. Szekely, P. Budd, L. Zou, Review of nanomaterials-assisted ion exchange membranes for electromembrane desalination, Npj Clean Water 1 (2018), https://doi.org/10.1038/s41545-018-0009-7.
[178] G.M. Geise, D.R. Paul, B.D. Freeman, Fundamental water and salt transport properties of polymeric materials, Prog. Polym. Sci. 39 (2014) 1–42, https://doi.org/10.1016/j.progpolymsci.2013.07.001.
[179] T. Luo, S. Abdu, M. Wessling, Selectivity of ion exchange membranes: a review, J. Membr. Sci. 555 (2018) 429–454, https://doi.org/10.1016/j.memsci.2018.03.051.
[180] H. Strathmann, A. Grabowski, G. Eigenberger, Ion-exchange membranes in the chemical process industry, Ind. Eng. Chem. Res. 52 (2013) 10364–10379, https://doi.org/10.1021/ie4002102.
[181] F. Helfferich, Ion-exchange, 1962.
[182] A. Kusoglu, A.Z. Weber, New insights into perfluorinated sulfonic-acid ionomers, Chem. Rev. 117 (2017) 987–1104, https://doi.org/10.1021/acs.chemrev.6b00159.
[183] J.R. Varcoe, P. Atanassov, D.R. Dekel, A.M. Herring, M.A. Hickner, P.A. Kohl, A. R. Kucernak, W.E. Mustain, K. Nijmeijer, K. Scott, T. Xu, L. Zhuang, Anion-exchange membranes in electrochemical energy systems, Energy Environ. Sci. 7 (2014) 3135–3191, https://doi.org/10.1039/c4ee01303d.
[184] D.W. Shin, M.D. Guiver, Y.M. Lee, Hydrocarbon-based polymer electrolyte membranes: importance of morphology on ion transport and membrane stability, Chem. Rev. 117 (2017) 4759–4805, https://doi.org/10.1021/acs.chemrev.6b00586.
[185] R. Epsztein, R.M. DuChanois, C.L. Ritt, A. Noy, M. Elimelech, Towards single-species selectivity of membranes with subnanometre pores, Nat. Nanotechnol. 15 (2020) 426–436, https://doi.org/10.1038/s41565-020-0713-6.
[186] S.A. Berlinger, P.J. Dudenas, A. Bird, X. Chen, G. Freychet, B.D. McCloskey, A. Kusoglu, A.Z. Weber, Impact of dispersion solvent on ionomer thin films and membranes, ACS Appl. Polym. Mater. 2 (2020) 5824–5834, https://doi.org/10.1021/acsapm.0c01076.
[187] R. Sujanani, M.R. Landsman, S. Jiao, J.D. Moon, M.S. Shell, D.F. Lawler, L.E. Katz, B.D. Freeman, Designing solute-tailored selectivity in membranes: perspectives for water reuse and resource recovery, ACS Macro Lett. 9 (2020) 1709–1717, https://doi.org/10.1021/acsmacrolett.0c00710.
[188] S. Holdcroft, Fuel cell catalyst layers: a polymer science perspective, Chem. Mater. 26 (2014) 381–393, https://doi.org/10.1021/cm401445h.
[189] J.L. Lutkenhaus, P. Flouda, Structural batteries take a load off, Sci. Robot. 5 (2020), eabd7026, https://doi.org/10.1126/scirobotics.abd7026.
[190] F. Mo, G. Liang, Z. Huang, H. Li, D. Wang, C. Zhi, An overview of fiber-shaped batteries with a focus on multifunctionality, scalability, and technical difficulties, Adv. Mater. 32 (2020), https://doi.org/10.1002/adma.201902151.
[191] P. Marchetti, M.F. Jimenez Solomon, G. Szekely, A.G. Livingston, Molecular separation with organic solvent nanofiltration: a critical review, Chem. Rev. 114 (2014) 10735–10806, https://doi.org/10.1021/cr500006j.
[192] R.P. Lively, D.S. Sholl, From water to organics in membrane separations: membrane materials provide economical means to achieve various separation processes - and their capabilities for processing organic fluids look set to expand significantly, Nat. Mater. 16 (2017) 276–279, https://doi.org/10.1038/nmat4860.
[193] M. Yu, M. Fathizadeh, Printable Graphene oxide Coatings and Membranes, 2019.
[194] M. Higa, A. Jikihara, K. Kobayashi, N. Fujiwara, Ion-Exchange Membrane and Method for Producing same, 2016.
[195] W.A. Phillip, S. Qu, Y. Shi, Copolymer Nanofilters with Charge- Patterned Domains, 2018.
[196] C.U. Hardwicke, A.J. Avagliano, G.R. Chambers, S.F. Rutkowski, E.J. Hall, Reverse Osmosis Membrane And Membrane Stack Assembly, 2009, https://doi.org/10.1016/j.ijpharm.2017.08.087%0A10.1016/j.ccr.2011.01.031.
[197] C.J. Arnusch, S. Badalov, E. Matzkin, N.C. Wardrip, Fabrication And Modification of Polymer Membranes Using Ink-Jet Printing, 2016.
[198] M.R. Chowdhury, J.R. McCutcheon, Smooth Polymer Membranes And Electrospray Printing Methods of Making Thereof, 2019.
[199] A. Alexiou Ayse, J. Lounder, Samuel, R. McCutcheon, Jeffrey, X. Qian, T. Ravindran, Additive Manufacturing of Self-Assembled Polymer Films, 2020.
[200] P. Campbell, S. Baker, M.C. Hernandez, J.M. Knipe, J.K. Stolaroff, Porous Ceramics for Additive Manufacturing, Filtration, And Membrane Applications, 2020.
[201] (n.d.), https://g2owatertech.com/.
[202] S. Atkinson, Nano Sun sets up Singapore's first 3D-printing plant for water filtration membranes, Membr. Technol. (2018) 10–11, https://doi.org/10.1016/s0958-2118(18)30208-8, 2018.
[203] (n.d.), https://aquamembranes.com/.
[204] J.J. Wu, L.M. Huang, Q. Zhao, T. Xie, 4D printing: history and recent progress, Chinese J. Polym. Sci. (English Ed. 36 (2018) 563–575, https://doi.org/10.1007/s10118-018-2089-8.
[205] S. Naficy, R. Gately, R. Gorkin, H. Xin, G.M. Spinks, 4D printing of reversible shape morphing hydrogel structures, Macromol. Mater. Eng. 302 (2017) 1–9, https://doi.org/10.1002/mame.201600212.
[206] H. Yang, W.R. Leow, T. Wang, J. Wang, J. Yu, K. He, D. Qi, C. Wan, X. Chen, 3D printed photoresponsive devices based on shape memory composites, Adv. Mater. 29 (2017) 1–7, https://doi.org/10.1002/adma.201701627.
[207] D. Raviv, W. Zhao, C. McKnelly, A. Papadopoulou, A. Kadambi, B. Shi, S. Hirsch, D. Dikovsky, M. Zyracki, C. Olguin, R. Raskar, S. Tibbits, Active printed materials for complex self-evolving deformations, Sci. Rep. 4 (2014) 1–9, https://doi.org/10.1038/srep07422.
[208] M. Zarek, M. Layani, I. Cooperstein, E. Sachyani, D. Cohn, S. Magdassi, 3D printing of shape memory polymers for flexible electronic devices, Adv. Mater. 28 (2016) 4449–4454, https://doi.org/10.1002/adma.201503132.
[209] S. Darvishmanesh, X. Qian, S.R. Wickramasinghe, Responsive membranes for advanced separations, Curr. Opin. Chem. Eng. 8 (2015) 98–104, https://doi.org/10.1016/j.coche.2015.04.002.
[210] Q. Zhang, K. Zhang, G. Hu, Smart three-dimensional lightweight structure triggered from a thin composite sheet via 3D printing technique, Sci. Rep. 6 (2016) 1–8, https://doi.org/10.1038/srep22431.
[211] M. Gillono, I. Roppolo, F. Frascella, L. Scaltrito, C.F. Pirri, A. Chiappone, CO2 permeability control in 3D printed light responsive structures, Appl. Mater. Today. 18 (2020) 100470, https://doi.org/10.1016/j.apmt.2019.100470.
[212] J.F. Hester, S.C. Olugebefola, A.M. Mayes, Preparation of pH-responsive polymer membranes by self-organization, J. Membr. Sci. 208 (2002) 375–388, https://doi.org/10.1016/S0376-7388(02)00317-4.
[213] J. De Grooth, M. Dong, W.M. De Vos, K. Nijmeijer, Building polyzwitterion-based multilayers for responsive membranes, Langmuir 30 (2014) 5152–5161, https://doi.org/10.1021/la500857b.
[214] S. Frost, M. Ulbricht, Thermoresponsive ultrafiltration membranes for the switchable permeation and fractionation of nanoparticles, J. Membr. Sci. 448 (2013) 1–11, https://doi.org/10.1016/j.memsci.2013.07.036.
[215] I. Gibson, D. Rosen, B. Stucker, Additive Manufacturing Technologies: 3D Printing, rapid Prototyping, and Direct Digital Manufacturing, second Edition, 2015, pp. 1–498, https://doi.org/10.1007/978-1-4939-2113-3. Addit. Manuf. Technol. 3D Printing, Rapid Prototyping, Direct Digit. Manuf. Second Ed.
[216] M. Carlotti, V. Mattoli, Functional materials for two-photon polymerization in microfabrication, Small 15 (40) (2019) 1–22, https://doi.org/10.1002/smll.201902687.
[217] S. Bruner, D. Xu, C. Phillips, 54.3: drop landing accuracy improvements in inkjet printed OLED displays, SID Symp. Dig. Tech. Pap. 38 (1) (2007) 1611–1612, https://doi.org/10.1889/1.2785628.
[218] P. Calvert, Inkjet printing for materials and devices, Chem. Mater. 13 (10) (2001) 3299–3305, https://doi.org/10.1021/cm0101632.
[219] C. Ho, et al., Electrospray ionisation mass spectrometry: principles and clinical applications, Clin. Biochem. Rev. 24 (1) (2003) 3–12, https://doi.org/10.1002/9781118307816.ch34.
[220] Stratasys, PolyJet 3D printers systems and materials [Online], https://www.stratasys.com/3d-printers/objet-350-500-connex3. Available.